Rossby Wave Turbulence

by

Katie Louise Harper

Thesis

Submitted to the University of Warwick Mathematics Department for the
degree of

Doctor of Philosophy

September 2015

THE UNIVERSITY OF
WARWICK

Contents

List of Figures

Acknowledgements

First and foremost, I would like to thank my PhD supervisor, Sergey Nazarenko, for his patience, support and guidance over the last four years. His knowledge of the subject and enthusiasm never ceases to amaze me and I feel very lucky to have been his student.

In addition, I would like to thank my collaborators, Miguel Bustamante, Sergey Medvedev and Colm Connaughton. I am especially grateful to Brenda Quinn for allowing me to use her numerical code and for all her help whilst I was learning Fortran. I would also like to express my sincere gratitude to Carole Fisher and all the staff in the Mathematics Institute at Warwick University who have helped me during my time there and to the fluid dynamics research group for many interesting discussions at our weekly coffee mornings.

And last but not least, thank you to my Mum, Dad and Richard for their continued support and belief in me. This wouldn't have been possible without you. I hope I have made you proud.

Declaration

This thesis is submitted to the University of Warwick in support of my application for the degree of Doctor of Philosophy. It has been composed by myself and has not been submitted for a degree at another university. I declare that the work contained in this thesis is my own except where otherwise stated.

Chapters 1 and 2 and the first section in chapter 3 contain no original work but provide a background on Rossby wave turbulence and quadratic invariants in the kinetic regime. Chapter 3 from section 3.2 onwards as well as chapter 4 is original work by myself, Sergey Nazarenko and Miguel Bustamante published in [1]. Chapter 5 is original work by myself and Sergey Nazarenko which has yet to be submitted for publication. A numerical code originally written by Brenda Quinn for small-scale turbulence was adapted by myself in order to find the numerical results for large-scale turbulence presented in this chapter. Chapter 6 contains original work which has been published by myself, Sergey Nazarenko, Sergey Medvedev and Colm Connaughton in [2], other than the derivation of the two-layer equations in section 6.1 which is based on work by Salmon [3]. The derivation in appendix A is based on working in Kozlov et al.'s paper [4].

Abstract

In this thesis, Rossby waves are considered within the one-layer Charney-Hasegawa-Mima (CHM) equation and two-layer quasi-geostrophic (QG) model. They are studied from a wave turbulence (WT) perspective. Since nonlinearity is quadratic, interactions take place between triplets of waves known as triads. A triad is said to be resonant if its wave vectors and frequencies satisfy $\mathbf{k}_1 + \mathbf{k}_2 - \mathbf{k}_3 = 0$ and $\omega(\mathbf{k}_1) + \omega(\mathbf{k}_2) - \omega(\mathbf{k}_3) = 0$ respectively. These triads can then be joined together to form resonant clusters of various sizes. The wave vectors can be continuous, in an unbounded domain, or discrete, in a bounded domain. Continuous, otherwise known as kinetic, WT has been extensively studied in the one-layer case. It is known that three quadratic invariants exist and they take part in a triple cascade in $\mathbf{k}$-space. This thesis is interested in finding quadratic invariants, of which there can be many, in the discrete regime. It begins by considering discrete clusters of resonant triads arising from a Hamiltonian three-wave equation. A cluster consists of N modes forming a total of M connected triads. It is shown that that finding quadratic invariants is equivalent to a basic linear algebra problem, consisting of finding the null space of a rectangular $M \times N$ matrix $\mathbb{A}$ with entries 1, -1 and 0. An algorithm is then formulated for decomposing large clusters into smaller ones to show how the quadratic invariants are related to topological parts of the cluster. Specific examples of clusters arising in the CHM wave model are considered.

The second part of this thesis focusses on the large-scale limit of the CHM equation. This limit has been studied the least; however, it would appear to be more relevant since Rossby waves in the ocean are large-scale. Recently a new quadratic invariant, known as semi-action, has been discovered in this limit. Its density is one in the meridional region $|k_y| < \sqrt{3}k_x$ and zero in the zonal region $|k_y| > \sqrt{3}k_x$. As a consequence of the conservation of semi-action, conditions are placed on the triad interactions involving zonal (Z) and meridional (M) modes. In this thesis it is proved directly, without appealing to conservation, that the following triad interactions are prohibited: $M \to M + M$, $M \to Z + Z$, $Z \to M + Z$ and $Z \to M + M$. The cascade directions are studied of the three invariants, the energy, enstrophy and, depending whether the initial spectrum is in the meridional or zonal sector, the semi-action or zonsotrophy respectively. The results are interpreted to explain the formation of unisotropic turbulence with dominating zonal scales.

In the final part of this thesis, a symmetric form of the two-layer kinetic equation for Rossby waves is derived using canonical variables, allowing the turbulent cascade of energy between the barotropic and baroclinic modes to be studied. It turns out that energy is transferred via local triad interactions from large-scale baroclinic modes to the baroclinic and barotropic modes at the Rossby deformation scale. From there it is transferred into large-scale barotropic modes via a non-local inverse transfer.

Acronyms

CHM Charney-Hasegawa-Mima

QG quasi-geostrophic

WT wave turbulence

2D two-dimensional

PDE partial differential equation

PV potential vorticity

KZ Kolmogorov-Zakharov

3D three-dimensional

1D one-dimensional

LHS left-hand-side

Z zonal

M meridional

RHS right-hand-side

BI baroclinic instability

DNS direct numerical simulation

1D one-dimensional

Chapter 1

Introduction

1.1 Quasi-geostrophic theory

The Rossby number is a dimensionless number which characterises the strength of inertial terms ($\mathbf{u}.\nabla\mathbf{u} \sim \frac{U^2}{L}$) to the Coriolis force terms ($\Omega \times \mathbf{u} = \Omega U$) in the Navier-Stokes equation. It is defined as:

$$Ro = U/fL, \tag{1.1}$$

where U and L are the characteristic horizontal velocity and length scales respectively and $f = 2\Omega\sin\varphi$ is the Coriolis parameter where Ω is the angular speed of the Earth and φ is the latitude. See figure 1.1.

When $Ro \ll 1$, inertial accelerations are negligible and Coriolis accelerations dominate. In this limit the geostrophic approximation can be used. However, for most large-scale atmospheric and oceanic flows the Rossby number is small but not so small that the inertial accelerations can be neglected completely. This gives us quasi-geostrophic (QG) motion.
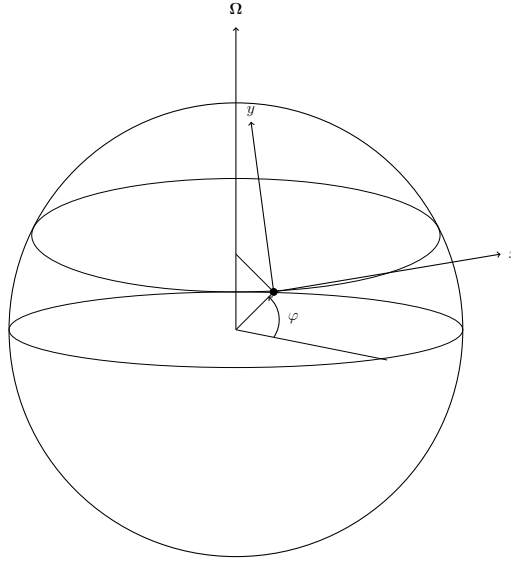
Figure 1.1: A rotating sphere.

Until the late 1940's equations governing atmospheric and oceanic dynamics were complicated, but in 1947 Charney [5] developed the QG approximation under the assumption that large-scale flows in the atmosphere and oceans were quasi-hydrostatic, quasi-adiabatic, quasi-horizontal, quasi-geostrophic and incompressible. He derived a single two-dimensional (2D) partial differential equation (PDE) expressing the conservation of potential vorticity (PV), known as the barotropic PV equation or the Charney-Hasegawa-Mima (CHM) equation:

$$\frac{\partial}{\partial t}(\nabla^2\psi - F\psi) + \beta\frac{\partial\psi}{\partial x} + J[\psi, \nabla^2\psi] = 0, \tag{1.2}$$

where $\psi(\mathbf{x}, t)$ is the geostrophic stream function, $\mathbf{x} = (x, y)$ is a 2D vector with x varying in the zonal direction and y in the meridional direction, $F = \frac{f^2}{gH}$ is one over the Rossby radius of deformation squared, β is the Rossby parameter measuring the variation of the Coriolis force with latitude and the Jacobian term:

$$J[\psi, \nabla^2\psi] = \frac{\partial\psi}{\partial x}\frac{\partial\nabla^2\psi}{\partial y} - \frac{\partial\psi}{\partial y}\frac{\partial\nabla^2\psi}{\partial x}, \tag{1.3}$$

represents the nonlinearity. The barotropic PV equation will not be derived in this thesis, for details on the derivation please refer to [6, 7, 8]; however, much more

detail will be given in chapter 6 on the derivation of the two-layer QG equations. The same equation governs drift waves in plasma [9] where F in this case represents the inverse of the gyroradius squared and β is a constant proportional to the gradient of the plasma density. Many of the findings discussed in this thesis, in a geophysical context, are relevant to plasma physics; however, drift waves will not be considered here.

Equation (1.2) is similar to the 2D Euler equation. It can be written in the form of an advection equation:

$$\frac{Dq}{Dt} = 0, \tag{1.4}$$

for the PV:

$$q = \nabla^2\psi + \beta y - F\psi, \tag{1.5}$$

where $\frac{D}{Dt} = \frac{\partial}{\partial t} + \mathbf{u} \cdot \nabla$ is the advective derivative and $\mathbf{u} = (u_x, u_y) = (-\frac{\partial\psi}{\partial y}, \frac{\partial\psi}{\partial x})$ is the velocity field. Like the 2D Euler equation, the CHM equation conserves two quadratic invariants, the energy:

$$E = \frac{1}{2}\int[(\nabla\psi)^2 + F\psi^2]d\mathbf{x}, \tag{1.6}$$

and potential enstrophy:

$$\Omega = \frac{1}{2}\int[\nabla^2\psi - F\psi]^2 d\mathbf{x}. \tag{1.7}$$

However, the CHM equation differs from the Euler equation by the presence of the linear term, $\beta\frac{\partial\psi}{\partial x}$. This extra term means that the CHM equation can support wave motions, unlike the Euler equation, and also has a weakly nonlinear limit since the linear term can be large compared with the nonlinear one.

If we neglect the nonlinear Jacobian in equation (1.2) it admits harmonic solutions of the form:

$$\psi(\mathbf{x}, t) = Re[A_\mathbf{k}e^{i(\mathbf{k}\cdot\mathbf{x} - \omega_\mathbf{k}t)}]. \tag{1.8}$$

These solutions are called Rossby waves and have the dispersion relation:

$$\omega_\mathbf{k} = -\frac{\beta k_x}{k^2 + F}. \tag{1.9}$$

1.2 Rossby waves

Rossby waves, also known as planetary waves, were first put forward by Carl-Gustaf Rossby in 1939 [10]. They are due to the variation of the Coriolis parameter with latitude (f is zero at the equator and increases towards the poles). This is known as the beta-effect, where:

$$\beta = \frac{\partial f}{\partial y}. \tag{1.10}$$

They are best understood by considering the conservation of PV for a single layer of fluid:

$$q = \frac{\zeta + f}{H}, \tag{1.11}$$

where $\zeta = \nabla^2 \psi$ is the relative vorticity and f is the planetary vorticity. Any latitudinal displacement of a parcel (north or south) to a region of larger/smaller planetary vorticity will require a decrease/increase in relative vorticity to keep the PV constant. Hence anti-cyclonic/cyclonic motion develops resulting in westward propagating Rossby waves. See figure 1.2.
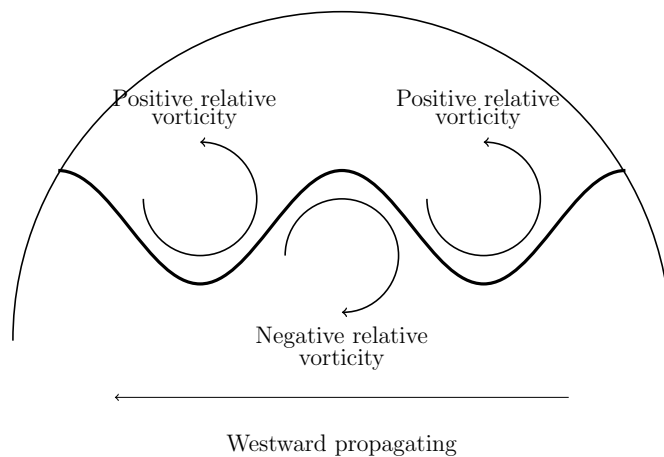
Figure 1.2: Rossby wave motion.

In the Earth's atmosphere Rossby waves are easy to observe as large-scale meanders of the jet stream, see figure 1.3. These meanders have a huge effect on the weather and climate experienced on Earth. This can be seen by considering the position of the polar jet stream over the United Kingdom. It is usually to the north of the UK meaning, in summer the weather is warm and settled and in winter it

4

ensures generally mild, and at times wet and windy weather. However, in 2007-2008 and 2009-2010 the jet stream dipped south causing usually wet and cooler summers and bitter but dry winters, see figure 1.4. One explanation for this is that it coincides with the El Nino taking place in the Equatorial Pacific, where weaker winds allow warmer water from the West Pacific to flow east, setting off an atmospheric chain reaction. The Met Office has already issued warnings of a harsh winter of 2015 as the El Nino is expected to take place.

In the Earth's oceans, Rossby waves are much harder to observe as they travel westward along the thermocline (the boundary between the warm upper layer and cold lower layer). They are large-scale waves, much longer than the Rossby radius of deformation, with a horizontal length of the order of hundreds of kilometres [11]. However, the amplitude of oscillation at the sea surface is just a few centimetres. They propagate slowly, with speed varying with latitude and increasing equatorward, but of the order of just a few kilometres per day. This means that at midlatitudes it may take several months, or even years, for a wave to cross the ocean.

Figure 1.3: The jet streams normal summer pattern. Sourced from www.bbc.co.uk.

Figure 1.4: The jet stream during summer 2008 and 2010. Sourced from www.bbc.co.uk.

Since Rossby waves are dispersive, wave turbulence (WT) theory is applicable when the waves are weak. In the next chapter a brief introduction to WT is presented, after which the theory is applied to the CHM equation.

Chapter 2

Wave turbulence

WT is defined as "out-of-equilibrium statistical mechanics of random nonlinear waves" [12]. As well as randomness, deviation from thermodynamic equilibrium and being statistical in nature, WT shares other properties with classical hydrodynamic turbulence such as conserving several positive quantities and being dominated by a flux or cascade of energy (or another conserved quantity such as waveaction or momentum) through the scales. It is often further assumed that waves are weakly nonlinear and dispersive, therefore allowing them to be approximated by independent linear waves for short time intervals. As it will later be seen, this leads to a systematic mathematical analysis of WT.

2.1   History and examples

The concept of WT originated from Peierls' work in 1929 [13] who derived what we now know as the kinetic equation for phonons in anharmonic crystals. However, it was not until the 1960's that the kinetic equation was derived for plasma physics [14] and for water waves [15]. Considerable progress in the area of weak WT was made by Zakharov in the mid 1960's when he showed that wave kinetic equations have exact power law solutions which are similar to Kolmogorov's spectrum of hydrodynamic turbulence. These stationary solutions are known as the Kolmogorov-Zakharov (KZ) spectra and they describe the transport of conserved quantities to small or large scales [16]. They were first discovered for weak turbulence in plasmas [17] and then

7

in the context of surface waves [18, 19]. Since then WT is a tool that has proved valuable and effective in a great variety of cases from quantum to astrophysical scales, i.e. quantum turbulence in superfluid helium [20], surface gravity and capillary waves [21, 22], magneto-hydrodynamic turbulence in astrophysics and laboratory plasmas [23, 24] and turbulence in rotating and stratified fluids [25, 26].

2.2 Three-wave resonant interactions

For a system of weakly interacting waves whose leading order nonlinearity is quadratic, like in the CHM equation, interactions take place between triplets of waves which form what is known as a triad. For a system with cubic nonlinearity, interactions would involve four waves and so on. It is convenient to represent the wave field in the 2D $\mathbf{k}$-space using Fourier coefficients, so let the system be a periodic box, with length L in all directions. A triad is then made up of three modes with wave vectors $\mathbf{k}_1, \mathbf{k}_2, \mathbf{k}_3 \in \mathbb{R}^2$, which satisfy the following three-wave condition:

$$\mathbf{k}_1 + \mathbf{k}_2 - \mathbf{k}_3 = 0. \tag{2.1}$$

Each wave vector has an associated frequency, $\omega(\mathbf{k}_1), \omega(\mathbf{k}_2)$ and $\omega(\mathbf{k}_3)$ respectively. By definition, a triad is called resonant if:

$$\omega(\mathbf{k}_1) + \omega(\mathbf{k}_2) - \omega(\mathbf{k}_3) = 0. \tag{2.2}$$

In the limit of weakly nonlinear waves, energy is only exchanged efficiently between modes which are members of resonant triads.

2.3 Wave turbulence regimes

The wave vectors $\mathbf{k}$ can either be continuous or discrete. For waves systems in an unbounded domain, the $\mathbf{k}$'s are continuous variables. Therefore, any $\mathbf{k}$ may be a member of infinitely many resonant triads. These resonant triads form a network in Fourier space to transfer energy throughout the system and this is the basis for the theory of WT [27]. This is the kinetic regime and the energy distribution between

modes is well described by the wave kinetic equation. WT theory is particularly well developed in the limit of infinite systems. However, it has become clear that the predictions of the classical theory of WT based on the continuous limit may not apply for oceanic Rossby waves bounded by the finite planet radius. The discreteness of the wavenumber space due to a finite size must be taken into account [28, 29]. Hence, a new regime was introduced - discrete WT. Here the wave vectors are discrete variables, i.e. $\mathbf{k} \in \mathbb{Z}^2$. As a result, the resonant conditions may be hard to satisfy and any $\mathbf{k}$ may be a member of only a few resonant triads (sometimes it could even be a single triad). If the energy of the system is initially concentrated in these triads, then an energy cascade cannot take place. An extreme version of such a situation is when there are no resonant triads at all, like in the case of the capillary surface waves [22], in which case turbulence is "frozen". In other words, mode interaction weakens or can even disappear completely, meaning no cascade can take place.

Resonant triads which are connected via common modes can be grouped together to form clusters of various sizes ranging from butterflies, where two triads are joined via one mode, to a multiple-triad cluster involving a complicated network of interconnected triads. These clusters have been studied in [1, 30, 31, 32, 33, 34].

These different regimes of weak WT are described in [12] and [29] by different relationships between the nonlinear frequency broadening Γ (approximately the inverse of the nonlinear timescale τ_{NL}) and the frequency spacing in the finite box:

$$\Delta_\omega = \left| \frac{\partial \omega_{\mathbf{k}}}{\partial \mathbf{k}} \right| \frac{2\pi}{L} \sim \frac{\omega_{\mathbf{k}}}{kL}, \tag{2.3}$$

where L is the length of the box. When wave amplitudes are very small (forcing is low), so that the nonlinear frequency broadening is much less than the frequency spacing,

$$\Gamma \ll \Delta_\omega,$$

WT is discrete with a finite number of modes where only waves that are in resonance (satisfying both (2.1) and (2.2)) can interact and exchange energy.

If the wave system's amplitudes are gradually increased (higher forcing but not too high so that the nonlinearity is still weak) the nonlinear frequency broadening

will eventually become large,

$$\Gamma \gg \Delta_\omega,$$

and WT becomes continuous. Alternatively, this condition may be realized by taking the infinite box limit while keeping the wave amplitudes constant. For example, if $L \to \infty$ then the frequency spacing Δ_ω decreases meaning the frequency spectrum becomes more dense and hence continuous.

For larger amplitudes originally isolated clusters may become connected via quasi-resonances, that is, resonances with small enough frequency detuning:

$$|\omega(\mathbf{k}_1) + \omega(\mathbf{k}_2) - \omega(\mathbf{k}_3)| \lesssim \Gamma. \tag{2.4}$$

This will allow energy to be transferred between waves which are not exactly resonant; however, this is less efficient than energy transfer between waves which are in exact resonance. It is also worth mentioning that the effects of frequency broadening also appear in the presence of dissipation for real systems.

On the other hand if,

$$\Gamma \sim \Delta_\omega,$$

then both types of WT - discrete and kinetic may coexist and the system may oscillate in time (or parts of the $\mathbf{k}$-space) between the two regimes giving rise to a new type of WT - mesoscopic [12, 29]. This so called sandpile behaviour and was first presented in [35]. Consider WT that is initially in the discrete regime with very weak intensity. If wave energy is permanently supplied at small $\mathbf{k}$ it will accumulate until the frequency broadening Γ_D becomes of order of the frequency spacing Δ_ω. An "avalanche" is then triggered and the turbulent cascade is released to higher $\mathbf{k}$. This is characterized by kinetic interactions, where $\Gamma = \Gamma_K \gg \Gamma_D$. At this point the mean wave amplitude will lower and the broadening Γ_K will become less than the frequency spacing Δ_ω. Thus, the system returns to the discrete WT regime, where energy accumulates and thus the cycle starts again.

The sandpile behaviour described here only occurs in forced systems. In this thesis we will be considering examples when forcing is absent or not important. It

is hypothetical and not known whether sandpile behaviour is realized or not in the CHM example since no one has considered it numerically yet; however, it would be interesting to consider in future work. From here onwards we will focus on the discrete and kinetic regimes.

2.4 Application of wave turbulence theory to the Charney-Hasegawa-Mima equation

Let us begin by putting the CHM equation (1.2) in Fourier or $\mathbf{k}$-space. For a 2D periodic box with period L in all directions, the Fourier transform of the stream function is:

$$\psi(\mathbf{x}, t) = \sum_{\mathbf{k}} \hat{\psi}(\mathbf{k}, t)e^{i\mathbf{k}\cdot\mathbf{x}}, \tag{2.5}$$

with Fourier coefficients:

$$\hat{\psi}(\mathbf{k}, t) = \frac{1}{L^2}\int_{Box} \psi(\mathbf{x}, t)e^{-i\mathbf{k}\cdot\mathbf{x}}d\mathbf{x}. \tag{2.6}$$

The CHM equation becomes:

$$\partial_t \hat{\psi}_{\mathbf{k}} = -i\omega_{\mathbf{k}}\hat{\psi}_{\mathbf{k}} + \sum_{\mathbf{k}_1,\mathbf{k}_2} T^{\mathbf{k}}_{\mathbf{k}_1,\mathbf{k}_2}\hat{\psi}_{\mathbf{k}_1}\hat{\psi}_{\mathbf{k}_2}\delta^{\mathbf{k}}_{\mathbf{k}_1,\mathbf{k}_2}, \tag{2.7}$$

where:

$$T^{\mathbf{k}}_{\mathbf{k}_1,\mathbf{k}_2} = -\frac{(\mathbf{k}_1 \times \mathbf{k}_2)_z(k_1^2 - k_2^2)}{k^2 + F}, \tag{2.8}$$

is the nonlinear interaction coefficient and $\delta^{\mathbf{k}}_{\mathbf{k}_1,\mathbf{k}_2} \equiv \delta(\mathbf{k} - \mathbf{k}_1 - \mathbf{k}_2)$ is the Kronecker symbol which is one if $\mathbf{k} - \mathbf{k}_1 - \mathbf{k}_2 = 0$ and zero otherwise. The densities of the energy and enstrophy in Fourier space become:

$$E_{\mathbf{k}} = (k^2 + F)|\hat{\psi}_{\mathbf{k}}|^2, \tag{2.9}$$

$$\Omega_{\mathbf{k}} = (k^2 + F)^2|\hat{\psi}_{\mathbf{k}}|^2. \tag{2.10}$$

Now let us introduce the waveaction variable:

$$a_{\mathbf{k}} = \frac{k^2 + F}{\sqrt{|\beta k_x|}} \hat{\psi}_{\mathbf{k}},$$ (2.11)

which is defined in order to relate the waveaction density:

$$n_{\mathbf{k}} = \left(\frac{L}{2\pi}\right)^2 |a_{\mathbf{k}}|^2,$$ (2.12)

to the energy density $E_{\mathbf{k}}$ by the relation $E_{\mathbf{k}} = |\omega_{\mathbf{k}}| n_{\mathbf{k}}$. Substituting (2.11) into equation (2.7) gives:

$$\dot{a}_{\mathbf{k}} = -i\omega_{\mathbf{k}} a_{\mathbf{k}} + \text{ sign}(k_x) \sum_{12} W_{12}^{\mathbf{k}} a_1 a_2 \delta_{12}^{\mathbf{k}},$$ (2.13)

where $\sum_{12} \equiv \sum_{\mathbf{k}_1,\mathbf{k}_2}$, $a_1 \equiv a_{\mathbf{k}_1}$, $a_2 \equiv a_{\mathbf{k}_2}$, $\dot{a}_{\mathbf{k}}$ denotes the derivative and the nonlinear interaction coefficient is now:

$$W_{12}^{\mathbf{k}} = \sqrt{\frac{\beta |k_{1x}||k_{2x}|}{|k_x|}} \frac{(\mathbf{k}_1 \times \mathbf{k}_2)_z (k_1^2 - k_2^2)}{(k_1^2 + F)(k_2^2 + F)}.$$ (2.14)

Such variables arise in the Hamiltonian formulation of the CHM equation which I will now introduce.

2.4.1 Hamiltonian formulation of the Charney-Hasegawa-Mima equation

In the limit of small amplitudes, the Hamiltonian $\mathcal{H}$ is a power series in the complex variables $a_{\mathbf{k}} = a(\mathbf{k}, t)$ and $a_{\mathbf{k}}^* = a^*(\mathbf{k}, t)$ where $*$ represents the complex conjugate,

$$i\dot{a}_{\mathbf{k}} = \frac{\delta \mathcal{H}}{\delta a_{\mathbf{k}}^*},$$ (2.15)

and:

$$\mathcal{H} = \mathcal{H}_2 + \mathcal{H}_3 + ...$$ (2.16)

The linear dispersion relation $\omega_{\mathbf{k}}$ contains all the information that is necessary for studying the propagation of non-interacting waves [36]. It is a coefficient in the first

term of the Hamiltonian which is quadratic with respect to the wave amplitudes:

$$\mathcal{H}_2 = \sum_{k_x \geq 0} \omega_{\mathbf{k}} |a_{\mathbf{k}}|^2. \tag{2.17}$$

$\mathcal{H}_3$ is the cubic term which describes the nonlinear wave interactions of a single wave decaying into two waves or the confluence of two waves into a single one:

$$\mathcal{H}_3 = \sum_{k_{1x}, k_{2x}, k_{3x} \geq 0} (V_{12}^3 a_1 a_2 a_3^* \delta_{12}^3 + c.c.). \tag{2.18}$$

Three-wave interactions dominate wave systems with small nonlinearity provided that $\mathcal{H}_3 \neq 0$, otherwise the leading nonlinear processes may be four-wave interactions or even higher. We are now considering only half of the $\mathbf{k}$-space, i.e. $k_x, k_{1x}, k_{2x} \geq 0$. This is because the CHM equation is for real variables $\psi(\mathbf{x}, t)$ and so $\mathbf{k}$ and $-\mathbf{k}$ represent the same modes via the property of the Fourier transform of real functions, $\hat{\psi}_{-\mathbf{k}} = \hat{\psi}_{\mathbf{k}}^*$. Rewriting equation (2.13) in Hamiltonian form gives the following three-wave equation:

$$i\dot{a}_{\mathbf{k}} = \omega_{\mathbf{k}} a_{\mathbf{k}} + \sum_{k_{1x}, k_{2x} \geq 0} (V_{12}^{\mathbf{k}} a_1 a_2 \delta_{12}^{\mathbf{k}} + 2 V_{\mathbf{k}2}^{1*} a_1 a_2^* \delta_{\mathbf{k}2}^1), \tag{2.19}$$

which now has the nonlinear interaction coefficient [12]:

$$V_{12}^{\mathbf{k}} = i\sqrt{\beta k_x k_{1x} k_{2x}} \left(\frac{k_{1y}}{k_1^2 + F} + \frac{k_{2y}}{k_2^2 + F} - \frac{k_y}{k^2 + F} \right). \tag{2.20}$$

$V_{12}^{\mathbf{k}}$ is only valid on the resonant manifold, i.e. when $\omega_{\mathbf{k}} = \omega_1 + \omega_2$ is satisfied. When this is true, (2.14) and (2.20) are equivalent. $V_{12}^{\mathbf{k}}$ has the following symmetries:

$$V_{12}^{\mathbf{k}} = V_{21}^{\mathbf{k}} = -V_{\mathbf{k}-1}^2 = -V_{-1-2}^{-\mathbf{k}}. \tag{2.21}$$

2.4.2   Interaction representation

We are considering waves that are weakly nonlinear and so for short time intervals their amplitudes are sufficiently small and time-independent and therefore can be approximated by independent linear waves. Over time however, the wave amplitudes

evolve and nonlinear interactions become apparent. But it is possible to average over the fast linear times due to the large difference between this nonlinear evolution and the linear wave period [12].

In order to separate the time scales, variables are introduced that do not change in the linear approximation, this is known as interaction representation. The interaction representation variable is defined as:

$$b_{\mathbf{k}} = \frac{a_{\mathbf{k}}}{\epsilon} e^{i\omega_{\mathbf{k}}t}, \tag{2.22}$$

where the parameter $\epsilon \ll 1$ is introduced to make the smallness of nonlinearity explicit. In terms of the interaction representation variable (2.22), the Hamiltonian (2.19) can be rewritten as:

$$i\dot{b}_{\mathbf{k}} = \epsilon \sum_{k_{1x}, k_{2x} \geq 0} (V_{12}^{\mathbf{k}} b_1 b_2 \delta_{12}^{\mathbf{k}} e^{i\omega_{12}^{\mathbf{k}}t} + 2V_{\mathbf{k}2}^{1*} b_1 b_2^* \delta_{\mathbf{k}2}^{1} e^{-i\omega_{\mathbf{k}2}^{1}t}), \tag{2.23}$$

where the triad detuning parameters $\omega_{12}^{\mathbf{k}} = \omega_{\mathbf{k}} - \omega_1 - \omega_2$ have been introduced to measure the deviation of each triad from resonance. The linear term $\omega_{\mathbf{k}} a_{\mathbf{k}}$ is not present as it is time independent and there is now explicit time-dependence in the nonlinear term. For very small amplitudes we can let $e^{i(\omega_{\mathbf{k}} - \omega_1 - \omega_2)t} = \delta(\omega_{12}^{\mathbf{k}})$ and $\tilde{V}_{12}^{\mathbf{k}} = \epsilon V_{12}^{\mathbf{k}} \delta_{12}^{\mathbf{k}} \delta(\omega_{12}^{\mathbf{k}})$, such that only resonant waves are left in equation (2.23) which becomes:

$$i\dot{b}_{\mathbf{k}} = \sum_{k_{1x}, k_{2x} \geq 0} (\tilde{V}_{12}^{\mathbf{k}} b_1 b_2 + 2\tilde{V}_{\mathbf{k}2}^{1*} b_1 b_2^*). \tag{2.24}$$

This equation governs the discrete WT regime. Sets of equations (2.24) can be divided into independent subsets, the so-called resonant clusters. Within each cluster the waves interact among themselves but not with the waves of the other clusters. The equations for the simplest possible cluster, shown in figure 2.1 consisting of one resonant triad only, are:

$$\dot{b}_1 = W^* b_2^* b_3, \tag{2.25}$$

$$\dot{b}_2 = W^* b_1^* b_3,$$

$$\dot{b}_3 = -W b_1 b_2,$$

where $W = 2i\epsilon V_{12}^3$.
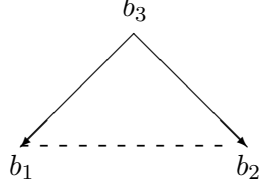
Figure 2.1: An isolated triad.

Now let us consider larger amplitudes that correspond to the kinetic regime. The governing kinetic equation can be derived from the Hamiltonian equation (2.23) using WT theory. The full derivation will not be given here as it is presented for the two-layer kinetic equation in chapter 6. For more information on deriving the one-layer kinetic equation see [12]. Below, the main steps are highlighted.

- After separating the linear τ_L and nonlinear τ_{NL} time scales, introduce an intermediate time T such that $\tau_L \ll T \ll \tau_{NL}$ and seek a solution for the wave amplitude $b_{\mathbf{k}}$ at time $t = T$ using an expansion in the small nonlinearity parameter ϵ :

$$b_{\mathbf{k}}(T) = b_{\mathbf{k}}^{(0)}(t) + \epsilon b_{\mathbf{k}}^{(1)}(t) + \epsilon^2 b_{\mathbf{k}}^{(2)}(t) + ... \qquad (2.26)$$

- The idea is then to substitute the weak nonlinearity expansion into $|b_{\mathbf{k}}(T)|^2$, and average over the random phases and amplitudes, $\langle |b_{\mathbf{k}}(T)|^2 \rangle$.

- Now take the large box limit $L \to \infty$, whereby Fourier sums are replaced by integrals:

$$\sum_{12} \to \int d\mathbf{k}_1 d\mathbf{k}_2 \left(\frac{L}{2\pi} \right)^4 . \qquad (2.27)$$

- Finally introduce the waveaction spectrum:

$$n_{\mathbf{k}} = \left(\frac{L}{2\pi} \right)^2 \langle |b_{\mathbf{k}}(T)|^2 \rangle, \qquad (2.28)$$

and take the weak nonlinearity limit $\epsilon \to 0$.

- As a result the kinetic equation is obtained, which describes the rate of change of the waveaction spectrum as a result of the spectral redistribution of energy by nonlinear interactions between waves:

$$\dot{n}_{\mathbf{k}} = \int_{k_{1x}, k_{2x} > 0} (\Re_{12\mathbf{k}} - \Re_{\mathbf{k}12} - \Re_{2\mathbf{k}1}) d\mathbf{k}_1 d\mathbf{k}_2, \qquad (2.29)$$

where:

$$\Re_{12\mathbf{k}} = 2\pi |V_{12}^{\mathbf{k}}|^2 (n_1 n_2 - n_{\mathbf{k}} n_1 - n_{\mathbf{k}} n_2) \delta_{12}^{\mathbf{k}} \delta(\omega_{12}^{\mathbf{k}}). \qquad (2.30)$$

Chapter 3

Quadratic invariants

3.1 Kinetic wave turbulence

The energy and enstrophy densities are defined in equations (2.9) and (2.10) in terms of the Fourier coefficients $\hat{\psi}_{\mathbf{k}}$, so now let us define them in terms of the waveaction spectrum $n_{\mathbf{k}}$. The energy and enstrophy become:

$$E = \int_{k_x>0} |\omega_{\mathbf{k}}| n_{\mathbf{k}} d\mathbf{k},$$

$$\Omega = \int_{k_x>0} k_x n_{\mathbf{k}} d\mathbf{k}. \tag{3.1}$$

where $\omega_{\mathbf{k}}$ is now the density of the energy and k_x the density of the enstrophy. Generally, one can write for a conserved quantity Φ with density $\varphi_{\mathbf{k}}$ as:

$$\Phi = \int_{k_x>0} \varphi_{\mathbf{k}} n_{\mathbf{k}} d\mathbf{k}. \tag{3.2}$$

This can easily be shown using equations (2.29) and (2.30):

$$
\begin{aligned}
\dot{\Phi} &= \int_{k_x>0} \varphi_{\mathbf{k}} \dot{n}_{\mathbf{k}} d\mathbf{k} \\
&= \int\int\int_{k_x,k_{1x},k_{2x}>0} (\varphi_{\mathbf{k}}\Re_{12\mathbf{k}} - \varphi_{\mathbf{k}}\Re_{\mathbf{k}12} - \varphi_{\mathbf{k}}\Re_{2\mathbf{k}1}) d\mathbf{k}_{12} d\mathbf{k} \\
&= \int\int\int_{k_x,k_{1x},k_{2x}>0} \Re_{12\mathbf{k}}(\varphi_{\mathbf{k}} - \varphi_1 - \varphi_2) d\mathbf{k}_{12} d\mathbf{k},
\end{aligned} \tag{3.3}
$$

where the integration variables are changed from $\mathbf{k}_1, \mathbf{k}_2, \mathbf{k} \to \mathbf{k}, \mathbf{k}_1, \mathbf{k}_2$ and $\mathbf{k}_1, \mathbf{k}_2, \mathbf{k} \to \mathbf{k}_2, \mathbf{k}, \mathbf{k}_1$ in the second and third terms in the integrand respectively. This proves the following theorem [37, 38]:

Theorem 3.1.1 *If the spectral density of quantity (3.2) satisfies:*

$$\varphi_{\mathbf{k}} - \varphi_1 - \varphi_2 = 0, \tag{3.4}$$

on the resonant manifold then, Φ is conserved, i.e.

$$\Phi = \int \varphi_{\mathbf{k}} n_{\mathbf{k}} d\mathbf{k} = const. \tag{3.5}$$

For the energy and enstrophy, the resonant condition (3.4) is obviously satisfied: $\mathbf{k} - \mathbf{k}_1 - \mathbf{k}_2 = 0$ and $\omega_{\mathbf{k}} - \omega_1 - \omega_2 = 0$, due to the respective δ-functions in the kinetic equation (2.29) which proves conservation of these quantities.

For a generic wave system no other invariant besides the energy and enstrophy has been found. However, it was discovered in [39] for kinetic WT that one extra conserved quantity exists for the system of Rossby waves. This quantity is conserved under the same conditions as the kinetic equation, namely weak nonlinearity and random phases, and it cannot be conserved in interactions of higher order so may be called the invariant of three-wave systems. It was first discovered in 1990 in the case of (i) large-scale turbulence ($\rho^2 k^2 \ll 1$) and (ii) anisotropic turbulence ($|k_y| \gg |k_x|$) after which it was generalised to all of $\mathbf{k}$-space in [40] where:

$$Z = \int_{k_x > 0} \eta_{\mathbf{k}} n_{\mathbf{k}} d\mathbf{k}, \tag{3.6}$$

with density:

$$\eta_{\mathbf{k}} = \arctan \frac{k_y + k_x \sqrt{3}}{\rho k^2} - \arctan \frac{k_y - k_x \sqrt{3}}{\rho k^2}, \tag{3.7}$$

and $\rho = \frac{1}{\sqrt{F}}$ is the Rossby radius of deformation. This extra invariant is unique to Rossby/drift waves and is known as zonostrophy, because as will be seen later, it causes energy to cascade to the zonal scales.

3.1.1 Cascades

In three-dimensional (3D) hydrodynamic turbulence it has long been known that the energy cascades from small to large wavenumbers [41, 42, 43]. In two dimensions, the introduction of a second invariant, the enstrophy, causes a dual cascade to form whereby the energy is transferred from large to small wavenumbers while the enstrophy is transferred from small to large wavenumbers [44, 45]. However, for Rossby waves with an extra invariant, it was found in [39] that the zonostrophy together with the energy and the enstrophy, are involved in the triple cascade process. Each of the invariants is forced by the other two to cascade into its own anisotropic sector of **k**-space and, in particular, the energy is forced to cascade to large zonal scales. Fjørtoft's argument [45] for the direction of the energy and enstrophy cascades in 2D turbulence was generalized in [46] to find the non-intersecting cascade directions of the three invariants in the case of small-scale turbulence. The non-intersecting sectors are shown in figure 3.1.
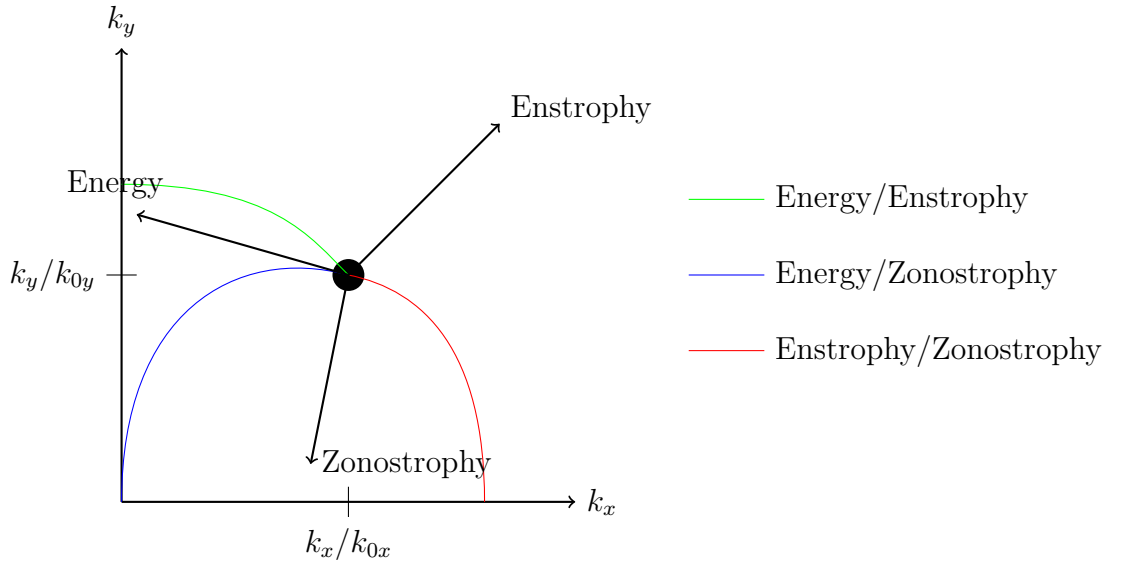
Figure 3.1: Non-intersecting sectors for the triple cascade as predicted by the generalized Fjørtoft argument.

In chapter 5, the cascade directions for the large-scale limit will be considered, where another invariant has recently been discovered.

3.2 Discrete wave turbulence

For the discrete regime it has been shown in [1], that the search of all quadratic invariants of system (2.24) is equivalent to a basic linear algebra problem, namely the search for the null space of a certain constant and sparse matrix, called the "cluster matrix".

3.2.1 The cluster matrix - $\mathbb{A}$

Consider a number of triads that are joined together forming a resonant cluster. Let the cluster consist of M triads and N modes $b_n(t)$ where index $n = 1, \ldots, N$ enumerates the modes in the cluster. Each mode n in the cluster has wavenumber $\mathbf{k}_n$. The three-wave resonance conditions for the m-th triad, defined by (2.1) and (2.2), can be put into the following matrix form:

$$\sum_{n=1}^{N} A_{mn} \mathbf{k}_n = \mathbf{0}, \qquad m \text{ fixed}, \ m = 1, \ldots, M, \tag{3.8}$$

where for each fixed m the set $\{A_{mn}\}_{n=1}^{N}$ contains exactly two elements with value 1, one element with value -1 and the remaining elements are equal to zero. In other words, the m-th row of the $M \times N$ matrix $\mathbb{A} = [A_{mn}]$ corresponds to the three-wave conditions for the m-th triad, i.e.

$$A_{mn_1} \mathbf{k}_{n_1} + A_{mn_2} \mathbf{k}_{n_2} + A_{mn_3} \mathbf{k}_{n_3} = 0,$$

where out of A_{mn_1}, A_{mn_2} and A_{mn_3}, two have value 1 and the third has value -1. From here on the matrix $\mathbb{A}$ will be referred to as the cluster matrix.

Definition 3.2.1 *The null space of the cluster matrix $\mathbb{A}$ is the linear vector space generated from a basis of linearly independent vectors $\boldsymbol{\varphi}^{(j)} \equiv (\varphi_1^{(j)}, \varphi_2^{(j)}, \ldots, \varphi_N^{(j)})^T$ for which:*

$$\mathbb{A} \boldsymbol{\varphi}^{(j)} = \mathbf{0}, \tag{3.9}$$

where $j = 1, \ldots, J$ and J is the dimension of the null space of $\mathbb{A}$.

3.2.2 Constructing quadratic invariants

The following theorem allows all of the independent quadratic invariants to be found.

Theorem 3.2.2 *Consider a resonant cluster of N interacting modes belonging to M triads. Let $\varphi_n \equiv \varphi_{\mathbf{k}_n}$ be a real function of the wavenumbers of the modes in the cluster, such that the vector $\boldsymbol{\varphi} \equiv (\varphi_1, \varphi_2, \ldots, \varphi_N)^T$ is in the null space of the cluster matrix: $\mathbb{A}\boldsymbol{\varphi} = \mathbf{0}$, or, in components: $\sum_{n=1}^{N} A_{mn}\varphi_n = 0$ for all triads in the cluster, i.e. for all $m = 1, \ldots, M$. Then,*

$$I = \sum_{n=1}^{N} \varphi_n \, |b_n(t)|^2 = const., \tag{3.10}$$

i.e. I is a quadratic invariant.

Conversely, let $I = \sum_{n=1}^{N} \varphi_n \, |b_n(t)|^2$ be a quadratic invariant of system (2.24), i.e. $\dot{I} = 0$ for all values of the complex amplitudes $b_n(t)$ such that (2.24) hold. Then the variables φ_n satisfy $\sum_{n=1}^{N} A_{mn}\varphi_n = 0$, for all $m = 1, \ldots, M$.

Proof. To show I is indeed an invariant, take the time derivative of (3.10):

$$\frac{dI}{dt} = \sum_{n=1}^{N} \varphi_n(\dot{b}_n b_n^* + b_n \dot{b}_n^*). \tag{3.11}$$

Substitute for $\dot{b}_n$ using equation (2.24) to get:

$$
\begin{aligned}
\dot{I} &= \sum_{n=1}^{N} \varphi_n b_n^* \sum_{12} (-i)(\tilde{V}_{12}^n b_1 b_2 + 2\tilde{V}_{n2}^{1*} b_2^* b_1) + c.c. \\
&= -i \sum_{123} (\varphi_3 b_3^* b_1 b_2 \tilde{V}_{12}^3 - \varphi_1 b_1^* b_2^* b_3 \tilde{V}_{12}^{3*} - \varphi_2 b_2^* b_1^* b_3 \tilde{V}_{12}^{3*} \\
&\quad + \varphi_3 b_3 b_1^* b_2^* \tilde{V}_{12}^{3*} - \varphi_1 b_1 b_2 b_3^* \tilde{V}_{12}^3 - \varphi_2 b_2 b_1 b_3^* \tilde{V}_{12}^3) \\
&= -i \sum_{123} (\varphi_3 - \varphi_1 - \varphi_2)(b_3^* b_1 b_2 \tilde{V}_{12}^3 + c.c.).
\end{aligned}
$$

It is clear that $\dot{I} = 0$ because $\varphi_3 - \varphi_1 - \varphi_2 = 0$ is guaranteed by equation (3.8) for every term in the sum.

The converse statement follows directly from the last equation for $\dot{I}$ indeed because each individual term in the sum depends on amplitude b which can be arbitrarily chosen. In general there can't be cancellation between these terms and the

result in general would be nonzero unless $\varphi_3 - \varphi_1 - \varphi_2 = 0$ in each term separately.

$\square$

3.2.3 Quick counting the number of independent quadratic invariants

The dimension J of the null space of the cluster matrix $\mathbb{A}$ was shown in theorem 3.2.2 to be equal to the total number of independent quadratic invariants of the cluster system (2.24). Direct application of linear algebra gives:

$$J \equiv N - M^* \geq N - M, \tag{3.12}$$

where M^* is the number of linearly independent rows in $\mathbb{A}$. In practice, this means that a quick counting is possible of the number of independent invariants, J, of a given cluster. Just take the number of modes involved minus the number of triads involved, and this gives a lower bound for J.

3.2.4 Connectivity of triads in a cluster and number of independent quadratic invariants

There are three general results in terms of connectivity:

(i) In order for the triads to be connected into a cluster, the following obvious condition must be satisfied:

$$2M + 1 \geq N.$$

For example, consider the triple-chain in figure 3.2. If $2M + 1 < N$, then N must be greater than 7. The only way to achieve this without adding a fourth triad to the cluster is to disconnect a triad from the chain.
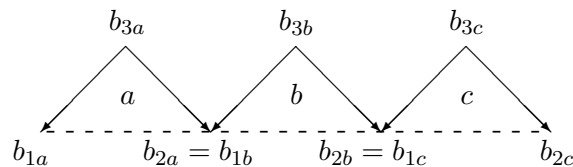
Figure 3.2: A triple chain.

(ii) If a cluster is formed exclusively by one-common-mode connections between triads, then one has $N = 2M + 1$. Using (3.12), $J \geq M + 1$. Most of the resonant clusters known in the literature are of this form. Therefore it is expected that the number of quadratic invariants increases with the number of triads.

(iii) If a cluster is formed exclusively by two-common-mode connections between triads, then one has $N = M + 2$. Using (3.12), $J \geq 2$. Most of the quasi-resonant clusters known in the literature are of this form. In these cases a small number of invariants are expected, but two of them always survive, up to the kinetic regime.

Three-common-mode connections between triads make no sense physically, so this ends the analysis in terms of connectivity properties of a cluster. In a general cluster, N will be between $M + 2$ and $2M + 1$, so J will vary accordingly.

3.2.5 Excluded cluster matrices

In real-life applications and numerical simulations, large clusters with many triads and modes are encountered. Therefore, it makes sense to try to understand the basic structures appearing within a cluster in terms of properties of the cluster matrix $\mathbb{A}$. Presented below are three physical requirements of the cluster matrices and their null spaces, so that the clusters represent physically sensible sets of interacting modes.

By writing out the resonant conditions for each triad from (3.8), one must admit only the matrices A_{mn} for which the solution set of wavenumbers $\mathbf{k}_n$, $n = 1, \ldots, N$, is physically sensible.

1. The first physical requirement is that in the solution of (3.8), no two wave vectors are equal, (i.e. $\mathbf{k}_n \neq \mathbf{k}_{n'}$ if $n \neq n'$).

   For example, any two rows $A_m, A_{m'}$ with $m \neq m'$, must not have the same values in more than one column. The reason being that two rows having equal values in two columns would imply that the corresponding columns of the third wave vector should be equal, so the two rows would represent exactly the same triad. Therefore the following matrices are not physically sensible:

$$\begin{bmatrix} \mathbf{1} & \mathbf{1} & -1 & 0 \\ \mathbf{1} & \mathbf{1} & 0 & -1 \end{bmatrix} \qquad\qquad \begin{bmatrix} \mathbf{1} & 1 & -\mathbf{1} & 0 \\ \mathbf{1} & 0 & -\mathbf{1} & 1 \end{bmatrix}$$

$$\mathbf{k}_1 + \mathbf{k}_2 - \mathbf{k}_3 = 0, \qquad\qquad \mathbf{k}_1 + \mathbf{k}_2 - \mathbf{k}_3 = 0,$$

$$\mathbf{k}_1 + \mathbf{k}_2 - \mathbf{k}_4 = 0, \qquad\qquad \mathbf{k}_1 - \mathbf{k}_3 + \mathbf{k}_4 = 0,$$

$$\implies \mathbf{k}_3 = \mathbf{k}_4. \qquad\qquad\qquad \implies \mathbf{k}_2 = \mathbf{k}_4.$$

The triads corresponding to these kind of cluster matrices are known as kites, with the first example pictured in figure 3.3.
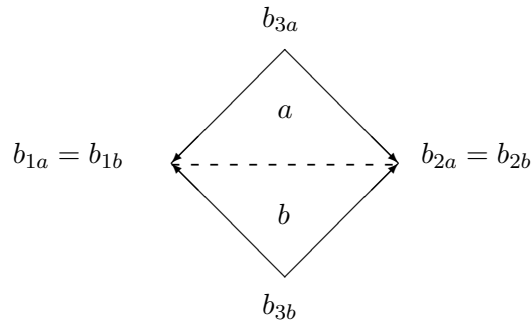
Figure 3.3: A kite.

2. Second, if the underlying PDE is for a real function, so that there is an iden- tification between the wave vectors $\mathbf{k}$ and $-\mathbf{k}$, such as in the case of the CHM equation, then an extra requirement is that in the solution of (3.8), no two wave vectors add up to zero, (i.e. $\mathbf{k}_n \neq -\mathbf{k}_{n'}$ if $n \neq n'$).

For example, any two rows $A_m, A_{m'}$ with $m \neq m'$, must not have values of opposite sign in two columns. If this was to happen the corresponding $\mathbf{k}$ of the third non-zero column of row A_m should be equal to minus the $\mathbf{k}$ of the third non-zero column of row $A_{m'}$. If the wave field is real in the physical space, as is the case for Rossby waves, the $\mathbf{k}$ and $-\mathbf{k}$ represent the same mode via $b_{-\mathbf{k}} = b_{\mathbf{k}}^*$ and therefore the two triads are identical. Consequently, the following matrix is not physically sensible:

$$\begin{bmatrix} \mathbf{1} & 1 & -\mathbf{1} & 0 \\ -\mathbf{1} & 0 & 1 & 1 \end{bmatrix} \qquad \begin{aligned} \mathbf{k}_1 + \mathbf{k}_2 - \mathbf{k}_3 &= 0, \\ \mathbf{k}_3 + \mathbf{k}_4 - \mathbf{k}_1 &= 0, \end{aligned}$$

$$\implies \mathbf{k}_2 = -\mathbf{k}_4.$$

3. Third, in cases when the zero-mode must be excluded, one must require that in the solution of (3.8), no wave vector is the zero vector, (i.e. $\mathbf{k}_n \neq \mathbf{0}$ for all n).

In the case of triad interactions, the violation of the third requirement will imply the violation of either the first or the second requirement for some modes. To see this, notice that, for example, if $\mathbf{k}_1 + \mathbf{k}_2 - \mathbf{k}_3 = 0$ and $\mathbf{k}_3 = \mathbf{0}$, then $\mathbf{k}_1 = -\mathbf{k}_2$.

An example of this third case is an excluded type of cluster which has the shape of a tetrahedron (see figure 4.4). This has the following cluster matrix:

$$\begin{bmatrix} 1 & -1 & 0 & 1 \\ -1 & 0 & 1 & 1 \\ 0 & 1 & -1 & 1 \end{bmatrix} \qquad \begin{aligned} \mathbf{k}_1 - \mathbf{k}_2 + \mathbf{k}_4 &= 0, \\ -\mathbf{k}_1 + \mathbf{k}_3 + \mathbf{k}_4 &= 0, \\ \mathbf{k}_2 - \mathbf{k}_3 + \mathbf{k}_4 &= 0, \end{aligned}$$

$$\implies \mathbf{k}_4 = \mathbf{0},$$

$$\implies \mathbf{k}_1 = \mathbf{k}_2 = \mathbf{k}_3.$$

This cluster is discussed in more detail in chapter 4.

3.3 Examples of low-dimensional clusters

3.3.1 An isolated triad

The cluster matrix corresponding to the resonant conditions for an isolated triad is:

$$\mathbb{A} = \begin{bmatrix} 1 & 1 & -1 \end{bmatrix}.$$

Its null space, the set of vectors $\boldsymbol{\varphi}^{(j)}$ for which $\mathbb{A}\boldsymbol{\varphi}^{(j)} = \mathbf{0}$ is:

$$\Phi = \begin{bmatrix} 1 & 1 \\ 0 & -1 \\ 1 & 0 \end{bmatrix}.$$

A triad has $J = N - M = 2$ independent quadratic invariants. Each column of Φ gives a quadratic invariant of the dynamical system:

$$I_1 = |b_1|^2 + |b_3|^2, \tag{3.13}$$

$$I_2 = |b_1|^2 - |b_2|^2.$$

These are known as Manley-Rowe invariants. They can also be derived using theorem 3.2.2 where I takes the form:

$$I = \varphi_1|b_1|^2 + \varphi_2|b_2|^2 + \varphi_3|b_3|^2. \tag{3.14}$$

Here, the resonant condition $\varphi_1 + \varphi_2 - \varphi_3 = 0$ is clearly satisfied when $\varphi_1 = \varphi_3 = 1$, $\varphi_2 = 0$ and $\varphi_1 = 1$, $\varphi_2 = -1$, $\varphi_3 = 0$ respectively.

Physically, this means that the energy ($\omega_{\mathbf{k}}$), the two components of momentum (k_x, k_y) and the zonostrophy ($\eta_{\mathbf{k}}$) will not be independent of one another. Only two may be linearly independent, e.g. k_x and $\omega_{\mathbf{k}}$ or k_y and $\eta_{\mathbf{k}}$ etc.

3.3.2 Double-triad clusters - butterflies

Two triads can be connected via one mode to form a butterfly. One example is shown in figure 3.4.

Its cluster matrix is:

$$\begin{array}{ccccc} b1a & b2a & b3a & b2b & b3b \end{array}$$
$$\mathbb{A} = \begin{bmatrix} 1 & 1 & -1 & 0 & 0 \\ 1 & 0 & 0 & 1 & -1 \end{bmatrix},$$
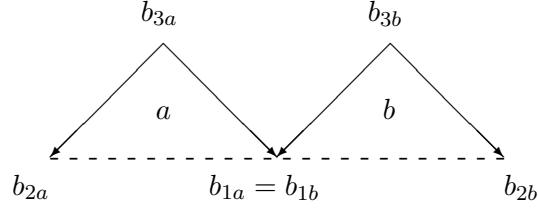
Figure 3.4: A butterfly.

and it's null space is:

$$\Phi = \begin{bmatrix} 0 & -1 & 1 \\ 1 & 1 & -1 \\ 1 & 0 & 0 \\ 0 & 1 & 0 \\ 0 & 0 & 1 \end{bmatrix} \begin{matrix} b1a \\ b2a \\ b3a \\ b2b \\ b3b \end{matrix} \quad .$$

This system has $N - M = 3$ independent quadratic invariants of the form:

$$I_1 = |b_{2a}|^2 + |b_{3a}|^2, \qquad (3.15)$$

$$I_2 = |b_{2a}|^2 + |b_{2b}|^2 - |b_{1a}|^2,$$

$$I_3 = |b_{1a}|^2 - |b_{2a}|^2 + |b_{3b}|^2.$$

As a result zonostrophy does not appear as an extra invariant to the energy, and momentum components. However, any three of the four invariants will be linearly independent. The situation becomes more interesting for larger, three-triad clusters, which have four invariants. The zonostrophy in these cases does appear as an extra invariant as all four of $k_x, k_y, \omega_{\mathbf{k}}$ and $\eta_{\mathbf{k}}$ are linearly independent of one another. For even bigger clusters there may be many more invariants than these four.

3.4   Application to the Charney-Hasegawa-Mima model

Resonant clusters have been found in [1] and [34] for the CHM equation in two limits, the small-scale limit and the large-scale limit.

3.4.1   Small-scale Rossby waves ($\rho k \to \infty$)

Let the frequency be that of small-scale Rossby waves, $\rho k \to \infty$. The dispersion relation can be obtained by putting $F = 1/\rho^2 = 0$ in (1.9) which gives:

$$\omega_{\mathbf{k}} = -\frac{\beta k_x}{k_x^2 + k_y^2}. \tag{3.16}$$

In the small-scale limit, the general expression for the zonostrophy density (3.7) becomes:

$$\eta_{\mathbf{k}} = \frac{k_x^3}{k^{10}}(k_x^2 + 5k_y^2). \tag{3.17}$$

Considering the region $1 \le k_x \le 100$ and $-100 \le k_y \le 100$ a total of thirty-four clusters (seventeen clusters plus their mirror images) were found numerically by searching for sets of wave vectors that satisfy the resonant conditions in the box. This consists of twenty-four isolated triads, four butterflies, two triple-chains, two seven-triad clusters and two thirteen-triad clusters, as shown in figure 3.5.
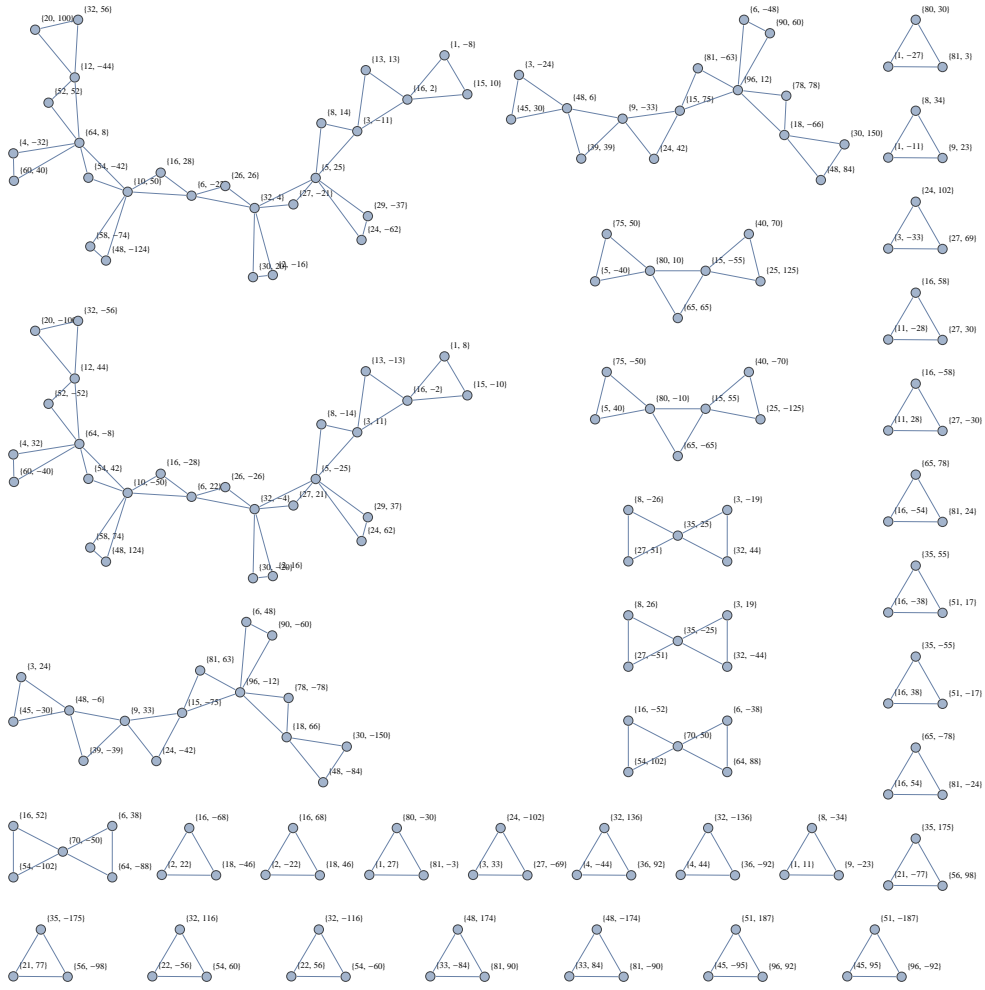
Figure 3.5: Small-scale Rossby waves in the region $1 \leq k_x \leq 100$, $-100 \leq k_y \leq 100$.

Consider the biggest cluster found in the small-scale limit, shown in the top left corner of figure 3.5, which is made up of thirteen triads, twenty-seven modes and has fourteen linearly independent invariants. Its cluster matrix and null space are as follows:

$$\mathbb{A} = \begin{bmatrix}
1 & 1 & -1 & 0 & 0 & 0 & 0 & 0 & 0 & 0 & 0 & 0 & 0 & 0 & 0 & 0 & 0 & 0 & 0 & 0 & 0 & 0 & 0 & 0 & 0 & 0 \\
0 & 0 & -1 & 1 & 1 & 0 & 0 & 0 & 0 & 0 & 0 & 0 & 0 & 0 & 0 & 0 & 0 & 0 & 0 & 0 & 0 & 0 & 0 & 0 & 0 & 0 \\
0 & 0 & 0 & 0 & 1 & -1 & 1 & 0 & 0 & 0 & 0 & 0 & 0 & 0 & 0 & 0 & 0 & 0 & 0 & 0 & 0 & 0 & 0 & 0 & 0 & 0 \\
0 & 0 & 0 & 0 & 0 & 0 & 1 & -1 & 1 & 0 & 0 & 0 & 0 & 0 & 0 & 0 & 0 & 0 & 0 & 0 & 0 & 0 & 0 & 0 & 0 & 0 \\
0 & 0 & 0 & 0 & 0 & 0 & 1 & 0 & 0 & -1 & 1 & 0 & 0 & 0 & 0 & 0 & 0 & 0 & 0 & 0 & 0 & 0 & 0 & 0 & 0 & 0 \\
0 & 0 & 0 & 0 & 0 & 0 & 0 & 0 & 0 & -1 & 0 & 1 & 1 & 0 & 0 & 0 & 0 & 0 & 0 & 0 & 0 & 0 & 0 & 0 & 0 & 0 \\
0 & 0 & 0 & 0 & 0 & 0 & 0 & 0 & 0 & -1 & 0 & 0 & 0 & 1 & 1 & 0 & 0 & 0 & 0 & 0 & 0 & 0 & 0 & 0 & 0 & 0 \\
0 & 0 & 0 & 0 & 0 & 0 & 0 & 0 & 0 & 0 & 0 & 0 & 0 & 1 & 0 & -1 & 1 & 0 & 0 & 0 & 0 & 0 & 0 & 0 & 0 & 0 \\
0 & 0 & 0 & 0 & 0 & 0 & 0 & 0 & 0 & 0 & 0 & 0 & 0 & 0 & 0 & 0 & 1 & -1 & 1 & 0 & 0 & 0 & 0 & 0 & 0 & 0 \\
0 & 0 & 0 & 0 & 0 & 0 & 0 & 0 & 0 & 0 & 0 & 0 & 0 & 0 & 0 & 0 & 1 & 0 & 0 & -1 & 1 & 0 & 0 & 0 & 0 & 0 \\
0 & 0 & 0 & 0 & 0 & 0 & 0 & 0 & 0 & 0 & 0 & 0 & 0 & 0 & 0 & 0 & 0 & 0 & 0 & -1 & 0 & 1 & 1 & 0 & 0 & 0 \\
0 & 0 & 0 & 0 & 0 & 0 & 0 & 0 & 0 & 0 & 0 & 0 & 0 & 0 & 0 & 0 & 0 & 0 & 0 & -1 & 0 & 0 & 0 & 1 & 1 & 0 \\
0 & 0 & 0 & 0 & 0 & 0 & 0 & 0 & 0 & 0 & 0 & 0 & 0 & 0 & 0 & 0 & 0 & 0 & 0 & 0 & 0 & 0 & 0 & 1 & -1 & 1
\end{bmatrix},$$

$$\Phi = \begin{bmatrix}
-\mathbf{1} & 1 & 0 & 0 & 0 & 0 & 0 & 0 & 0 & 0 & 0 & 0 & 0 & 0 \\
\mathbf{1} & 0 & 0 & 0 & 0 & 0 & 0 & 0 & 0 & 0 & 0 & 0 & 0 & 0 \\
0 & 1 & 0 & 0 & 0 & 0 & 0 & 0 & 0 & 0 & 0 & 0 & 0 & 0 \\
0 & 1 & -1 & 0 & 0 & 0 & 0 & 0 & 0 & 0 & 0 & 0 & 0 & 0 \\
0 & 0 & 1 & 0 & 0 & 0 & 0 & 0 & 0 & 0 & 0 & 0 & 0 & 0 \\
0 & 0 & 1 & 0 & 1 & 0 & 0 & 0 & 0 & 0 & 0 & 0 & 0 & 0 \\
0 & 0 & 0 & 0 & 1 & 0 & 0 & 0 & 0 & 0 & 0 & 0 & 0 & 0 \\
0 & 0 & 0 & \mathbf{1} & 1 & 0 & 0 & 0 & 0 & 0 & 0 & 0 & 0 & 0 \\
0 & 0 & 0 & \mathbf{1} & 0 & 0 & 0 & 0 & 0 & 0 & 0 & 0 & 0 & 0 \\
0 & 0 & 0 & 0 & 0 & 0 & 1 & 0 & 0 & 0 & 0 & 0 & 0 & 0 \\
0 & 0 & 0 & 0 & -1 & 0 & 1 & 0 & 0 & 0 & 0 & 0 & 0 & 0 \\
0 & 0 & 0 & 0 & 0 & -\mathbf{1} & 1 & 0 & 0 & 0 & 0 & 0 & 0 & 0 \\
0 & 0 & 0 & 0 & 0 & \mathbf{1} & 0 & 0 & 0 & 0 & 0 & 0 & 0 & 0 \\
0 & 0 & 0 & 0 & 0 & 0 & 0 & 1 & 0 & 0 & 0 & 0 & 0 & 0 \\
0 & 0 & 0 & 0 & 0 & 0 & 1 & -1 & 0 & 0 & 0 & 0 & 0 & 0 \\
0 & 0 & 0 & 0 & 0 & 0 & 0 & 1 & 0 & 1 & 0 & 0 & 0 & 0 \\
0 & 0 & 0 & 0 & 0 & 0 & 0 & 0 & 0 & 1 & 0 & 0 & 0 & 0 \\
0 & 0 & 0 & 0 & 0 & 0 & 0 & 0 & \mathbf{1} & 1 & 0 & 0 & 0 & 0 \\
0 & 0 & 0 & 0 & 0 & 0 & 0 & 0 & \mathbf{1} & 0 & 0 & 0 & 0 & 0 \\
0 & 0 & 0 & 0 & 0 & 0 & 0 & 0 & 0 & 0 & 0 & 1 & 0 & 0 \\
0 & 0 & 0 & 0 & 0 & 0 & 0 & 0 & 0 & -1 & 0 & 1 & 0 & 0 \\
0 & 0 & 0 & 0 & 0 & 0 & 0 & 0 & 0 & 0 & -\mathbf{1} & 1 & 0 & 0 \\
0 & 0 & 0 & 0 & 0 & 0 & 0 & 0 & 0 & 0 & \mathbf{1} & 0 & 0 & 0 \\
0 & 0 & 0 & 0 & 0 & 0 & 0 & 0 & 0 & 0 & 0 & 1 & -1 & 0 \\
0 & 0 & 0 & 0 & 0 & 0 & 0 & 0 & 0 & 0 & 0 & 0 & 1 & 0 \\
0 & 0 & 0 & 0 & 0 & 0 & 0 & 0 & 0 & 0 & 0 & 0 & 1 & \mathbf{1} \\
0 & 0 & 0 & 0 & 0 & 0 & 0 & 0 & 0 & 0 & 0 & 0 & 0 & \mathbf{1}
\end{bmatrix}.$$

It can be seen from the null space that it has six Manley-Rowe invariants in columns 1,4,6,9,11 and 14.

3.4.2 Large-scale Rossby waves $(\rho k \to 0)$

Now consider large-scale Rossby waves, $\rho^2 k^2 \ll 1$, with the frequency obtained from the general dispersion relation:

$$\omega_{\mathbf{k}} = -\frac{\beta \rho^2 k_x}{1 + \rho^2 k^2}, \tag{3.18}$$

by Taylor expansion in small $\rho^2 k^2$:

$$\omega_{\mathbf{k}} = -\beta k_x \rho^2 (1 - \rho^2 k^2). \tag{3.19}$$

Since the first part in this expression is equal to k_x, for the purpose of finding the resonances a simpler expression can be used:

$$\omega_k = k_x k^2. \tag{3.20}$$

In the region $1 \leq k_x \leq 20$ and $-20 \leq k_y \leq 20$ a total of four clusters were found. This consists of two isolated triads, one ten-triad cluster and one 104-triad cluster, as shown in figure 3.6.
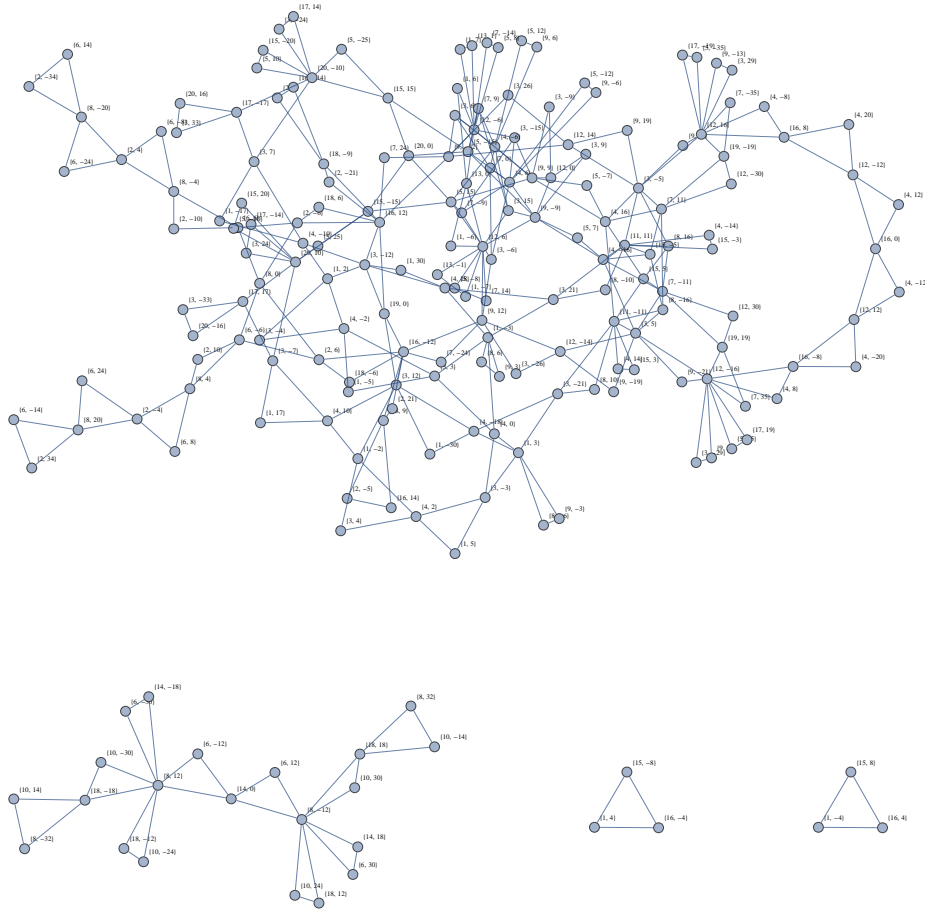
Figure 3.6: Large-scale Rossby waves in the region $1 \leq k_x \leq 20$, $-20 \leq k_y \leq 20$.

It can be seen that in a much smaller domain of the large-scale limit there is

already a much larger cluster than in the small-scale limit. This tells us that the resonance conditions are much easier to satisfy in the large-scale limit than in the small-scale limit.

In the next section we will study both the thirteen-triad cluster from the small-scale limit and the 104-triad cluster from the large-scale limit in more detail and see how, in symbolic cluster space, the invariants are related to specific parts of the cluster.

3.5 Comparison of quadratic invariants in kinetic and discrete wave turbulence

In this chapter we have considered the conservation of quadratic invariants in both kinetic and discrete WT. It turns out that the condition for conservation is very similar in both regimes - the $\mathbf{k}$-space density of the quadratic invariant must satisfy the same resonance conditions as does the wave vectors (2.1) and frequencies (2.2).

The kinetic regime has well known quadratic invariants, the energy with density $\varphi_{\mathbf{k}} = \omega_{\mathbf{k}}$ and the momenta with density $\varphi_{\mathbf{k}}$ equal to each of the d components of the wave vector $\mathbf{k}$. These invariants along with a more recently discovered additional invariant for Rossby waves, zonostrophy, take part in a triple cascade. However, in the discrete regime many more invariants may be conserved. The total number of independent quadratic invariants of the cluster is equal to $J \equiv N - M^* \geq N - M$ where M^* is the number of linearly independent rows in the cluster matrix $\mathbb{A}$. The resonance conditions are much harder to satisfy in a discrete system and therefore there are fewer triads than in the kinetic case. Hence $N - M$ increases and there are many more invariants in discrete WT than kinetic WT.

It is not yet known how the presence of numerous additional quadratic invariant affects the turbulent cascades in $\mathbf{k}$-space. It would therefore be interesting to simulate numerically WT in large discrete clusters, such as the one in figure 3.6, to see how their behaviour is different from their counterparts in kinetic WT. Equally, quasi-resonant clusters contain more triads than resonant clusters. Thus, as the detuning in a cluster increases, $N - M$ decreases, and generally there will be fewer

invariants. Therefore, it would also be interesting to study the dynamical consequences of such a loss of the quadratic invariants when triads with higher frequency detuning start to become available due to an increase in the nonlinearity of the WT.

Chapter 4

Relating the quadratic invariants to the topological properties of the cluster

As we have seen, finding the cluster matrix of a system of interacting triads is a straightforward matter, regardless of the size of the cluster. Moreover, finding its null space takes seconds using basic linear-algebra commands from computer programs such as Matlab. What is less trivial is that the number of these invariants is deeply related to the structure of the cluster in symbolic space. In [1] an algorithm was found for decomposing large clusters into smaller ones to show how various quadratic invariants are related to certain parts of a cluster. The full details of the algorithm are presented below.

Part 1

- Consider a cluster, like in figure 4.1, with an unconnected mode, call it mode 1 for simplicity. Being unconnected, means that mode 1 will not be joined to any other triad in the cluster other than the one it belongs to, call it triad 1.

- Consider the cluster matrix $\mathbb{A}$. Since mode 1 is unconnected, the rest of column 1 in the cluster matrix will contain zeros. Here n and m denote the positions of the non-zero entries in row 1 (other than the first position).
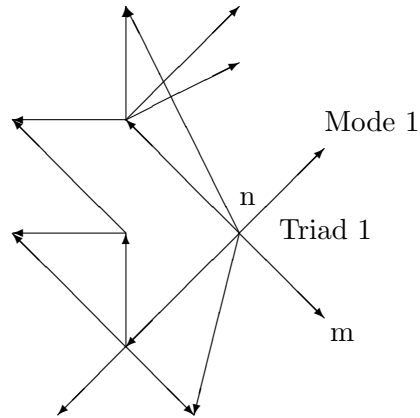
Figure 4.1: A cluster before reduction.

- Delete column/mode 1 and row/triad 1 to leave a new reduced matrix $\mathbb{A}'$ with $M' = M - 1$ rows and $N' = N - 1$ columns:

$$
\mathbb{A} = \begin{matrix} 1 & & & n & & m & \\ \end{matrix}
\begin{bmatrix}
1 & 0 & 0 & -1 & 0 & 1 & \cdots \\
0 & . & . & . & . & . & . \\
0 & . & & & & & \\
0 & . & & & \mathbb{A}' & & \\
0 & . & & & & & \\
0 & . & & & & & \\
\end{bmatrix}.
$$

- Consider a vector from the null space of $\mathbb{A}$ (a column of matrix Φ):

$$
\begin{matrix}
1 \qquad\quad n \qquad\quad m \\
\begin{bmatrix}
1 & 0 & 0 & -1 & 0 & 1 & \cdots \\
0 & . & . & . & . & . & . \\
0 & . & & & & & \\
0 & . & & \mathbb{A}' & & & \\
0 & . & & & & & \\
0 & . & & & & &
\end{bmatrix}
\end{matrix}
\begin{bmatrix}
\varphi_1 \\
\varphi_2 \\
. \\
\varphi_n \\
. \\
\varphi_m \\
. \\
. \\
. \\
. \\
\varphi_N
\end{bmatrix}
= \mathbf{0}.
$$

- Solve $\mathbb{A}' \begin{bmatrix} \varphi_2 \\ \vdots \\ \varphi_N \end{bmatrix} = \mathbf{0}$, to find the null space of $\mathbb{A}'$.

- Then solving for φ_1 gives:

$$
\varphi_1 - \varphi_n + \varphi_m = 0 \longrightarrow
\begin{bmatrix}
\varphi_1 \\
\varphi_2 \\
. \\
. \\
. \\
\varphi_N
\end{bmatrix}
=
\begin{bmatrix}
\varphi_n - \varphi_m \\
\varphi_2 \\
\vdots \\
\varphi_N
\end{bmatrix}.
\tag{4.1}
$$

Thus finding the null space of $\mathbb{A}$ is reduced to finding the null space of a smaller matrix $\mathbb{A}'$. By eliminating one row which is linearly independent from the rest of the rows in $\mathbb{A}$, and eliminating the respective column, the null space dimension has not been changed. Therefore, the number of independent invariants is the same for $\mathbb{A}$ and the smaller matrix $\mathbb{A}'$.

- Two situations may arise:

1. Triad 1 has one unconnected mode. $\mathbb{A}'$ is a cluster matrix of a cluster obtained from $\mathbb{A}$ by eliminating triad/row 1 and column/mode 1 only. It is clear that such reduced clusters will have the same number of invariants as the original bigger cluster.

2. Triad 1 has two unconnected modes, e.g. 1 and m in the example below:

$$
\mathbb{A} = \begin{array}{ccc} 1 & n & m \\ \end{array}
\begin{bmatrix}
1 & 0 & 0 & -1 & 0 & 1 & \cdots \\
0 & . & . & . & . & 0 & . \\
0 & . & & & & 0 & \\
0 & . & & \mathbb{A}' & & 0 & \\
0 & . & & & & 0 & \\
0 & . & & & & 0 &
\end{bmatrix}.
$$

In this case there is a column of zeros in matrix $\mathbb{A}'$ (column m). Thus, one can now choose φ_m arbitrarily as follows:

$$
\begin{bmatrix}
\varphi_1 = \varphi_n - \varphi_m \\
\varphi_2 \\
\vdots \\
\varphi_m \\
\vdots \\
\varphi_N
\end{bmatrix}
=
\begin{bmatrix}
\varphi_n \\
\varphi_2 \\
\vdots \\
0 \\
\vdots \\
\varphi_N
\end{bmatrix}
+ c
\begin{bmatrix}
-1 \\
0 \\
\vdots \\
1 \\
\vdots \\
0
\end{bmatrix}.
\tag{4.2}
$$

The second contribution here, $[-1, 0, ..., 1, ..., 0]^T$, gives one of the linearly independent invariants of $\mathbb{A}$, and all the other columns in the null space of $\mathbb{A}$ must have zero entries in the position number m. Note that this invariant is an attribute solely of the triad with two unconnected ends which are being eliminated and in fact it has a simple Manley-Rowe form, $I = |b_m|^2 - |b_1|^2$. Equally if modes 1 and n are unconnected then we have the Manley-Rowe $I = |b_1|^2 + |b_n|^2$.

- Hence a triad with two unconnected ends will contribute a Manley-Rowe invariant which depends only on the two free modes and so it is "local". Note that being local in symbolic cluster space does not imply being local in wavenumber Fourier space. However, being non-local in symbolic cluster space implies being non-local in wavenumber Fourier space.

- Note that removing triads with unconnected modes may possibly disjoin the remaining cluster into independent clusters, which must then be treated separately.

- Repeat until only fully connected cluster(s) are left, i.e. one in which all modes are connected to more than one triad.

- If matrix $\mathbb{A}'$ cannot be reduced any further via this method move to part 2. Note however, that some clusters can be fully decomposed by repeating part 1 only and part 2 will not be necessary.

Part 2

Suppose in the remaining cluster there are two triads (triad 1 and 2 in figure 4.2 below) that are joined together by two modes and that these modes are not connected to any other triad.
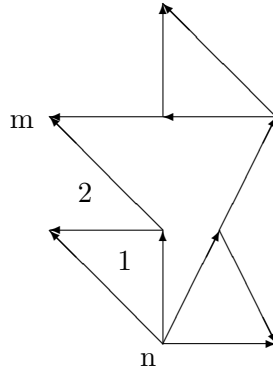
Figure 4.2: A cluster after all unconnected ends have been removed by part 1.

- Rearrange the rows/columns of $\mathbb{A}'$ to form a 2×2 matrix in the top left hand corner, (i.e. renumber the modes in the triad in an appropriate way). The only

2×2 matrix possible is $\begin{bmatrix} 1 & 1 \\ 1 & -1 \end{bmatrix}$ or any permutation of it because it must satisfy the exclusion principles in section 3.2.5, meaning the following matrices are not allowed: $\begin{bmatrix} 1 & 1 \\ 1 & 1 \end{bmatrix}$, $\begin{bmatrix} 1 & -1 \\ 1 & -1 \end{bmatrix}$, $\begin{bmatrix} 1 & -1 \\ -1 & 1 \end{bmatrix}$.

- Delete the pair of modes in column/row 1 and 2 to get matrix $\mathbb{A}''$ as follows:

$$
\mathbb{A}' =
\begin{array}{cc}
 n m \\
\begin{bmatrix}
1 & 1 & 0 & -1 & 0 & 0 & \cdots \\
1 & -1 & 0 & 0 & 1 & 0 & \cdots \\
0 & 0 & . & . & . & . & . \\
0 & 0 & . & & & & \\
0 & 0 & . & & \mathbb{A}'' & & \\
0 & 0 & . & & & &
\end{bmatrix}
\end{array}.
$$

- This 2×2 matrix is always non-degenerate, i.e. it has a non-zero determinant.

- Removing a pair of connected triads may disjoin the remaining cluster into two independent clusters, in which case each must be treated separately. Or the remaining part may stay as a single cluster.

- Solve $\mathbb{A}'' \begin{bmatrix} \varphi_3 \\ \vdots \\ \varphi_N \end{bmatrix} = \mathbf{0}$, to find the null space of $\mathbb{A}''$.

- Then solving for φ_1 and φ_2 gives:

$$\varphi_1 + \varphi_2 - \varphi_n = 0 \text{ and } \varphi_1 - \varphi_2 + \varphi_m = 0$$

$$\longrightarrow \begin{bmatrix} \varphi_1 \\ \varphi_2 \\ \varphi_3 \\ . \\ . \\ . \\ \varphi_N \end{bmatrix} = \begin{bmatrix} 1/2(\varphi_n - \varphi_m) \\ 1/2(\varphi_n + \varphi_m) \\ \varphi_3 \\ \vdots \\ \varphi_N \end{bmatrix}. \tag{4.3}$$

Therefore, the null space of $\mathbb{A}$ is uniquely constructed from the null space of $\mathbb{A}''$ and has the same dimension. In other words, by eliminating two triads as described above, it leads to a smaller cluster (or two disjoint clusters) whose total number of independent invariants is equal to the number of independent invariants in the original cluster.

It is not possible to have any zero columns in $\mathbb{A}''$ since these should have been eliminated in part 1. The necessity to remove zero columns may arise only at the level of eliminating single triads and not at the level of triad pairs.

- Look at $\mathbb{A}''$ (single or two disjoint clusters) and again search for unconnected single modes (part 1) and triad pairs (part 2) of the type $\begin{bmatrix} 1 & 1 \\ 1 & -1 \end{bmatrix}$. Repeat the procedure until part 1 and part 2 cannot be applied any more.

Part 3

After a number of successive applications of part 1 and part 2 one inevitably arrives at reduced cluster(s) for which the steps of neither part 1 nor part 2 can be carried out. Such reduced cluster(s) are usually significantly smaller than the original one but will still have the same number of invariants. Moreover the invariants for the big cluster can be easily reconstructed from the respective invariants of such a reduced cluster by expressing the entries of the eliminated modes in the null space

41

as shown in (4.1), (4.2) and (4.3). Because of the fact that this smaller cluster will completely determine the conservation properties of the original large cluster it is called the "cluster kernel" of the original cluster. Note that not all clusters will have kernels as they can be taken apart completely by the steps of part 1 and part 2.

- Consider a cluster kernel (irreducible by parts 1 and 2). Following the logic of part 1 and part 2 now consider 3×3 blocks in the top left hand corner (arising after appropriate renumbering of the rows/triads and columns/modes) such that the rest of the entries below the 3×3 block contains zeros only, e.g.

$$
\mathbb{A}'' = \begin{bmatrix}
1 & 1 & -1 & 0 & 0 & 0 & \cdots \\
1 & -1 & 0 & 0 & 1 & 0 & \cdots \\
1 & 0 & 1 & 0 & -1 & 0 & \cdots \\
0 & 0 & 0 & . & . & . & . \\
0 & 0 & 0 & . & & \mathbb{A}''' & \\
0 & 0 & 0 & . & & &
\end{bmatrix}.
$$

Call these 3×3 blocks $\mathbb{A}^{3\times3}$. Of course $\mathbb{A}^{3\times3}$ must again satisfy the exclusion principles discussed above. Either $\mathbb{A}^{3\times3}$ is:

1. non-degenerate with a non-zero determinant, in which case the system of equations for $\varphi_1, \varphi_2, \varphi_3$ has a unique solution and consequently the complete system has the same number of invariants as $\mathbb{A}'''$.

2. or degenerate with a zero determinant, in which case, one or two independent solutions are to be obtained by putting $\varphi_4 = ... = \varphi_N = 0$. Further solutions are to be sought for $(\varphi_4, ..., \varphi_N)$ given by solutions of $\mathbb{A}'''(\varphi_4, ..., \varphi_N)^T = \mathbf{0}$. For each of these solutions, the resulting system of equations for $\varphi_1, \varphi_2, \varphi_3$ has either:

   (a) a unique solution,

   (b) infinite solutions or

   (c) no solutions at all.

   This can be determined by the following Rouché-Capelli theorem [47].

Theorem 4.0.1 *A system of linear equations with n variables has a solution if and only if the rank of its coefficient matrix $\mathbb{A}^{3\times3}$ is equal to the rank of its augmented matrix $[\mathbb{A}^{3\times3}|\mathbf{b}]$. If the number of unknowns $n = rank(\mathbb{A}^{3\times3})$, the solution is unique, otherwise there are an infinite number of solutions.*

Situation 2 is new with respect to 1×1 and 2×2 matrix eliminations above, since only starting at the 3×3 matrix level can we get degenerate matrices.

In case (2b) the system $\mathbb{A}''$ has more invariants than $\mathbb{A}'''$. Note that the value of $N - M$ is the same for matrix $\mathbb{A}'''$ as for the original matrix $\mathbb{A}$ because the size of $\mathbb{A}'''$ is less than the size of $\mathbb{A}$ by an equal amount of rows and columns. This means that in case (2b) the number of linearly independent rows in the original matrix $\mathbb{A}$, M^* is less than the total number of rows M, i.e. the number of independent invariants of the full system is: $J = N - M^* > N - M$. An example of (2b) can be found figure 4.3.
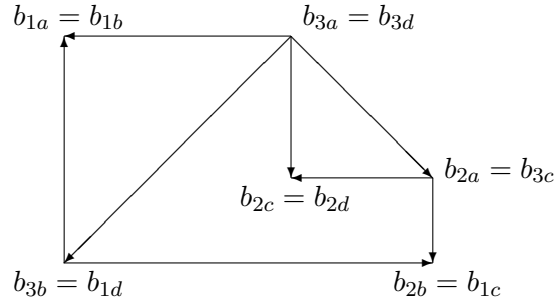
Figure 4.3: A cluster demonstrating case (2b) where $M^* < M$.

It has the cluster matrix:

$$\mathbb{A}'' = \begin{bmatrix} 1 & 1 & -1 & 0 & 0 & 0 \\ 1 & 0 & 0 & 1 & -1 & 0 \\ 0 & -1 & 0 & 1 & 0 & 1 \\ 0 & 0 & -1 & 0 & 1 & 1 \end{bmatrix}.$$

43

This cluster is fully connected and cannot be reduced by part 1 or part 2. Rearrange $\mathbb{A}''$ to form a 3×3 matrix, $\mathbb{A}^{3\times3}$, in the top left corner:

$$
\mathbb{A}'' = \left[\begin{array}{ccc|ccc}
1 & 1 & 0 & -1 & 0 & 0 \\
1 & 0 & 1 & 0 & -1 & 0 \\
0 & -1 & 1 & 0 & 0 & 1 \\
\hline
0 & 0 & 0 & -1 & 1 & 1
\end{array} \right].
$$

Since the determinant of $\mathbb{A}^{3\times3}$ is zero, the Rouché-Capelli theorem can be used. The rank of $\mathbb{A}^{3\times3}$ is two. From $\mathbb{A}'''$ (the lower-right part in $\mathbb{A}''$) it can be seen that $\varphi_4 = \varphi_5 + \varphi_6$. So there are two independent solutions, either $\varphi_4 = \varphi_5 = 1, \varphi_6 = 0$ or $\varphi_4 = \varphi_6 = 1, \varphi_5 = 0$. To find $\mathbf{b}$ corresponding to these solutions, multiply the rectangular matrix in the top-right of $\mathbb{A}''$ by $(\varphi_4, \varphi_5, \varphi_6)^T$. So either:

$$
\mathbf{b}_1 = \left[\begin{array}{ccc}
-1 & 0 & 0 \\
0 & -1 & 0 \\
0 & 0 & 1
\end{array} \right] \left[\begin{array}{c}
1 \\ 1 \\ 0
\end{array} \right] = \left[\begin{array}{c}
-1 \\ -1 \\ 0
\end{array} \right],
$$

or

$$
\mathbf{b}_2 = \left[\begin{array}{ccc}
-1 & 0 & 0 \\
0 & -1 & 0 \\
0 & 0 & 1
\end{array} \right] \left[\begin{array}{c}
1 \\ 0 \\ 1
\end{array} \right] = \left[\begin{array}{c}
-1 \\ 0 \\ 1
\end{array} \right].
$$

Using these in the augmented matrix $[\mathbb{A}^{3\times3}|\mathbf{b}]$ it can be seen that the rank is again two. Since both have the same rank there exists at least one solution by theorem 4.0.1. And since their rank is less than the number of unknowns, the latter being three, there are an infinite number of solutions. Hence, the number of linearly independent rows of $M^* = 3$ is less than the number of rows $M = 4$ and hence $\mathbb{A}$ has an extra invariant.

This explains why the null space for $\mathbb{A}$,

$$\Phi = \begin{bmatrix} -1 & 1 & 0 \\ 1 & 0 & 1 \\ 1 & 0 & 0 \\ 0 & 1 & 1 \\ 0 & 1 & 0 \\ 0 & 0 & 1 \end{bmatrix},$$

doesn't satisfy the rule $J = N - M = 2$ but instead $J = N - M^* = 3$, i.e. $J = N - M^* \geq N - M$.

In case (2c), solutions may be "lost", i.e. extra solutions gained by solving for $\varphi_1, \varphi_2, \varphi_3$ with $\varphi_4 = ... = \varphi_N = 0$ may be compensated by an equal or larger loss because some solutions $(\varphi_4, ..., \varphi_N)$ of $\mathbb{A}'''(\varphi_4, ..., \varphi_N)^T = \mathbf{0}$ do not correspond to any solution of the full system $\mathbb{A}$. Therefore in case (2c) the number of independent solutions of the original cluster $\mathbb{A}$ may be the same or less than $\mathbb{A}'''$. To see this take the following "tetrahedron cluster":
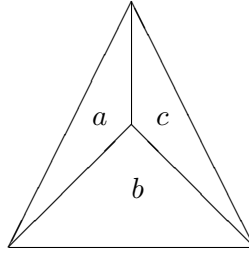
Figure 4.4: A tetrahedron cluster.

This cluster is unphysical (since the resulting null space is such that $\mathbf{k}_4 = \mathbf{0}$, thus violating the third physical requirement in subsection 3.2.5) but for illustrating case (2c) it is a simple example to consider. The cluster matrix which has been rearranged to form a 3×3 matrix, $\mathbb{A}^{3 \times 3}$, on the

left-hand-side (LHS) and a column $\mathbf{b}$ on the right is:

$$
\mathbb{A}'' = \left[\begin{array}{ccc|c} 1 & -1 & 0 & 1 \\ -1 & 0 & 1 & 1 \\ 0 & 1 & -1 & 1 \end{array} \right].
$$

The determinant of $\mathbb{A}^{3\times3}$ is zero. Now in order to solve the system of equations:

$$
\begin{bmatrix} 1 & -1 & 0 & 1 \\ -1 & 0 & 1 & 1 \\ 0 & 1 & -1 & 1 \end{bmatrix} \begin{bmatrix} \varphi_1 \\ \varphi_2 \\ \varphi_3 \\ \varphi_4 \end{bmatrix} = \mathbf{0},
$$

form an augmented matrix $\left[\mathbb{A}^{3\times3} | \mathbf{b} \right]$ with $\mathbf{b} = (\varphi_4, \varphi_4, \varphi_4)$, i.e.

$$
\mathbb{A}^{3\times3} \begin{bmatrix} \varphi_1 \\ \varphi_2 \\ \varphi_3 \end{bmatrix} + \varphi_4 \mathbf{b} = \mathbf{0}.
$$

Since there is no $\mathbb{A}'''$ in this case, φ_4 can be chosen arbitrarily, e.g. $\varphi_4 = 1$. The rank of the coefficient matrix $\mathbb{A}^{3\times3}$ is two and the rank of the augmented matrix $[\mathbb{A}^{3\times3} | \mathbf{b}]$ is three. Hence, by the Rouché-Capelli theorem no solutions exist.

Now let $\varphi_4 = 0$ and solve $\mathbb{A}^{3\times3}(\varphi_1, \varphi_2, \varphi_3)^T = \mathbf{0}$. Since the rank of $A^{3\times3}$ is two, there exists one independent solution, $(\varphi_1, \varphi_2, \varphi_3) = (1, 1, 1)$. Consequently, the tetrahedron cluster has $N - M = 1$ invariant and its null space is:

$$
\Phi = \begin{bmatrix} 1 \\ 1 \\ 1 \\ 0 \end{bmatrix}.
$$

Therefore, for the tetrahedron cluster the number of invariants corresponds to the "$N - M$" rule (which holds for non-degenerate cases) even

46

though its $\mathbb{A}^{3\times 3}$ matrix is degenerate.

4.1 Applying the algorithm to the two Charney-Hasegawa-Mima examples

Let us apply the algorithm to the two CHM examples from section 3.4.

All the clusters given in the example for the small-scale Rossby waves (figure 3.5) can be fully decomposed by part 1 of the algorithm. In particular the largest (thirteen-triad cluster) has a total of fourteen invariants. From these, six are local, each depending only on a pair of loose ends. These are indicated via bold print in the cluster matrix in section 3.4. From the null space, it is clear that triads with two loose ends have Manley-Rowe invariants. These triads are eliminated in the first application of part 1 after which a seven-triad chain remains which will be further reduced by successive elimination of triads with double unconnected ends. Of the remaining eight invariants, four depend on three modes each and another four on four modes each. All of the invariants in this example are relatively local within the cluster. Their existence is probably imposing severe restrictions on moving energy in and out of these triads and propagating them throughout the cluster. It is expected that invariants involving three or four modes are a bit more efficient than the invariants involving two modes, in stirring the energy through the $\mathbf{k}$-space.

Applying this algorithm to the largest 104-triad cluster in the large-scale limit (figure 3.6) leads to two cluster kernels after applying three times the procedure part 1. The two reduced cluster kernels are made up of eight triads each and twelve modes as shown in figures 4.5 and 4.6. Note that each of these clusters are mirror symmetric, i.e. each cluster maps onto itself when transformation $\mathbf{k}_y \rightarrow -\mathbf{k}_y$ is applied. The fact that both clusters are the same size is interesting but probably coincidental. When applying the algorithm further to each of these clusters, we conclude that for each of these "kernel" clusters the null space basis contains one extra vector, and so the 104-triad cluster will contain two extra invariants in total.
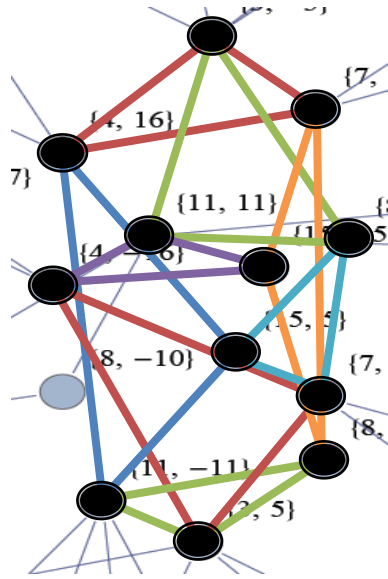
Figure 4.5: The first cluster kernel taken from figure 3.6 such that each triad is connected to other triads and neither part 1 or part 2 can be applied.
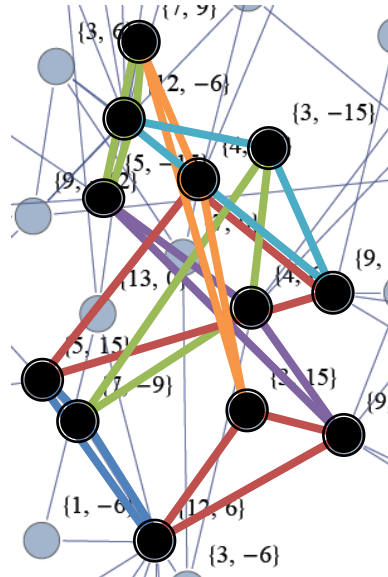
Figure 4.6: The second cluster kernel taken from figure 3.6.

Both of these kernels appear to be so tightly linked that no further reduction is possible by removing triad pairs, triple- or even four-triad blocks. This brings us straight to considering 5×5 blocks.

Figure 4.5: $\mathbb{A}''$ has been rearranged to form a 5×5 matrix in the top left hand corner:

$$
\left[
\begin{array}{ccccc|ccccccc}
1 & 1 & -1 & 0 & 0 & 0 & 0 & 0 & 0 & 0 & 0 & 0 \\
1 & 0 & 0 & 0 & -1 & 0 & 0 & 0 & 1 & 0 & 0 & 0 \\
0 & 1 & 0 & 0 & 0 & 1 & -1 & 0 & 0 & 0 & 0 & 0 \\
0 & 0 & 0 & -1 & 1 & 0 & 0 & 1 & 0 & 0 & 0 & 0 \\
0 & 0 & 1 & -1 & 0 & 0 & 0 & 0 & 0 & 1 & 0 & 0 \\
\hline
0 & 0 & 0 & 0 & 0 & 0 & -1 & 0 & 1 & 0 & 1 & 0 \\
0 & 0 & 0 & 0 & 0 & 0 & 0 & 1 & 0 & 0 & -1 & 1 \\
0 & 0 & 0 & 0 & 0 & -1 & 0 & 0 & 0 & 1 & 0 & 1 \\
\end{array}
\right].
$$

The determinant of $\mathbb{A}^{5 \times 5}$ is zero and the rank is four. Now find the vector $\mathbf{b}$ from $\mathbb{A}'''$:

$$-\varphi_7 + \varphi_9 + \varphi_{11} = 0, \tag{4.4}$$

$$\varphi_8 - \varphi_{11} + \varphi_{12} = 0,$$

$$-\varphi_6 + \varphi_{10} + \varphi_{12} = 0.$$

One independent solution is $\varphi_7 = \varphi_8 = \varphi_9 = \varphi_{10} = 1$, $\varphi_{12} = -1$ and $\varphi_6 = \varphi_{11} = 0$. So:

$$
\mathbf{b} =
\begin{bmatrix}
0 & 0 & 0 & 0 & 0 & 0 & 0 \\
0 & 0 & 0 & 1 & 0 & 0 & 0 \\
1 & -1 & 0 & 0 & 0 & 0 & 0 \\
0 & 0 & 1 & 0 & 0 & 0 & 0 \\
0 & 0 & 0 & 0 & 1 & 0 & 0 \\
\end{bmatrix}
\begin{bmatrix}
0 \\ 1 \\ 1 \\ 1 \\ 1 \\ 0 \\ -1
\end{bmatrix}
=
\begin{bmatrix}
0 \\ 1 \\ -1 \\ 1 \\ 1
\end{bmatrix}.
$$

The rank of $[\mathbb{A}^{5 \times 5}|\mathbf{b}]$ is four. So by the Rouché-Capelli theorem the cluster kernel in figure 4.5 has an infinite number of solutions and since the rank of the coefficient

matrix is one less than its size, one extra invariant. The null space for figure 4.5 is:

$$
\Phi =
\begin{bmatrix}
-1 & 1 & 0 & 0 & 1 \\
1 & 0 & -1 & 0 & -1 \\
0 & 1 & -1 & 0 & 0 \\
1 & 0 & 0 & -1 & 0 \\
0 & 1 & 0 & -1 & 1 \\
0 & 0 & 1 & 0 & 1 \\
1 & 0 & 0 & 0 & 0 \\
0 & 0 & 0 & 1 & -1 \\
0 & 1 & 0 & 0 & 0 \\
0 & 0 & 1 & 0 & 0 \\
0 & 0 & 0 & 1 & 0 \\
0 & 0 & 0 & 0 & 1
\end{bmatrix}.
$$

Figure 4.6: Once again $\mathbb{A}''$ has been rearranged to form a 5×5 matrix in the top left hand corner:

$$
\left[
\begin{array}{ccccc|ccccccc}
1 & 1 & -1 & 0 & 0 & 0 & 0 & 0 & 0 & 0 & 0 & 0 \\
-1 & 0 & 0 & 1 & 0 & 1 & 0 & 0 & 0 & 0 & 0 & 0 \\
0 & 0 & -1 & 0 & 1 & 0 & 1 & 0 & 0 & 0 & 0 & 0 \\
0 & 1 & 0 & 0 & 0 & 0 & 0 & 1 & -1 & 0 & 0 & 0 \\
0 & 0 & 0 & 1 & -1 & 0 & 0 & 0 & 0 & 1 & 0 & 0 \\
\hline
0 & 0 & 0 & 0 & 0 & 0 & 0 & 0 & 0 & 1 & 1 & -1 \\
0 & 0 & 0 & 0 & 0 & 0 & 1 & 1 & 0 & 0 & -1 & 0 \\
0 & 0 & 0 & 0 & 0 & 1 & 0 & 0 & 1 & 0 & 0 & -1
\end{array}
\right].
$$

The determinant of $\mathbb{A}^{5 \times 5}$ is zero and the rank is four. Now find the vector $\mathbf{b}$ from

$\mathbb{A}'''$:

$$\varphi_{10} + \varphi_{11} - \varphi_{12} = 0, \tag{4.5}$$

$$\varphi_7 + \varphi_8 - \varphi_{11} = 0,$$

$$\varphi_6 + \varphi_9 - \varphi_{12} = 0.$$

One independent solution is $\varphi_6 = \varphi_7 = \varphi_{10} = \varphi_{12} = 1$, $\varphi_8 = -1$ and $\varphi_9 = \varphi_{11} = 0$.
So:

$$\mathbf{b} = \begin{bmatrix} 0 & 0 & 0 & 0 & 0 & 0 & 0 \\ 1 & 0 & 0 & 0 & 0 & 0 & 0 \\ 0 & 1 & 0 & 0 & 0 & 0 & 0 \\ 0 & 0 & 1 & -1 & 0 & 0 & 0 \\ 0 & 0 & 0 & 0 & 1 & 0 & 0 \end{bmatrix} \begin{bmatrix} 1 \\ 1 \\ -1 \\ 0 \\ 1 \\ 0 \\ 1 \end{bmatrix} = \begin{bmatrix} 0 \\ 1 \\ 1 \\ -1 \\ 1 \end{bmatrix}.$$

The rank of $[\mathbb{A}^{5\times5}|\mathbf{b}]$ is four. So by the Rouché-Capelli theorem the cluster kernel in figure 4.6 has an infinite number of solutions and since the rank of the coefficient matrix is one less than its size, one extra invariant. The null space for figure 4.6 is:

$$\Phi = \begin{bmatrix} 1 & 0 & -1 & 1 & 0 \\ 0 & -1 & 1 & 0 & 0 \\ 1 & -1 & 0 & 1 & 0 \\ 1 & 0 & 0 & 1 & -1 \\ 0 & 0 & -1 & 0 & 1 \\ 1 & 0 & 0 & 0 & 0 \\ 0 & -1 & 0 & 1 & 0 \\ 0 & 1 & 0 & 0 & 0 \\ 0 & 0 & 1 & 0 & 0 \\ 0 & 0 & 0 & -1 & 1 \\ 0 & 0 & 0 & 1 & 0 \\ 0 & 0 & 0 & 0 & 1 \end{bmatrix}.$$

Thus, both kernels have an additional invariant each. Therefore, the original 104-triad cluster has two extra invariants, $J = N - M + 2 = 178 - 104 + 2 = 76$.

Chapter 5

An additional invariant in the large-scale limit

Much of the research into WT has concentrated on the small-scale limit of the CHM equation. This limit is applicable to the atmosphere, where the Rossby radius of deformation is of the order of thousands of kilometres. However, the Rossby radius of deformation in a middle-latitude ocean is tens of kilometres and since Rossby waves can be hundreds of kilometres in length, the large-scale limit is more appropriate. The large-scale limit is also more relevant to plasma physics since the gyroradius is very small, of the order of just a few millimetres, whereas the tokamak diameter is much larger being tens of metres. So now let us turn our attention to the large-scale limit.

Since all large-scale waves travel at the same speed in the x-direction, it is convenient to work in a coordinate frame moving with them. Therefore, let us Doppler shift the frequency using the x-component of the phase speed $c_{\mathbf{k}}$ as follows:

$$
\begin{aligned}
\Omega_{\mathbf{k}} &= \omega_{\mathbf{k}} - c_{\mathbf{k}} k_x \\
&= \omega_{\mathbf{k}} + \beta \rho^2 k_x \\
&= -\beta k_x \rho^2 + \beta \rho^4 k_x k^2 + \beta \rho^2 k_x \\
&= \beta \rho^4 k_x k^2.
\end{aligned}
\tag{5.1}
$$

Therefore, assuming for simplicity that $\beta \rho^4 = 1$, we can replace the dispersion

relation (??) with a simpler expression:

$$\omega_{\mathbf{k}} = k_x k^2 + O(\rho^2).\tag{5.2}$$

The waveaction variable for the large-scale limit is:

$$a_{\mathbf{k}} = \frac{\hat{\psi}_{\mathbf{k}}}{\sqrt{|k_x|}},\tag{5.3}$$

which when substituted into the CHM equation in Fourier space (2.7) gives us equation (2.13) but now with the interaction coefficient:

$$W_{12}^{\mathbf{k}} = \left|\frac{k_{1x}k_{2x}}{k_x}\right|^{1/2}(\mathbf{k}_1 \times \mathbf{k}_2)_z(k_1^2 - k_2^2).\tag{5.4}$$

This can be rearranged as follows:

$$\left|\frac{k_{1x}k_{2x}}{k_x}\right|^{1/2}(k_{1x}k_{2y} - k_{1y}k_{2x})(k_1^2 - k_2^2)\tag{5.5}$$

$$= \left|\frac{k_{1x}k_{2x}}{k_x}\right|^{1/2}((k_{1x} + k_{2x})k_{2y} - (k_{1y} + k_{2y})k_{2x})(k_1^2 - k_2^2)$$

$$= -2|k_{1x}k_{2x}k_x|^{1/2}\left(k_{2y} - \frac{k_y k_{2x}}{k_x}\right)k_2^2$$

$$= -|k_{1x}k_{2x}k_x|^{1/2}\left(k_{2y}k_2^2 - \frac{k_y k_{2x}}{k_x}k_2^2 + k_{1y}k_1^2 - \frac{k_y k_{1x}}{k_x}k_1^2\right).$$

Assuming that the frequency resonance condition is satisfied, i.e. $k_{1x}k_1^2 + k_{2x}k_2^2 = k_x k^2$, we get:

$$V_{12}^{\mathbf{k}} = -\sqrt{|k_{1x}k_{2x}k_x|}(k_{1y}k_1^2 + k_{2y}k_2^2 - k_y k^2),\tag{5.6}$$

which is only valid on the resonant manifold. In the large-scale limit, the zonostrophy density becomes:

$$\eta_{\mathbf{k}} = \frac{k_x^3}{k_y^2 - 3k_x^2}.\tag{5.7}$$

It has recently been discovered in [48] that this expression arises in $O(\rho^1)$ in the Taylor expansion of (3.7) for $\rho k^2 \to 0$ and another invariant arises in $O(\rho^0)$. This

54

additional invariant is defined as follows:

$$\varphi_{\mathbf{k}} = \begin{cases} 1 & \text{for} \quad |k_y| < \sqrt{3}k_x, \\ 0 & \text{for} \quad |k_y| > \sqrt{3}k_x, \\ \frac{1}{2} & \text{for} \quad |k_y| = \sqrt{3}k_x. \end{cases} \tag{5.8}$$

Both invariants are conserved independently for $\omega_{\mathbf{k}} = k_x k^2$ since this expression for the frequency is valid up to order ρ^2 corrections in the original expression (1.9). The new expression has since been named semi-action in [49] because its density coincides with the one of waveaction in the sector where it is not zero. Figure 5.1 shows the distribution of $\varphi_{\mathbf{k}}$ in 2D wavenumber space. The dividing line is $|k_y| = \sqrt{3}k_x$, $\varphi_{\mathbf{k}}$ is equal to zero in the shaded region ($|k_y| > \sqrt{3}k_x$) which is the zonal region with zonal (Z) modes and $\varphi_{\mathbf{k}}$ is equal to one outside this region ($|k_y| < \sqrt{3}k_x$) where the modes are meridional (M) modes.
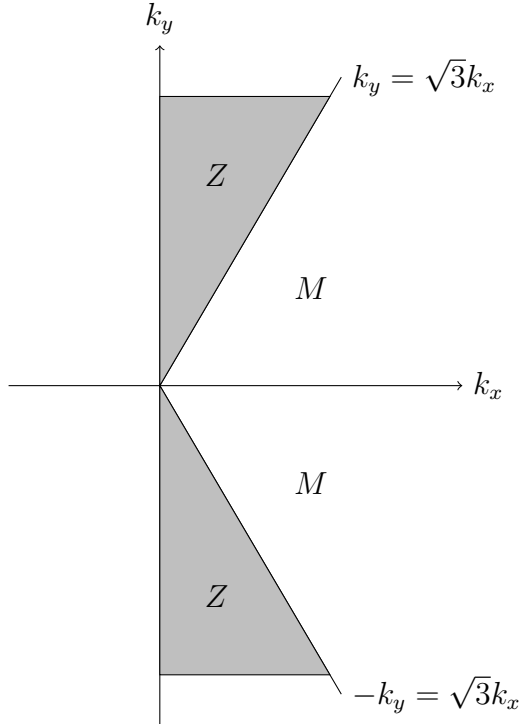
Figure 5.1: The distribution of $\varphi_{\mathbf{k}}$ in 2D wavenumber space.

In order for the semi-action (5.8) to be conserved it must satisfy the resonance condition (3.4), $\varphi_{\mathbf{k}} - \varphi_1 - \varphi_2 = 0$. So we have, $1 = 1 + 0$ for triads of type $M \to M + Z$

and $0 = 0 + 0$ for $Z \to Z + Z$. In other words, an excitation that is in a M-mode can transfer to a M- and a Z-mode but not to two M-modes ($1 \neq 1 + 1$) or two Z-modes ($1 \neq 0 + 0$) otherwise (3.4) would not be satisfied. On the other hand, an excitation that is in a Z-mode can only move to other Z-modes and not to M-modes. This behaviour follows from the conservation of semi-action, but in this thesis we would like to prove the following proposition directly.

Proposition 1 *Let M stand for meridional modes and Z stand for zonal modes of the system with frequency $\omega_{\mathbf{k}} = k_x k^2$. Then the following triad processes are prohibited:*

1. $M \to M + M$,

2. $M \to Z + Z$,

3. $Z \to M + Z$,

4. $Z \to M + M$.

Depending on whether we are considering the kinetic or discrete regime, either one or both of the following triad processes may be realised, $M \to M + Z$ and/or $Z \to Z + Z$.

5.1 Proof

Let $\mathbf{k} = (p, q)$, $p > 0$ and $\omega = p(p^2 + q^2)$. Let us begin by writing out the resonance condition:

$$\omega = \omega_1 + \omega_2, \tag{5.9}$$

$$p(p^2 + q^2) = p_1(p_1^2 + q_1^2) + (p - p_1)((p - p_1)^2 + (q - q_1)^2), \tag{5.10}$$

where we rewrote $p_2 = p - p_1$ and $q_2 = q - q_1$. Rearrange to get a quadratic for q_1:

$$pq_1^2 + 2(p_1 - p)qq_1 + 3pp_1^2 - 3p^2p_1 - p_1q^2 = 0, \tag{5.11}$$

from which we can find the discriminant:

$$
\frac{D}{4} = (p_1 - p)^2 q^2 - 3p^2 p_1^2 + 3p^3 p_1 + p_1 p q^2 \tag{5.12}
$$

$$
= p_2^2 q^2 + 3p^2 p_1 p_2 + p_1 p q^2, \tag{5.13}
$$

and the roots:

$$
q_{1\pm} = \frac{p_2 q}{p} \pm \frac{1}{p}\sqrt{\frac{D}{4}}. \tag{5.14}
$$

Taking $q > 0$ we can see that $q_{1+} > 0$ and $q_{1-} < 0$. Using $q_{2\pm} = q - q_{1\pm}$ gives:

$$
q_{2\pm} = \frac{p_1 q}{p} \mp \frac{1}{p}\sqrt{\frac{D}{4}}, \tag{5.15}
$$

where $q_{2+} < 0$ and $q_{2-} > 0$.

We must first prove that $\frac{q_{1\pm}}{p_1}$ and $\frac{q_{2\pm}}{p_2}$ are monotonic functions in the interval $0 < p_{1,2} < p$, i.e. they have no local extrema in this range. So from equation (5.14):

$$
\frac{q_{1\pm}}{p_1} = \frac{p_2 q}{p p_1} \pm \frac{1}{p p_1}\sqrt{\frac{D}{4}} \tag{5.16}
$$

$$
= \frac{q}{p_1} - \frac{q}{p} \pm \frac{1}{p p_1}\sqrt{(p_1^2 - p_1 p + p^2) q^2 + 3p^2 p_1 (p - p_1)}. \tag{5.17}
$$

Differentiating with respect to p_1 gives:

$$
\frac{\partial}{\partial p_1}\left(\frac{q_{1\pm}}{p_1}\right) = -\frac{q}{p_1^2} \mp \frac{\sqrt{(p_1^2 - p_1 p + p^2) q^2 + 3p^2 p_1 (p - p_1)}}{p p_1^2} \tag{5.18}
$$

$$
\pm \frac{q^2(2p_1 - p) + 3p^3 - 6p^2 p_1}{2 p p_1 \sqrt{(p_1^2 - p_1 p + p^2) q^2 + 3p^2 p_1 (p - p_1)}} = 0.
$$

Rearrange to get:

$$
\frac{\partial}{\partial p_1}\left(\frac{q_{1\pm}}{p_1}\right) = p_1^2 (q^4 - 3p^2 q^2 - \frac{9}{4}p^4 + \frac{3}{2}q^2 p^2 - \frac{1}{4}q^4) = 0, \tag{5.19}
$$

from which it can be seen that $p_1 = 0$ is the extremum location for both $\frac{q_{1+}}{p_1}$ and $\frac{q_{1-}}{p_1}$ and hence no extrema exist in the range $0 < p_1 < p$. Now do the same for $\frac{q_{2\pm}}{p_2}$.

Rewriting equation (5.15) using $p_1 = p - p_2$ gives:

$$\frac{q_{2\pm}}{p_2} = \frac{(p-p_2)q}{pp_2} \mp \frac{1}{p}\sqrt{q^2 + \frac{3(p-p_2)p^2}{p_2} + \frac{p(p-p_2)q^2}{p_2^2}} \qquad (5.20)$$

$$= \frac{q}{p_2} - \frac{q}{p} \mp \frac{1}{pp_2}\sqrt{q^2(p_2^2 + p^2 - pp_2) + 3p^3p_2 - 3p_2^2p^2}. \qquad (5.21)$$

Differentiate with respect to p_2 to get:

$$\frac{\partial}{\partial p_2}\left(\frac{q_{2\pm}}{p_2}\right) = -\frac{q}{p_2^2} \pm \frac{\sqrt{q^2(p_2^2 + p^2 - pp_2) + 3p^3p_2 - 3p_2^2p^2}}{pp_2^2} \qquad (5.22)$$

$$\mp \frac{q^2(2p_2 - p) + 3p^3 - 6p_2p^2}{2pp_2\sqrt{q^2(p_2^2 + p^2 - pp_2) + 3p^3p_2 - 3p_2^2p^2}} = 0.$$

Rearrange to get:

$$\frac{\partial}{\partial p_2}\left(\frac{q_{2\pm}}{p_2}\right) = p_2^2(q^2 - \frac{q^2}{4} - \frac{9}{4}\frac{p^4}{q^2} + \frac{3}{2}p^2 - 3p^2) = 0, \qquad (5.23)$$

from which it can be seen that $p_2 = 0$, so again there are no extrema in the range $0 < p_2 < p$, which is the same as $0 < p_1 < p$.

Secondly, we need to find out whether $\frac{q_{1\pm}}{p_1}$ and $\frac{q_{2\pm}}{p_2}$ are increasing or decreasing functions of p_1. To do this we must compare their values at $p_1 \to 0$ and $p_1 \to p$.

1. $p_1 \to 0 \quad (p_2 \to p)$

From (5.17):

$$\frac{q_{1\pm}}{p_1} \to \frac{q}{p_1} - \frac{q}{p} \pm \frac{pq}{pp_1}\sqrt{1 + \frac{(-pq^2 + 3p^3)}{p^2q^2}p_1}, \qquad (5.24)$$

where we have ignored p_1^2 terms since they are very small. Taylor expanding we get:

$$\frac{q_{1\pm}}{p_1} \to \frac{q}{p_1} - \frac{q}{p} \pm \frac{q}{p_1}\left[1 + \frac{(3p^2 - q^2)}{2pq^2}p_1\right]. \qquad (5.25)$$

Therefore we can see that:

$$\frac{q_{1+}}{p_1} \to \frac{2q}{p_1} \to +\infty, \qquad (5.26)$$

since $p_1 \to 0$ and:

$$\frac{q_{1-}}{p_1} \to -\frac{q}{p} - \frac{3p^2 - q^2}{2pq}. \tag{5.27}$$

Similarly, we find:

$$\frac{q_{2\pm}}{p_2} \to \mp\frac{q}{p}. \tag{5.28}$$

2. $p_1 \to p \quad (p_2 \to 0)$

From (5.21), ignoring p_2^2 terms:

$$\frac{q_{1\pm}}{p_1} \to \frac{p_2 q}{pp_1} \pm \frac{pq}{pp_1}\sqrt{1 + \frac{(-pq^2 + 3p^3)}{p^2 q^2}p_2}. \tag{5.29}$$

Taylor expanding and letting $p_1 \to p$ gives:

$$\frac{q_{1\pm}}{p_1} \to \frac{p_2 q}{p^2} \pm \frac{pq}{p^2}\left[1 + \frac{(3p^2 - q^2)}{2pq^2}p_2\right], \tag{5.30}$$

and letting $p_2 \to 0$ gives:

$$\frac{q_{1\pm}}{p_1} \to \pm\frac{q}{p}. \tag{5.31}$$

Similarly, we find:

$$\frac{q_{2-}}{p_2} \to \frac{2q}{p_2} \to +\infty, \tag{5.32}$$

$$\frac{q_{2+}}{p_2} \to -\frac{q}{p} - \frac{3p^2 - q^2}{2pq}. \tag{5.33}$$

Therefore we can see that $\frac{q_{1\pm}}{p_1}$ are increasing functions and $\frac{q_{2\pm}}{p_2}$ are decreasing functions.

Let us now denote $x = \frac{q}{p} > 0$. Substituting this into equations (5.27) and (5.33) gives:

$$f(x) = -\frac{1}{2}x - \frac{3}{2x}. \tag{5.34}$$

By taking the derivative and putting it equal to zero we find that there is an extremum at $x = \sqrt{3}$. And since the second derivative is less than zero we know that this is a maximum. Hence, the maximum value of $\frac{q_{1-}}{p_1}$ and $\frac{q_{2+}}{p_2}$ is $-\sqrt{3}$. It can also

be seen that:

$$\frac{q_{1+}}{p_1} > \frac{q}{p} > \sqrt{3} \quad \text{and} \quad \frac{q_{2-}}{p_2} > \frac{q}{p} > \sqrt{3}. \tag{5.35}$$

Putting this all together, we get the following graph for the case when $q > p\sqrt{3}$, i.e. $\mathbf{k} \in Z$.
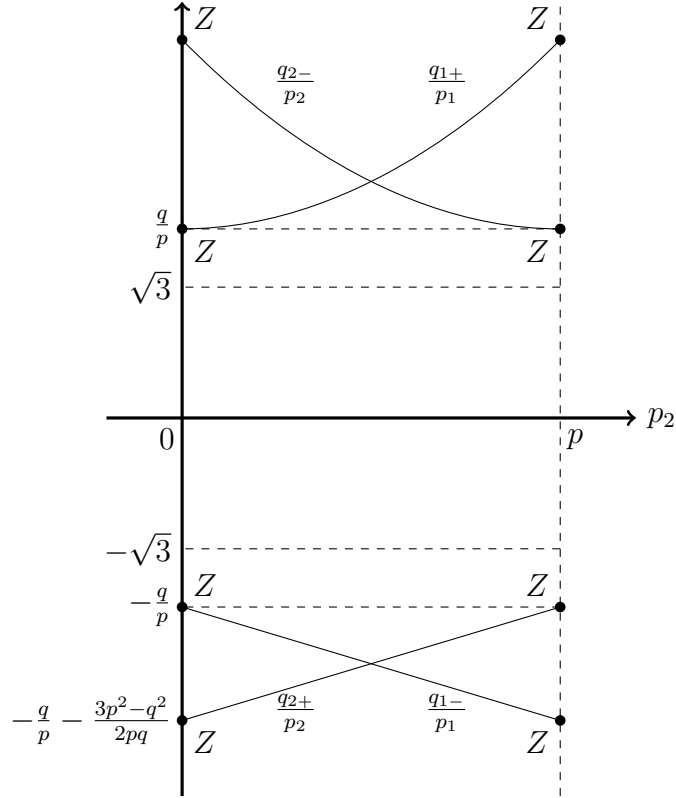
Figure 5.2: Graph summarizing the case when $q > p\sqrt{3}$.

Hence we have proved numbers 3 and 4 of the proposition, semi-action already in a Z-mode must stay in a Z-mode and cannot be transferred to M-modes.

When $q < p\sqrt{3}$, i.e. $\mathbf{k} \in M$ we get the following graph.
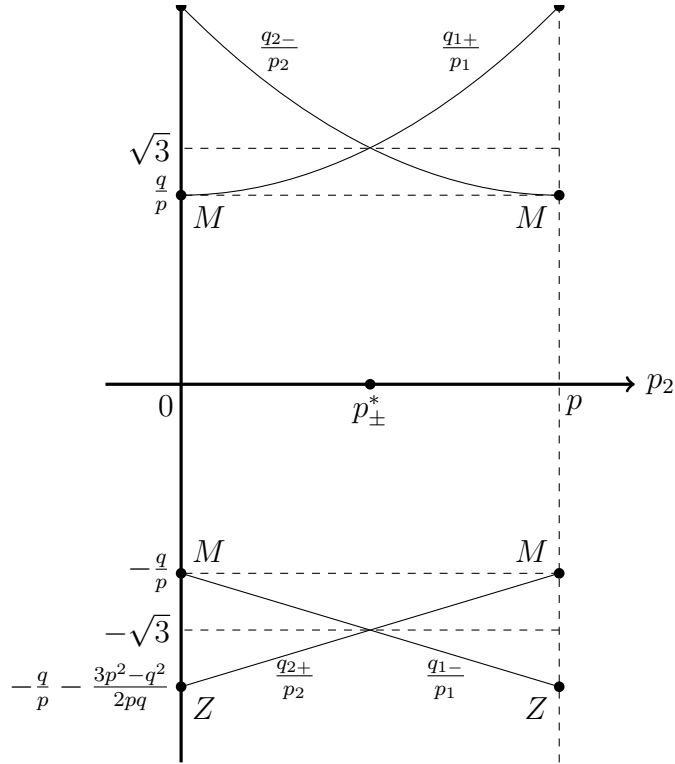
Figure 5.3: Graph summarizing the case when $q < p\sqrt{3}$.

We can see that all curves change from $M \to Z$ or $Z \to M$ at some point p^* within the range $0 < p_1 < p$. We need to prove that this point is the same for (1.) $\frac{q_{1+}}{p_1}$ and $\frac{q_{2+}}{p_2}$ as well as for (2.) $\frac{q_{1-}}{p_1}$ and $\frac{q_{2-}}{p_2}$.

1.

$$q_{1+} = \sqrt{3}p_1 = \frac{p_2 q}{p} + \frac{1}{p}\sqrt{\frac{D}{4}}, \tag{5.36}$$

$$(\sqrt{3}p_1 p - p_2 q)^2 = p_2^2 q^2 + 3p^2 p_1 p_2 + p_1 p q^2. \tag{5.37}$$

Rearranging we get:

$$p_1 = \frac{p + \frac{q}{\sqrt{3}}}{2}. \tag{5.38}$$

From this we can see that:

$$p_1 < p \quad \text{if} \quad p + \frac{q}{\sqrt{3}} < 2p \to q < p\sqrt{3}. \tag{5.39}$$

61

2.

$$q_{2+} = -\sqrt{3}p_2 = \frac{p_1 q}{p} - \frac{1}{p}\sqrt{\frac{D}{4}}, \tag{5.40}$$

$$(\sqrt{3}p_2 p + p_1 q)^2 = p_2^2 q^2 + 3p^2 p_1 p_2 + p_1 p q^2. \tag{5.41}$$

Rearranging we get:

$$p_2 = \frac{p}{2} - \frac{q}{2\sqrt{3}}. \tag{5.42}$$

We can see that:

$$p_2 > 0 \quad \text{if} \quad q < p\sqrt{3} \quad \text{and} \quad p_2 < p \quad \text{if} \quad p - \frac{q}{\sqrt{3}} < 2p. \tag{5.43}$$

$p_1 = p - p_2 = \frac{p}{2} + \frac{q}{2\sqrt{3}}$, hence:

$$p_{\pm}^* = \frac{1}{2}\left(p \pm \frac{q}{\sqrt{3}}\right). \tag{5.44}$$

So we have proved numbers 1 and 2 of the proposition.

5.2 Cascade boundaries

Similar to the work carried out by Nazarenko and Quinn in [46], where they found the cascade paths of the energy, enstrophy and zonostrophy in the small-scale limit, we will now do the same for the large-scale case taking into account the extra invariant. It is now qualitatively different depending on which sector the initial spectrum is in. In the small-scale case all three invariants are positive; however, in the large-scale case, zonostrophy is not sign definite in the meridional sector so instead we use the semi-action. When the initial spectrum is in the zonal sector, zonostrophy is positive.

When the density of the invariant is positive we can apply Fjørtoft's argument [45] to find the cascade directions of the three invariants, the energy E, enstrophy Ω and depending whether the initial spectrum is in the meridional or zonal sector, the semi-action Φ or zonsotrophy Z, respectively.

Each of the invariants must cascade to the scales where its density is dominant

over the densities of the other two invariants and the boundaries between the cascade sectors are found when the ratios of the invariant densities remain constant. Let us begin by considering the case when the initial spectrum is in the meridional sector at $\mathbf{k}_0 = (k_{0x}, k_{0y})$.

5.2.1 Initial spectrum in the meridional sector

From the invariant densities:

$$E = \int k_x k^2 n_{\mathbf{k}} d\mathbf{k}, \tag{5.45}$$

$$\Omega = \int k_x n_{\mathbf{k}} d\mathbf{k}, \tag{5.46}$$

$$\Phi = \int n_{\mathbf{k}} d\mathbf{k} \quad \text{for} \quad |k_y| < \sqrt{3} k_x. \tag{5.47}$$

the boundaries are as follows:

- $E\Omega$: $k^2 = k_0^2$,

- $E\Phi$: $k_x k^2 = k_{0x} k_0^2$,

- $\Omega\Phi$: $k_x = k_{0x}$.

It is clear that the semi-action, Φ must remain in the meridional sector as its density is zero outside of this sector. However, E and Ω can flow freely from M to Z modes. The $E\Omega$ boundary separates the energy and the enstrophy cascades which means that E cannot be transferred to $\mathbf{k} \ll \mathbf{k}_0$ and Ω to $\mathbf{k} \gg \mathbf{k}_0$. Hence E is dissipated at large $\mathbf{k}$ and Ω is dissipated at small $\mathbf{k}$. Further, since the $E\Phi$ and the $\Omega\Phi$ boundaries are only in the meridional sector, we have $\mathbf{k}/2 \leq k_x \leq \mathbf{k}$. The boundaries are "soft" in a sense that the invariants are allowed to cross to each other's sector but not too deeply, as a result we can take $k_x \sim \mathbf{k}$, and find that all three boundaries, $E\Omega$, $E\Phi$ and $\Omega\Phi$, approximately coincide in the meridional sector. This means that Φ cannot flow to large $\mathbf{k}$, and, assuming that it should move far from the initial scale $\mathbf{k}_0$, it must move to modes with small $\mathbf{k}$ (while remaining in M modes). On the other hand, Ω cannot be transferred to neither large nor small wave vectors in the meridional sector. The only remaining choice for Ω is to flow to small

wave vectors in the zonal sector. The latter choice does not contradict conservation of Φ because its density is zero in the zonal sector. This is depicted in figure 5.4.
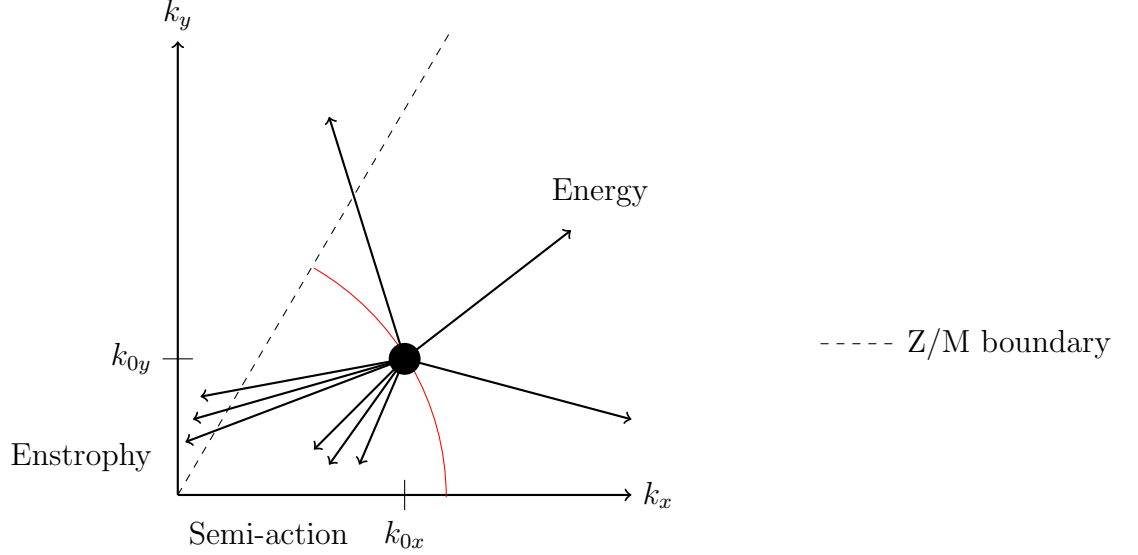
Figure 5.4: Cascade boundaries and dissipation regions when the initial spectrum is in the meridional sector.

5.2.2 Initial spectrum in the zonal sector

Let us now put the initial spectrum in the zonal sector. Since the semi-action density is zero in this sector and the zonostrophy density is positive we will study the cascades of energy, enstrophy and zonostrophy. The zonostophy in the large-scale limit is:

$$Z = \int \frac{k_x^3}{k_y^2 - 3k_x^2} n_{\mathbf{k}} d\mathbf{k}, \tag{5.48}$$

and the boundaries between the three invariants are as follows:

- $E\Omega$: $k^2 = k_0^2$,

- ΩZ: $\left(\frac{k_y}{k_x}\right)^2 = \left(\frac{k_{0y}}{k_{0x}}\right)^2$

- EZ: $\left[\left(\frac{k_y}{k_x}\right)^2 - 3\right] k^2 = \left[\left(\frac{k_{0y}}{k_{0x}}\right)^2 - 3\right] k_0^2$

The cascade picture is depicted in figure 5.5. It can been seen that the energy cascades to large $\mathbf{k}$, the enstrophy to small $\mathbf{k}$ becoming progressively more zonal and

the zonostrophy towards the line $k_y = \sqrt{3}k_x$. Note that no turbulence can leave the zonal sector otherwise the conservation of Φ is broken.
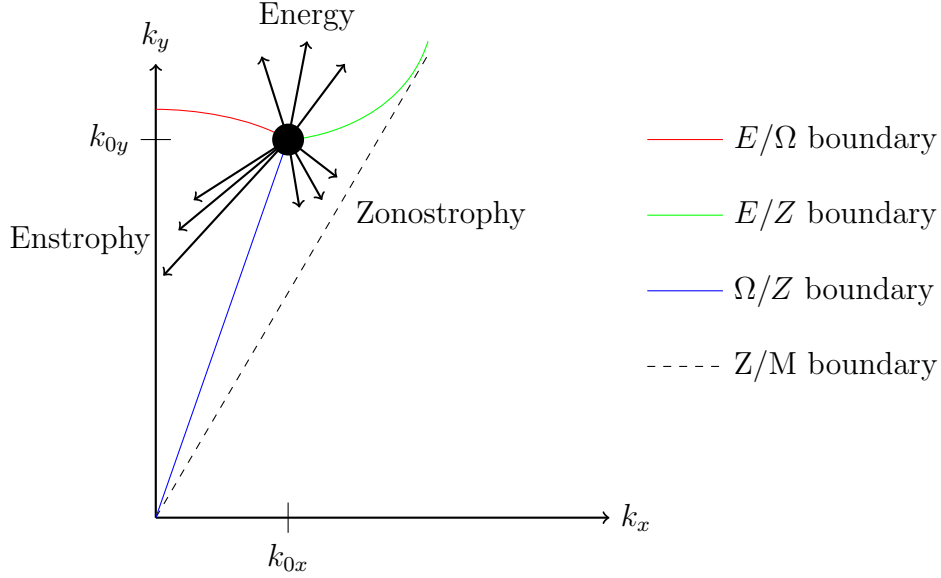
Figure 5.5: Cascade boundaries and dissipation regions when the initial spectrum is in the zonal sector.

5.3 Numerics

In order to numerically test the theoretical predictions of this chapter, a pseudo-spectral code, originally used for the small-scale case in [46], has been used. This code solves the CHM equation in order to check both the conservation and cascade directions of the invariants in the case of large-scale turbulence. The initial condition is defined as follows:

$$\hat{\psi}_{\mathbf{k}}|_{t=0} = Ae^{\left(\frac{|\mathbf{k}-\mathbf{k}_0|^2}{k_*^2} + i\phi_{\mathbf{k}}\right)} + \text{image}, \tag{5.49}$$

which is a Gaussian spot centred at $\mathbf{k}_0$ with width k_* and its mirror image with respect to the k_x-axis. $\phi_{\mathbf{k}}$ are random independent phases and A is the constant amplitude. Again we consider when the initial spectrum is in the meridional sector and the zonal sector for both weak and strong nonlinearity.

5.3.1 Meridional sector

Let us begin by putting the initial spectrum in the meridional sector, centred at $\mathbf{k}_0 = (40, 20)$ with a width of $k_* = 8$. The initial amplitude was chosen as $A = 1.875 \times 10^{-4}$ so as to make the run weakly nonlinear. The resolution was 256^2, $\beta = 10$ and the time step $\delta t = 1.25 \times 10^{-8}$.

Figure 5.6 shows the conservation of the energy, enstrophy, semi-action and zonostrophy. The energy, enstrophy and semi-action are well conserved to within $0.25\%, 0.1\%$ and 1.5% respectively. However, it can be seen that the zonostrophy is more sensitive; this is probably since its density becomes singular when it reaches the zonal/meridional boundary, i.e. the denominator of (5.48) is zero on the line $|k_y| = \sqrt{3}k_x$.

Figure 5.7 shows the cascade directions of the energy, enstrophy and semi-action. They are plotted in-terms of the paths followed by the centroids defined as follows:

$$\mathbf{k}_E(t) = \frac{1}{E} \int \mathbf{k} k^2 |\hat{\psi}_{\mathbf{k}}|^2 d\mathbf{k}, \tag{5.50}$$

$$\mathbf{k}_\Omega(t) = \frac{1}{\Omega} \int \mathbf{k} |\hat{\psi}_{\mathbf{k}}|^2 d\mathbf{k},$$

$$\mathbf{k}_Z(t) = \frac{1}{Z} \int \mathbf{k} \frac{k_x^2}{k_y^2 - 3k_x^2} |\hat{\psi}_{\mathbf{k}}|^2 d\mathbf{k},$$

$$\mathbf{k}_\Phi(t) = \frac{1}{\Phi} \int \mathbf{k} \frac{|\hat{\psi}_{\mathbf{k}}|^2}{k_x} d\mathbf{k}, \quad \text{for} \quad |k_y| < \sqrt{3}k_x.$$

The centroids are normalised by their initial values so that the centroid paths start from the same point. It can be seen that each invariant cascades into the sector predicted in section 5.2.1.

Figure 5.8 shows three successive frames of the ψ spectrum in 2D $\mathbf{k}$-space at the start, middle and end of the run.

Figure 5.6: Plot showing the conservation of the energy, enstrophy, zonostrophy and semi-action when the initial spectrum is in the meridional sector and nonlinearity is weak.

Figure 5.7: Plot showing the cascade paths of the energy, enstrophy and semi-action when the initial spectrum is in the meridional sector and nonlinearity is weak.
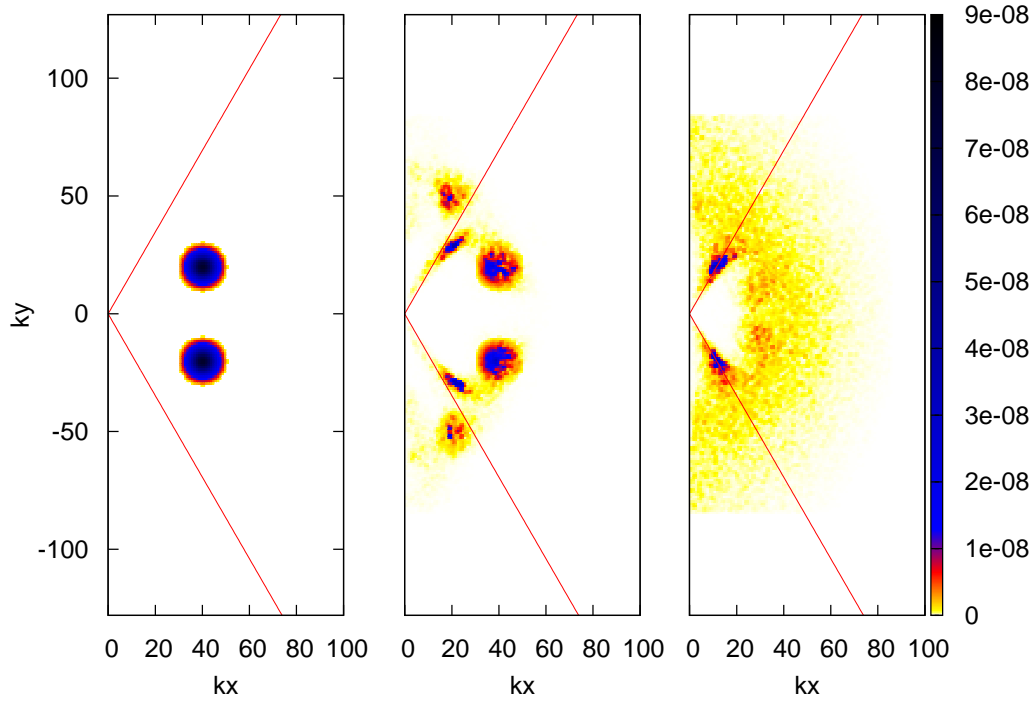
Figure 5.8: Three successive frames of the ψ spectrum in 2D **k**-space.

To see what happens when nonlinearity is increased the following parameters were chosen: $\mathbf{k}_0 = (40, 20), k_* = 8, \beta = 10, A = 1 \times 10^{-3}$ and $\delta t = 2.5 \times 10^{-9}$. Figures 5.9, 5.10 and 5.11 show the conservation, cascade directions and ψ spectrum respectively. The zonostrophy line has been removed from the conservation plot as it quickly looses conservation. On the other hand, the energy, enstrophy and semi-action are conserved to within $4\%, 1\%$ and 17% respectively.

Figure 5.9: Plot showing the conservation of the energy, enstrophy and semi-action when the initial spectrum is in the meridional sector and nonlinearity is strong.

Figure 5.10: Plot showing the cascade paths of the energy, enstrophy and semi-action when the initial spectrum is in the meridional sector and nonlinearity is strong.
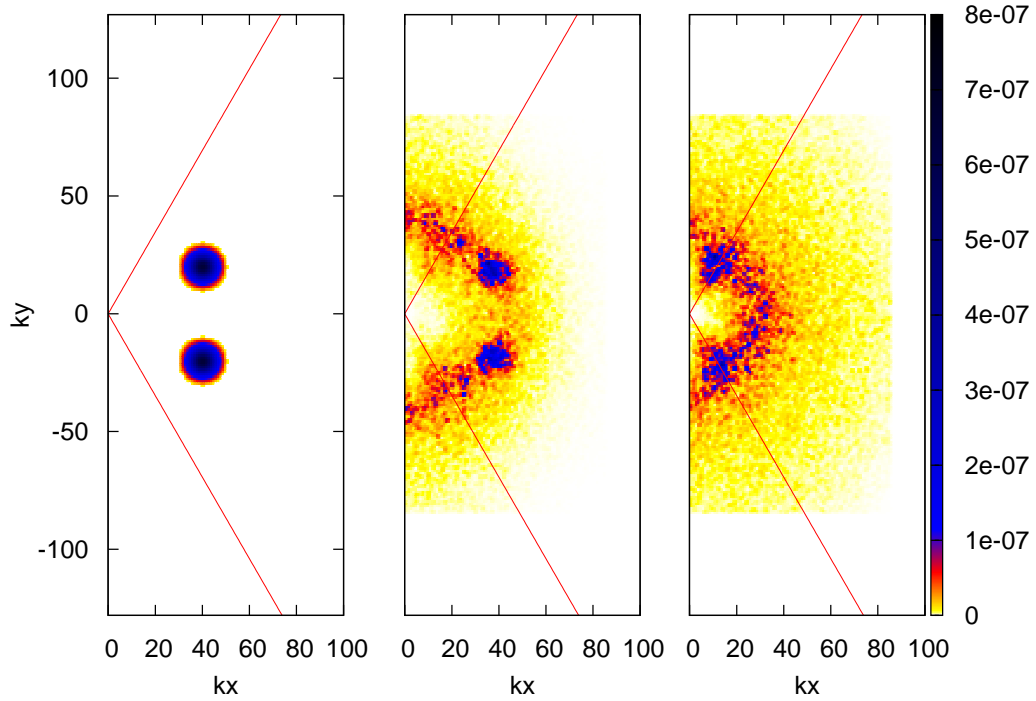
Figure 5.11: Three successive frames of the ψ spectrum in 2D **k**-space.

5.3.2 Zonal sector

Let us now put the initial spectrum in the zonal sector and again consider weak nonlinearity. Figures 5.12 and 5.13 show the conservation and cascade directions of the energy, enstrophy and zonostrophy respectively, when we considered a resolution of 512^2 with the following parameters: $\mathbf{k}_0 = (20, 65), k_* = 8, \beta = 10, A = 5 \times 10^{-5}$ and $\delta t = 1.25 \times 10^{-8}$.
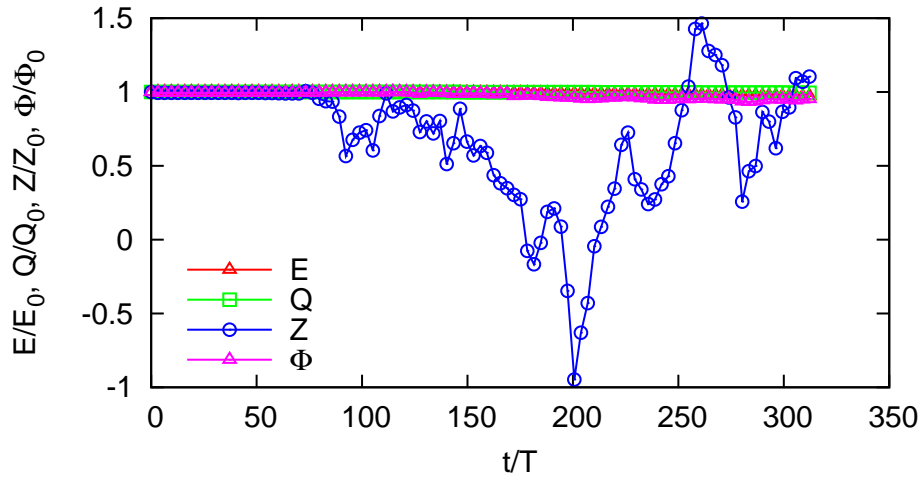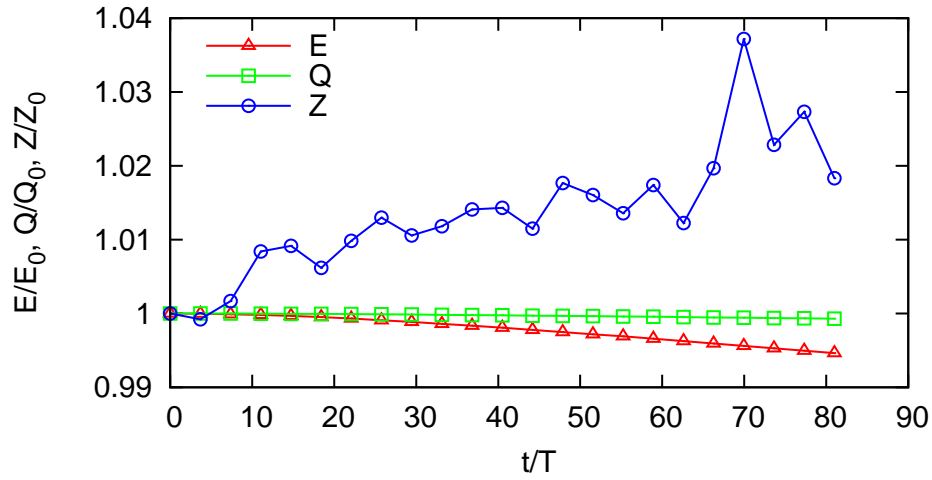
Figure 5.12: Plot showing the conservation of the energy, enstrophy and zonostrophy when the initial spectrum is in the zonal sector and nonlinearity is weak.
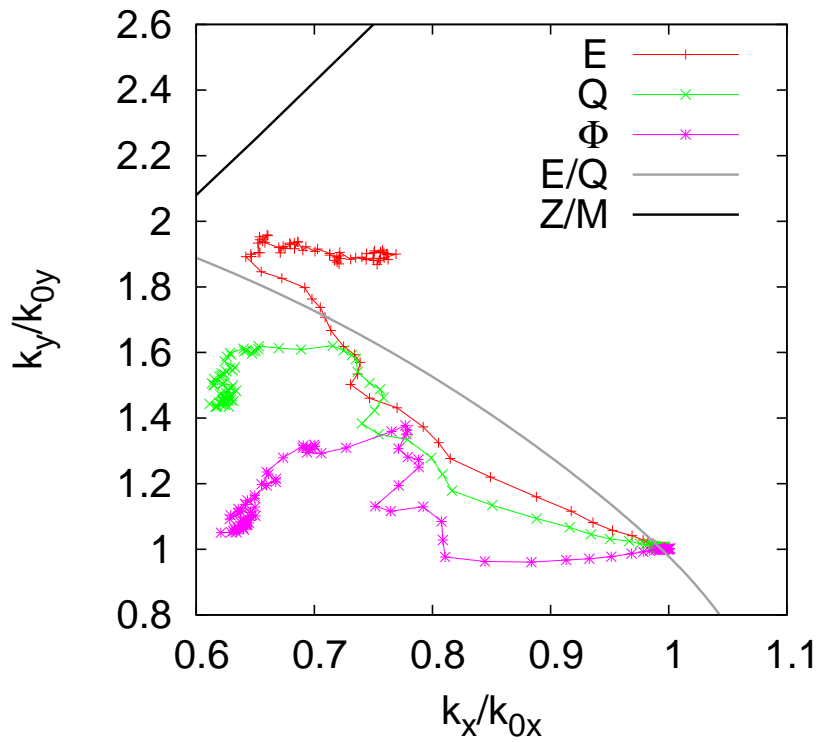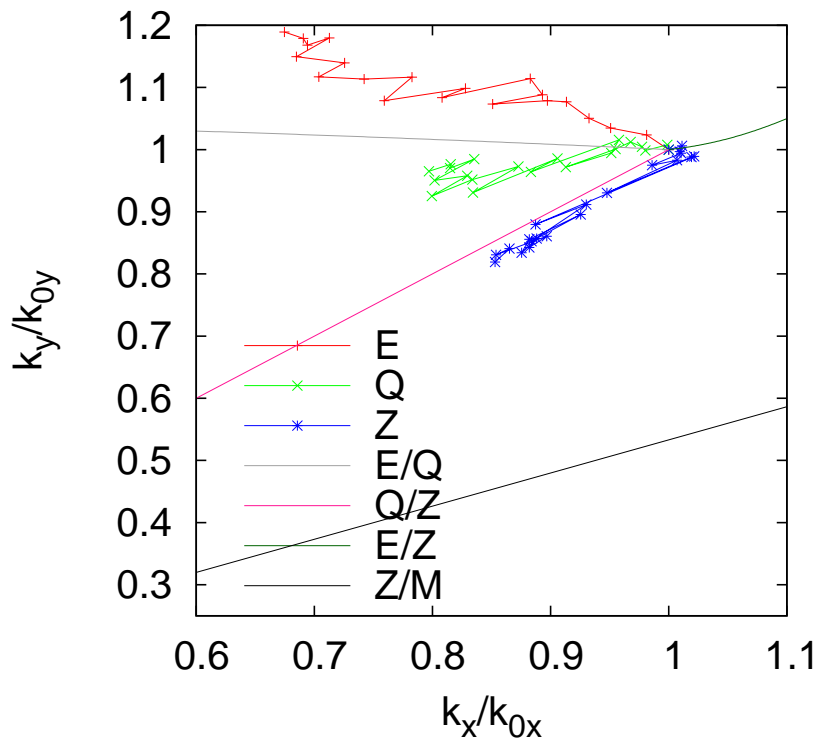

Figure 5.13: Plot showing the cascade paths of the energy, enstrophy and zonostrophy when the initial spectrum is in the zonal sector and nonlinearity is weak.

It can be seen that the energy and enstrophy are conserved to within 0.55% and 0.1% respectively and the zonostrophy to within 4%. Each invariant cascades into the sector predicted in section 5.2.2. The zonostrophy follows the Ω/Z boundary. This has been observed before for energy in the small-scale case.
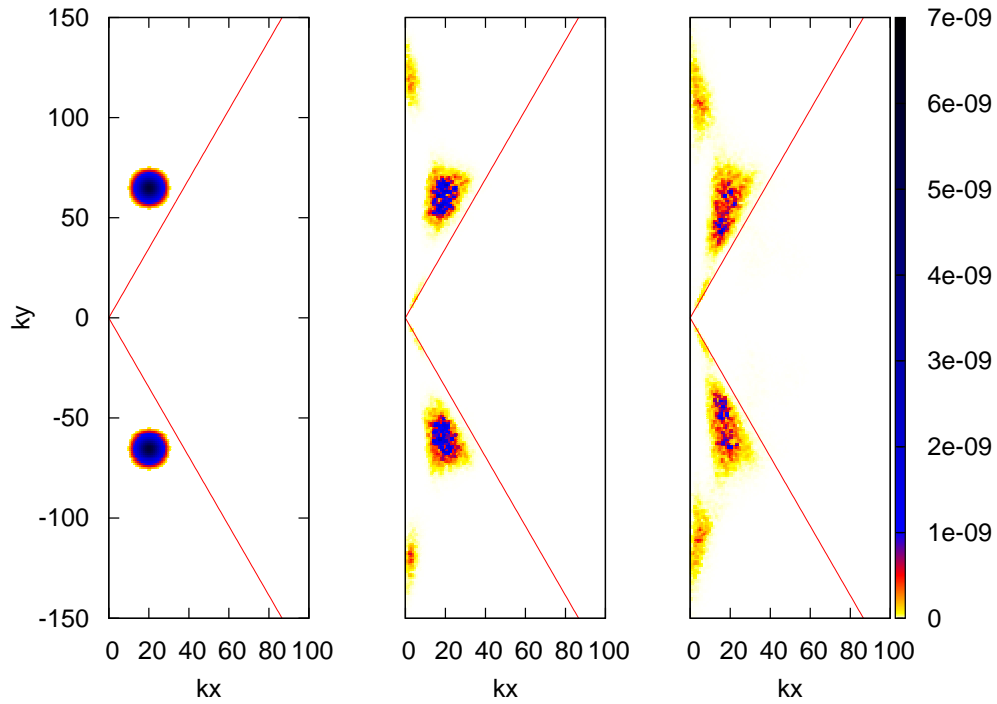
Figure 5.14: Three successive frames of the ψ spectrum in 2D **k**-space.

The ψ spectrum in 2D **k**-space is shown in figure 5.14 and figure 5.15 shows the ratio of waveaction $n_{\mathbf{k}}$ in the meridional sector to that in the whole of **k**-space. It can be seen that ψ remains in the zonal sector and the spectrum evolves towards the origin with zonal flow forming at low **k** and also high **k**. The action plot confirms that less than 0.2% of semi-action escapes into the meridional sector.
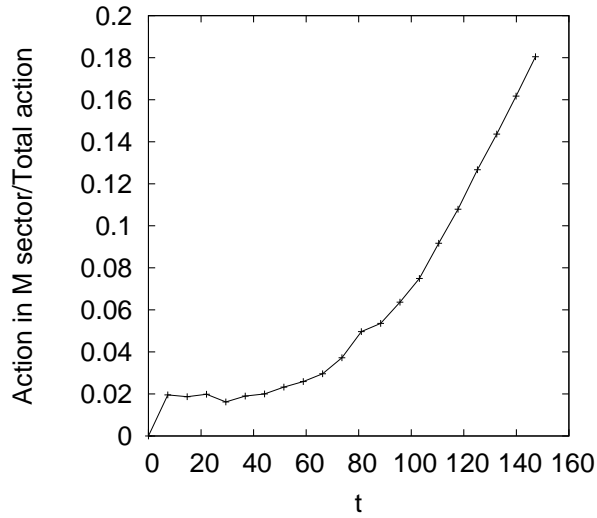
Figure 5.15: Plot showing the ratio of action $n_{\mathbf{k}}$ in the meridional sector to that in the whole of $\mathbf{k}$-space.

When the amplitude is increased to $A = 1 \times 10^{-3}$ and the time step decreased to $\delta t = 2.5 \times 10^{-10}$ so as to make the run strongly nonlinear we get the following plots.
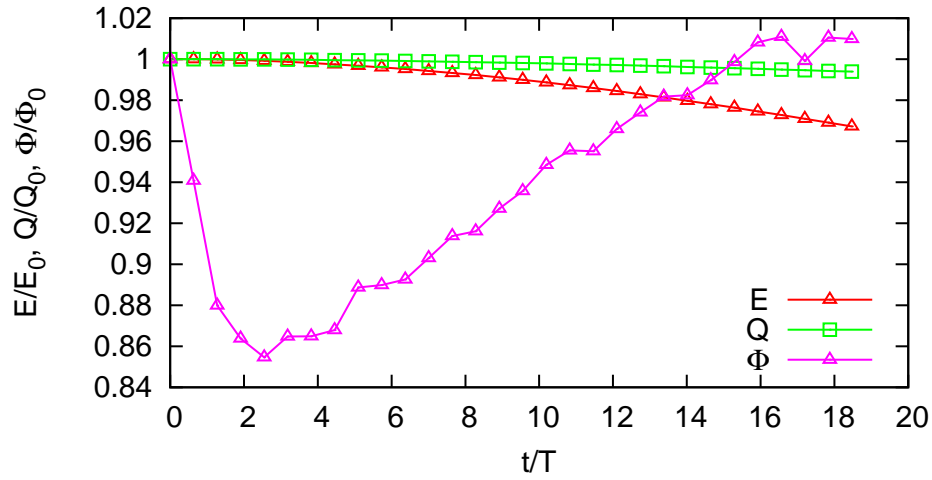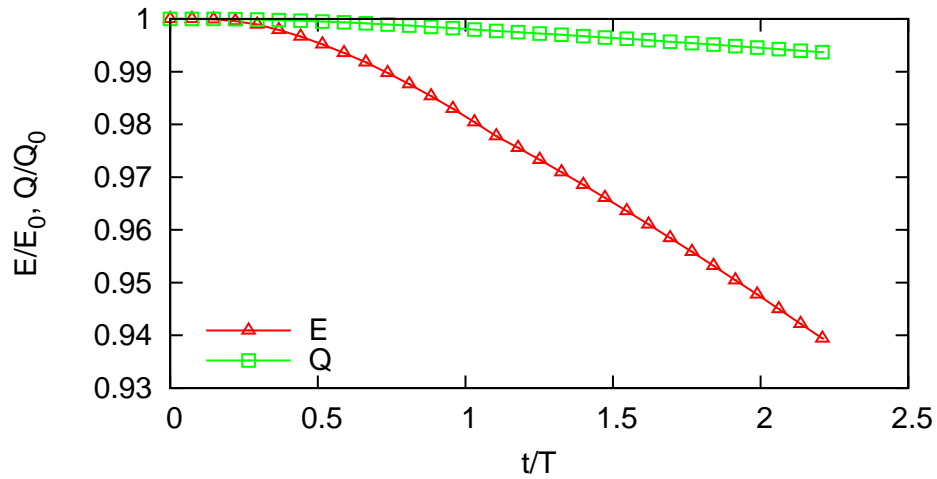

Figure 5.16: Plot showing the conservation of the energy and enstrophy when the initial spectrum is in the zonal sector and nonlinearity is strong.

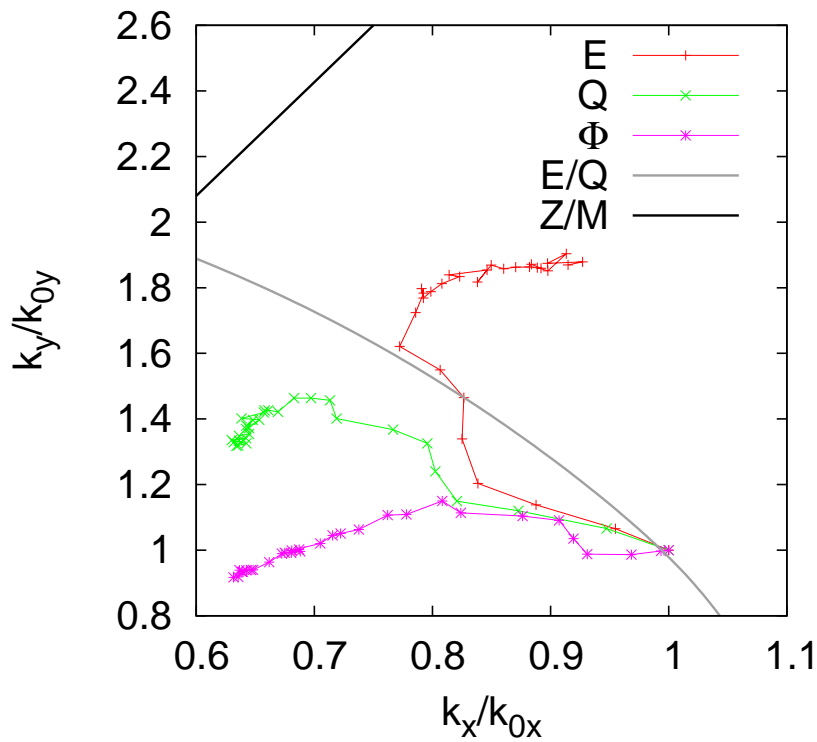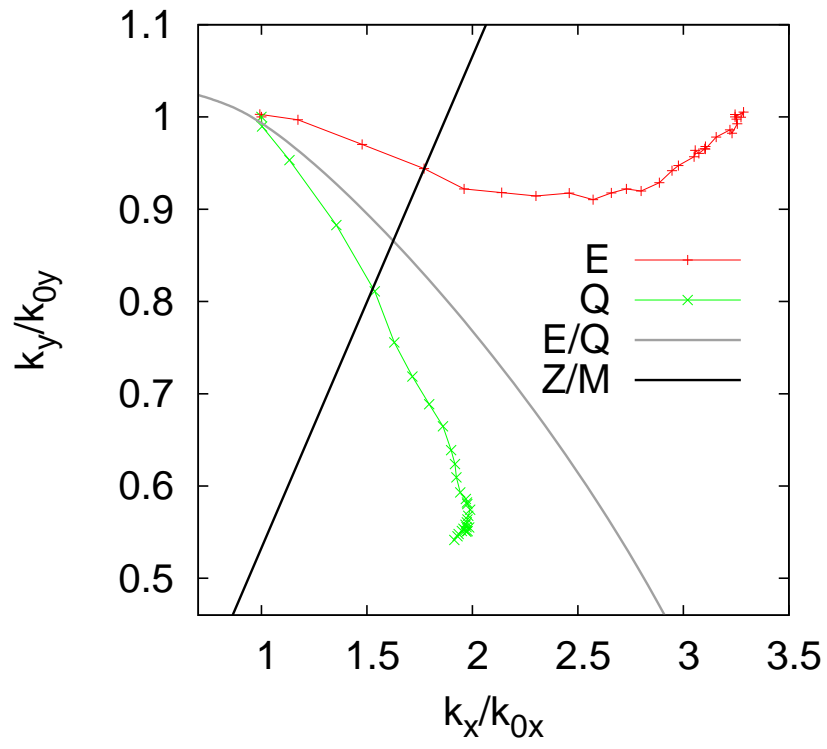Figure 5.17: Plot showing the cascade paths of the energy and enstrophy when the initial spectrum is in the zonal sector and nonlinearity is strong.
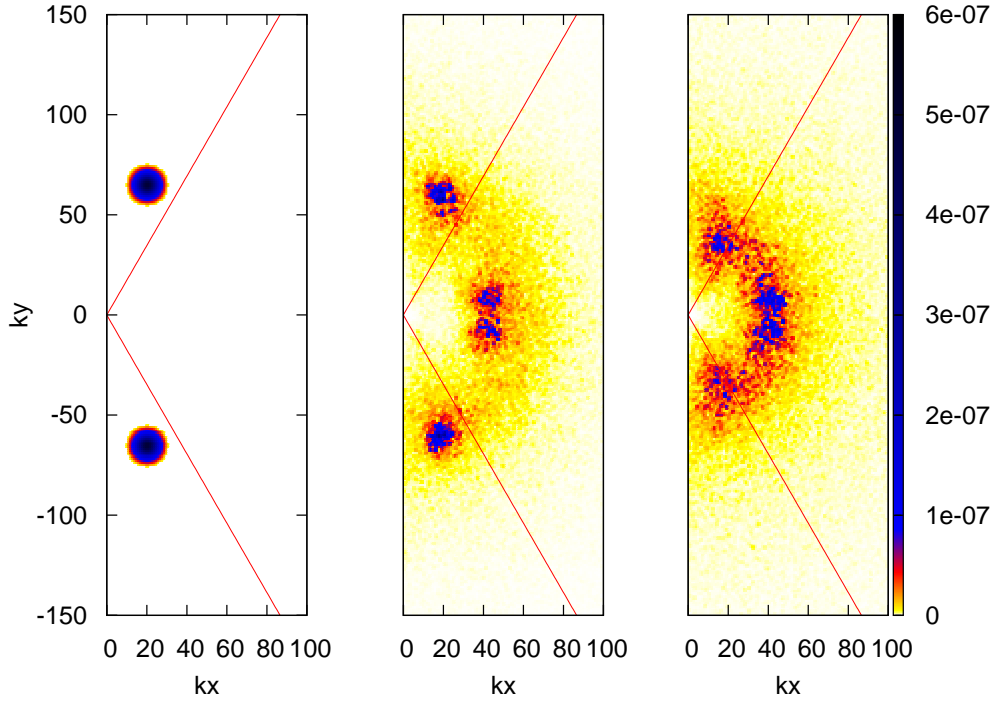
Figure 5.18: Three successive frames of the ψ spectrum in 2D **k**-space.
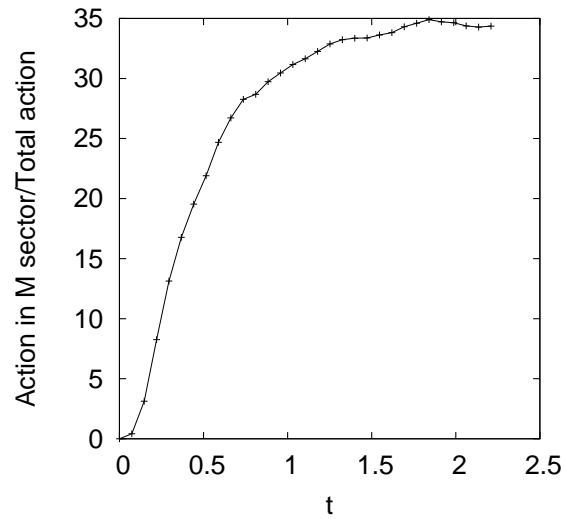
Figure 5.19: Plot showing the ratio of action $n_{\mathbf{k}}$ in the meridional sector to that in the whole of **k**-space.

Again we have removed the zonostrophy from the conservation and cascade plots

as it has twice the magnitude and the opposite sign by the middle of the run making the cascade path very erratic and lacking any structure. It can be seen that the energy and enstrophy still move in opposite directions but the cascade paths are not as predicted, crossing the zonal/meridional boundary. Now that nonlinearity is strong and three-wave resonances no longer dominate, it can be seen that the spectrum moves into the meridional sector and proposition 1 is no longer valid.

Hence, we have shown, both theoretically and numerically, that proposition 1 holds when nonlinearity is weak and three-wave interactions dominate. If the initial spectrum is zero outside the zonal sector then it must remain zero else conservation is violated. We showed numerically that this is indeed the case, when the initial spectrum is in the zonal sector it remains in the zonal sector. On the other hand, when the initial spectrum is in the meridional sector, small amounts can move into the zonal sector, but not all can transfer as otherwise semi-action would be lost. However, when nolinearity is strong, we showed that the proposition no longer holds.

We considered a continuous **k**-space; however, our proposition also holds when wavenumbers take discrete values. In the discrete regime the resonance conditions are harder to satisfy and hence fewer triads exist. Therefore triads that we proved don't exist in the continuous case also don't exist in the discrete case. However, we can't say that if a triad exists in the continuous case it also exists in the discrete case.

5.4 ρ^2 small but finite

We have seen in the previous section, that for the large-scale limit ($\rho^2 \to 0$), when nonlinearity is weak and three-wave interactions dominate, proposition 1 is satisfied. However, what happens when ρ^2 is small but finite?

It turns out that forbidden triads exist. They are concentrated along the zonal/meridional boundary and their deviation of $\frac{k_y}{k_x}$ from $\sqrt{3}$ shrinks as $\rho^2 \to 0$. In other words, as ρ^2 increases, the angle containing forbidden triads around the zonal/meridional boundary also increases. See figures 5.20 and 5.21 below. Letting $\mathbf{k}_3 = (\cos(\theta), \sin(\theta))$, the closer θ is to the boundary, the bigger the angle containing forbidden triads.
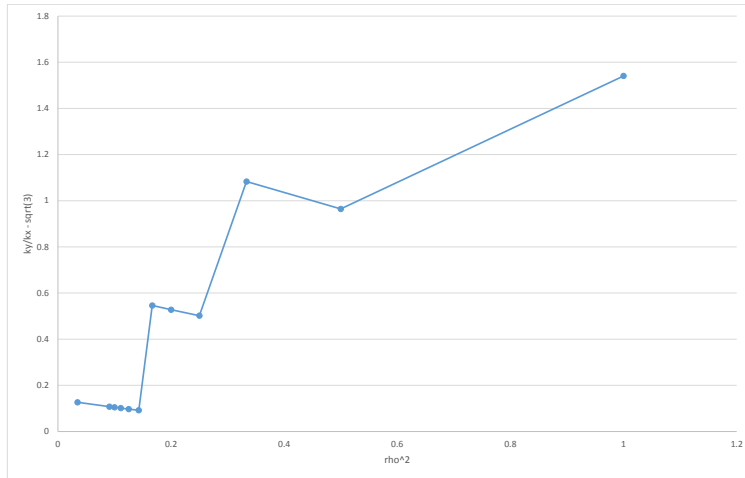
Figure 5.20: Plot showing for $\theta = \pi/4$, as ρ^2 increases the angle containing forbidden triads around the zonal/meridional boundary also increases.
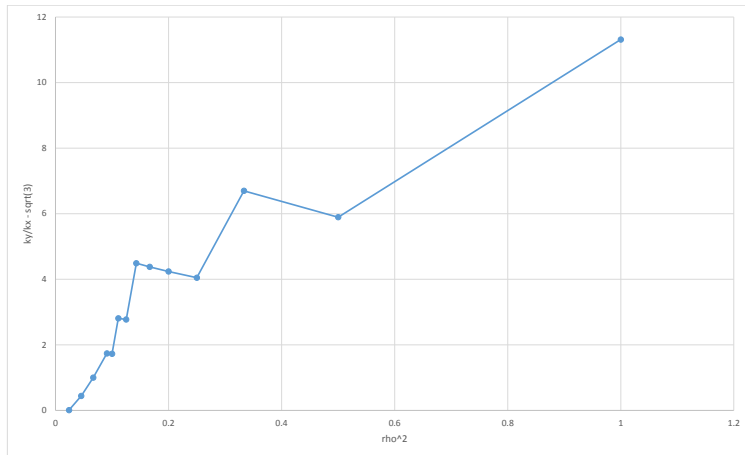
Figure 5.21: Plot showing for $\theta = 5\pi/16$, as ρ^2 increases the angle containing forbidden triads around the zonal/meridional boundary also increases.

It has further been found, that for θ less than the boundary, all forbidden triads are of the type $Z + Z \to M$. And for θ greater than the boundary no forbidden triad exist for $k_x > 0$. Hence, the forbidden triads $M + M \to Z$, $M + Z \to Z$ and $M + M \to M$ don't exist for finite but small ρ^2 either.

77

Chapter 6

Two-layer quasi-geostrophic turbulence

In oceanography, idealized models of the full equations of motion, such as the CHM equation (1.2), have proven to be useful tools in the study of large-scale geophysical flows. On the other hand, barotropic equations often do not adequately represent reality, as they lack the mechanism for energy injection and generation of turbulence. The two-layer model first introduced by Phillips in 1951 [50] represents the next level of realism in describing geophysical fluid dynamics. Indeed, this model allows for baroclinic motions and as a result baroclinic instabilities (BIs) which are believed to be the main source of energy for large-scale geophysical turbulence.

Similar to the picture of 2D barotropic motion [44, 45] with the inverse energy and direct enstrophy cascades, there have been ideas put forward for two-layer baroclinic motion. Rhines [51] and Salmon [52, 53] suggested the following. Energy enters at large horizontal scales, k_F, in the baroclinic mode. It then moves towards higher wavenumbers until it reaches the Rossby deformation scale, k_R (one over the Rossby deformation radius), where eddies generated through BI energise the barotropic mode, a process known as barotropization. Barotropization refers to the tendency of a QG flow to reach the gravest vertical mode [54, 55, 56]. Energy then moves back towards large scales via an inverse barotropic cascade similar to that of 2D turbulence. At scales smaller than the Rossby deformation scale, there is a direct enstrophy cascade in each layer until it is scattered into 3D turbulence. If

planetary rotation is fast enough, the inverse cascade is influenced by the beta-effect and the large-scale flow becomes anisotropic, leading to the formation of zonal jets [57, 58, 59].

As we have already seen, in one-layer turbulence energy is transferred between scales via triplets of modes whose wavenumbers sum to zero. This is also the case for two-layer QG turbulence, the only difference being, that the vertical wavenumbers in a triad must also sum to zero. Salmon [3] and Vallis [8] studied the various types of triads involving barotropic and baroclinic modes. A barotropic triad is made up of three barotropic modes (with vertical wavenumber zero) and a baroclinic triad is made up of one barotropic and two baroclinic modes (with vertical wavenumber plus or minus one). Both Salmon and Vallis studied two layers of equal depth; however, this is not always the case.

One of the main differences between the ocean and atmosphere, apart from the Rossby deformation scale lengths, of the order of 1000s of kms in the atmosphere and 10s of kms in the ocean, is that in the atmosphere the mean stratification is fairly uniform, whereas in the ocean, the stratification is surface intensified making Salmons two-layer model with equal layers unrealistic.

Fu and Flierl [60] studied a more realistic model to that of Salmon and Vallis, considering several baroclinic modes instead of only considering the first baroclinic mode. They found that most of the energy cascaded from the higher baroclinic modes into the first baroclinic mode at small scales, rather than directly to barotropic modes. This energy then remains in the first baroclinic mode as it cascades up to the Rossby deformation radius. However, they found that once the energy has become barotropic, it remains barotropic and increases in scale with the energy transferring into zonal modes as previously predicted.

Smith and Vallis [61] and Arbic [62] found that as the upper layer becomes thinner, energy is expected to concentrate in the first baroclinic mode and then transfer to the barotropic mode with reduced efficiency. They stated that with uniform stratification, energy in high baroclinic modes transfers "directly, quickly and almost completely" to the barotropic mode. However, for unequal layers, energy in high baroclinic modes transfers intermediately to the first baroclinic mode, from

where it transfers "inefficiently and incompletely" to the barotropic mode. This could help us to understand why, in the ocean, the first baroclinic mode is frequently energetic.

Until recently it has been very difficult to collect near-simultaneous measurements of ocean currents covering large regions over long time periods and as a result, this has made the theory-data comparisons challenging. However, the advent of satellite altimetry has meant that we can now study turbulence in the oceans more easily. Scott and Wang [63] provided the first evidence of inverse cascades observed directly in the South Pacific Ocean using sea surface height measurements from satellites. They found that, contradictory to previous theory, an inverse energy cascade takes place in the first baroclinic mode at the ocean surface but this upscale cascade would only partially reduce the forward flux of baroclinic energy.

Three dimensional general circulation models (GCMs) are currently one of the most advanced and realistic ways to study physical processes in the atmosphere and oceans. Using GCMs to study the Earths atmosphere, Schneider and Walker [64] found that there is no evidence of an inverse energy cascade beyond the scale of the linearly most unstable baroclinic waves. The barotropic energy spectrum does not exhibit the $-5/3$ spectrum at large scales that would be expected in an inverse energy cascade. They suggest that the scale at which the barotropic energy is maximal is the same order of magnitude as the Rossby radius of deformation.

Many laboratory experiments have also studied quasi-two-dimensional turbulence. Wordsworth et al. [65] investigated a differentially heated rotating annulus which was cooled and heated at its inner and outer walls, respectively, causing baroclinic instability to develop in the fluid inside. Spectral analysis of the flow indicated a distinct separation between jets and eddies in wavenumber space, with direct energy transfer occurring nonlocally between them. Berloff and Kamenkovich [66] later agreed that the transfer of energy to the jets is most likely nonlocal. Kaspi and Flierl [67] demonstrated this point by considering a truncated baroclinic model without all the intermediate length scales. They found that the model qualitatively reproduced the jets and the associated energy transfers.

Galperin et al. [68] asks how important the inverse energy cascade is for planetary

dynamics. Some recent studies suggest that energy transfer to the zonal flow need not necessarily involve an inverse cascade [69, 70] however, this research is only in its early stages.

It is also interesting to compare these results with what has been discovered on Jovian planets such as Jupiter and Saturn. Like the ocean, they have Rossby deformation radii that are very small compared to their size meaning large-scales are important. However, interior convection is thought to be the dominant forcing mechanism rather than baroclinic instability and on Jupiter, due to the absence of a solid surface and hence reduced bottom friction zonal jets can be much stronger. Schneider and Liu [71] found, using GCMs, that on Jupiter there may be an inverse energy cascade from small scales to the Rossby deformation radius [72] but not beyond it. This is similar to what was observed in the Earths atmosphere in [64], whereby the fact that the energy-containing scale coincides with the Rossby deformation radius indicates that the zonal jets form without an inverse cascade of barotropic energy.

Similar to Salmon, Arbic et al. [73, 74] considered the f-plane, i.e. no beta-effect. They demonstrated that nonlinearities in a baroclinically unstable mean flow drive energy toward lower frequencies, alongside the well-known inverse cascade to lower wavenumbers.

Salmon and Vallis studied the dynamics of the energy exchange within an individual non-resonant triad, a triad in which the frequency resonant condition (2.2) is not satisfied. However, in real geophysical turbulence many modes are excited simultaneously and therefore many coupled triads are active and mutually interacting. Such complex multi-dimensional systems call for a statistical description and this brings us to the domain of the WT approach.

For the two-layer baroclinic model, the WT approach was first introduced by Kozlov et al. [4], who derived kinetic equations for the barotropic and baroclinic Rossby wave components. They used a direct derivation with the physical variables for the normal barotropic and baroclinic modes, which meant that the resulting kinetic equations were complicated, making them difficult to use for further analysis. In the following sections, we will revisit WT theory for a two-layer ocean model.

The symmetric form of the Hamiltonian dynamical equations are derived using the waveaction variables, which allows a kinetic equation to be obtained that is compact and symmetric and therefore easier to use for modelling. The kinetic equation is then used to study Salmon's energy transfer diagram from a WT perspective, in particular considering the locality of the direct and inverse cascades. Further, we will study the situation when the baroclinic and barotropic modes are scale separated. This gives a very simple equation for the baroclinic energy spectrum, which has the form of a diffusion equation in wavenumber space. This equation can then be used to give a qualitative description of the coupled two-component system, small-scale baroclinic waves and large-scale, zonally dominated barotropic turbulence.

Let us begin this chapter by deriving the two-layer QG equations.

6.1 Derivation of the two-layer equations
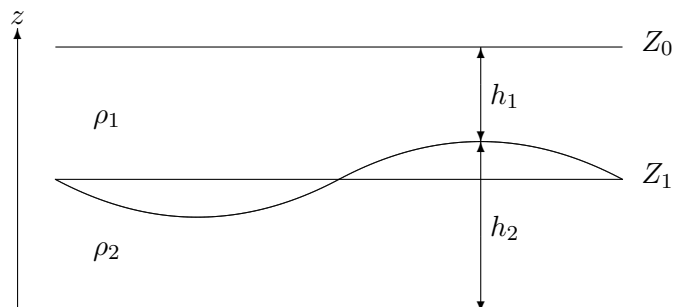
Figure 6.1: The two-layer ocean model.

The derivation of the two-layer QG equations below has the following set-up [3, 75]:

1. Consider two immiscible, i.e. unmixing fluid layers each with constant density. Let ρ_1 denote the upper layer density and ρ_2 the lower layer density where ρ_1 must be less than ρ_2 for gravitational stability.

2. Assume that there is a fluid of negligible density above this so the pressure can be taken to be zero at the surface.

3. Let h_1 and h_2 be the depth of the upper and lower layer respectively.

4. Assume a rigid-lid approximation and neglect the surface displacements compared to interface displacements.

5. Assume also a flat bottom topography.

6. The depth of the fluid in each layer is much shallower than the horizontal length and so it is assumed that hydrostatic balance applies and the pressure at any point may be found by integrating the density times gravity downward.

We start with the shallow-water momentum equation:

$$\frac{D\mathbf{u}}{Dt} + (f \times \mathbf{u}) = -\frac{1}{\rho}\nabla p, \tag{6.1}$$

where $\mathbf{u}$ is the horizontal velocity and:

$$\frac{D}{Dt} = \frac{\partial}{\partial t} + u\frac{\partial}{\partial x} + v\frac{\partial}{\partial y}. \tag{6.2}$$

The pressure in layer 1 at height z is:

$$p_1 = \rho_1 g(Z_0 - z), \tag{6.3}$$

and in layer 2 at height z:

$$p_2 = \rho_1 g(Z_0 - Z_1) + \rho_2 g(Z_1 - z) = \rho_1 g Z_0 + \rho_2 g' Z_1 - \rho_2 g z, \tag{6.4}$$

where:

$$g' = \frac{\rho_2 - \rho_1}{\rho_2}g, \tag{6.5}$$

is the reduced gravity. Using p_1 and p_2, the momentum equations for layers 1 and 2 become:

$$\frac{D\mathbf{u}_1}{Dt} + (f \times \mathbf{u}_1) = -g\nabla Z_0, \tag{6.6}$$

$$\frac{D\mathbf{u}_2}{Dt} + (f \times \mathbf{u}_2) = -\frac{\rho_1}{\rho_2}g\nabla Z_0 - g'\nabla Z_1. \tag{6.7}$$

Let us assume the Boussinesq approximation, i.e. that density differences are sufficiently small to be neglected, except where they appear in terms multiplied by g, so that $\rho_1/\rho_2 = 1$. Now take the curl of the momentum equations (6.6) and (6.7) to obtain the vorticity equation for each layer:

$$\frac{\partial(\zeta_i + f)}{\partial t} + \mathbf{u}_i.\nabla(\zeta_i + f) = -(\zeta_i + f)\nabla.\mathbf{u}_i, \quad i = 1, 2. \tag{6.8}$$

We can use the mass conservation equation:

$$\frac{Dh_i}{Dt} + h_i\nabla.\mathbf{u}_i = 0, \tag{6.9}$$

to eliminate horizontal divergence in the right-hand-side (RHS) of equation (6.8) giving:

$$\frac{\partial(\zeta_i + f)}{\partial t} + \mathbf{u}_i.\nabla(\zeta_i + f) = \frac{\zeta_i + f}{h_i}\frac{Dh_i}{Dt}. \tag{6.10}$$

Writing the LHS as a material derivative and using the product rule yields the two-layer PV equation:

$$\frac{D}{Dt}\left(\frac{\zeta_i + f}{h_i}\right) = 0, \quad i = 1, 2. \tag{6.11}$$

Therefore:

$$\frac{Dq_i}{Dt} = 0 \quad \text{where} \quad q_i = \frac{\zeta_i + f}{h_i}. \tag{6.12}$$

Let us now put this into QG form. Let the height of each layer $h_i = H_i + h_i'$ where H_i is the mean and h_i' is the perturbation and make the following assumptions:

1. The Rossby number is small, i.e. $R_0 \ll 1$.

2. Variations in thickness of each layer are small.

3. Variations in the Coriolis parameter with latitude are small.

The PV then becomes:

$$q_i = \frac{\zeta_i + f}{H_i + h_i'} = \frac{\zeta_i + f}{H_i}\left(1 + \frac{h_i'}{H_i}\right)^{-1}. \tag{6.13}$$

Since $|h_i'|/H_i \ll 1$ we can Taylor expand to get:

$$q_i = \frac{1}{H_i}\left(\zeta_i + f - \frac{\zeta_i h_i'}{H_i} - \frac{f h_i'}{H_i}\right). \tag{6.14}$$

Retaining only terms of order R_0 and letting $f = f_0$ since variations in the Coriolis parameter are small, the PV becomes:

$$q_i = \zeta_i + \beta y - f_0 \frac{h_i'}{H_i}. \tag{6.15}$$

In the QG limit the PV equation reduces to an equation containing a single dependent variable, so use the geostrophic balance equations to rewrite it in terms of the geostrophic steam function $\psi_i(x,y,t)$. Letting $Z_0 = h_1' + h_2'$ and $Z_1 = h_2'$ we get:

$$f_0 \times \mathbf{u}_1 = -g\nabla(h_1' + h_2'), \tag{6.16}$$

$$f_0 \times \mathbf{u}_2 = -g\nabla(h_1' + h_2') - g'\nabla h_2'. \tag{6.17}$$

Since the geostrophic stream function is related to the geostrophic velocities by:

$$u_g = -\frac{\partial \psi}{\partial y}, \quad v_g = \frac{\partial \psi}{\partial x}, \tag{6.18}$$

the geostrophic stream functions in each layer can be written as:

$$\psi_1 = \frac{g}{f_0}(h_1' + h_2'), \tag{6.19}$$

$$\psi_2 = \frac{g}{f_0}(h_1' + h_2') + \frac{g'}{f_0}h_2'. \tag{6.20}$$

Rewriting the layer depths in terms of the stream functions we get:

$$h_2' = \frac{f_0}{g'}(\psi_2 - \psi_1), \tag{6.21}$$

$$h_1' = \frac{f_0}{g'}(\psi_1 - \psi_2), \tag{6.22}$$

where we have assumed $g'/g \ll 1$. The relative vorticity ζ_i can also be rewritten in terms of the stream function:

$$
\begin{aligned}
\zeta_i &= \frac{\partial v_g}{\partial x} - \frac{\partial u_g}{\partial y} &\text{(6.23)}\\
&= \frac{\partial^2 \psi}{\partial x^2} + \frac{\partial^2 \psi}{\partial y^2}\\
&= \nabla^2 \psi_i.
\end{aligned}
$$

Substituting (6.21-6.23) into (6.15) we arrive at the QG version of the PV in terms of the stream function:

$$
\frac{Dq_i}{Dt} = \frac{\partial q_i}{\partial t} + J[\psi_i, q_i] = 0, \tag{6.24}
$$

where $J[a,b] = \partial_x a \partial_y b - \partial_y a \partial_x b$ is the nonlinear Jacobian and:

$$
q_1 = \nabla^2 \psi_1 + \beta y - \frac{f_0^2}{g' H_1}(\psi_1 - \psi_2), \tag{6.25}
$$

$$
q_2 = \nabla^2 \psi_2 + \beta y + \frac{f_0^2}{g' H_2}(\psi_1 - \psi_2). \tag{6.26}
$$

Putting it all together and rewriting $\frac{\partial}{\partial t}\beta y$ as $\beta v = \beta \frac{\partial \psi_i}{\partial x}$ gives the QG PV equations for a two-layer fluid:

$$
\frac{\partial}{\partial t}\left[\nabla^2 \psi_1 + \frac{f_0^2}{g' H_1}(\psi_2 - \psi_1)\right] + \beta \frac{\partial \psi_1}{\partial x} = -J\left[\psi_1, \nabla^2 \psi_1 + \frac{f_0^2}{g' H_1}(\psi_2 - \psi_1)\right], \tag{6.27}
$$

$$
\frac{\partial}{\partial t}\left[\nabla^2 \psi_2 + \frac{f_0^2}{g' H_2}(\psi_1 - \psi_2)\right] + \beta \frac{\partial \psi_2}{\partial x} = -J\left[\psi_2, \nabla^2 \psi_2 + \frac{f_0^2}{g' H_2}(\psi_1 - \psi_2)\right]. \tag{6.28}
$$

6.2 Derivation of the baroclinic kinetic equation

For the kinetic framework to be used, these equations must first be modified so that each linear part contains only one unknown function. Doing this is equivalent to introducing normal modes:

$$
\psi^\sigma = \psi_1 + s^\sigma \psi_2, \quad \sigma = +, - \tag{6.29}
$$

where $\psi^+ = \psi_1 + s^+ \psi_2$ is the barotropic normal mode and $\psi^- = \psi_1 + s^- \psi_2$ is the baroclinic normal mode. Kozlov et al. [4] used this approach to derive the following

equation (for the working see appendix A):

$$\frac{\partial}{\partial t}(\nabla^2 \psi^\sigma - F^\sigma \psi^\sigma) + \beta \frac{\partial \psi^\sigma}{\partial x} = -\lambda \sum_{\mu\nu} [p^\sigma_{\mu\nu} J(\psi^\mu, \nabla^2 \psi^\nu) + F^\sigma g^\sigma_{\mu\nu} J(\psi^\mu, \psi^\nu)], \quad (6.30)$$

where $\lambda = \frac{1}{(s^+ - s^-)^2}$ and:

$$p^+_{++} = s^+ + (s^-)^2, \quad p^+_{--} = s^+(1 + s^+), \quad (6.31)$$

$$p^-_{++} = s^-(1 + s^-), \quad p^-_{--} = s^- + (s^+)^2,$$

$$p^+_{+-} = -s^+(1 + s^-) = p^+_{-+}, \quad p^-_{+-} = -s^-(1 + s^+) = p^-_{-+},$$

$$g^+_{+-} = -g^+_{-+} = -\frac{1}{2}(s^+ - s^-) = g^-_{+-} = -g^-_{-+}.$$

These are known as the coupling coefficients because they describe the intensity of coupling between different modes.

$$F^\sigma = \frac{f_0^2}{g' H_1} - \frac{f_0^2}{g' H_2} s^\sigma, \quad (6.32)$$

where $(F^\sigma)^{-1/2}$ are the barotropic ($\sigma = +$) and the baroclinic ($\sigma = -$) Rossby deformation radii respectively. Here, $s^\pm$ are solutions of the following quadratic equation:

$$\frac{1}{H_2} s^2 + \left(\frac{1}{H_2} - \frac{1}{H_1}\right) s - \frac{1}{H_1} = 0, \quad (6.33)$$

hence:

$$s^+ \simeq \frac{H_2}{H_1} \quad \text{and} \quad s^- \simeq -1. \quad (6.34)$$

6.2.1 Fourier space

Now put equation (6.30) into Fourier space. As before, let the system be in a periodic box, with period L in both directions. Fourier series representation of the barotropic and baroclinic stream function is as follows:

$$\psi^\sigma(\mathbf{x}, t) = \sum_{\mathbf{k}} \hat{\psi}^\sigma(\mathbf{k}, t) e^{i\mathbf{k}\cdot\mathbf{x}}, \quad (6.35)$$

with Fourier coefficients:

$$\hat{\psi}^\sigma(\mathbf{k}, t) = \frac{1}{L^2} \int_{Box} \psi^\sigma(\mathbf{x}, t) e^{-i\mathbf{k}\cdot\mathbf{x}} d\mathbf{x}. \tag{6.36}$$

Fourier transforming equation (6.30) gives:

$$
\frac{\partial}{\partial t}(-k^2 - F^\sigma)\hat{\psi}^\sigma_{\mathbf{k}} + i\beta k_x \hat{\psi}^\sigma_{\mathbf{k}} = -\lambda \sum_{\mu\nu} \sum_{12} [p^\sigma_{\mu\nu}(k_{1x}k_{2y}k_2^2 - k_{1y}k_{2x}k_2^2) \tag{6.37}
$$
$$
+ F^\sigma g^\sigma_{\mu\nu}(k_{1x}k_{2y} - k_{1y}k_{2x})]\hat{\psi}^\mu_1 \hat{\psi}^\nu_2 \delta^{\mathbf{k}}_{12}.
$$

Finally dividing by $-(k^2 + F^\sigma)$ we get:

$$\partial_t \hat{\psi}^\sigma_{\mathbf{k}} + i\omega^\sigma_{\mathbf{k}} \hat{\psi}^\sigma_{\mathbf{k}} = \lambda \sum_{\mu\nu} \sum_{12} D^{\sigma\mu\nu}_{12} \hat{\psi}^\mu_1 \hat{\psi}^\nu_2 \delta^{\mathbf{k}}_{12}, \tag{6.38}$$

where:

$$\delta^{\mathbf{k}}_{12} = \delta(\mathbf{k} - \mathbf{k}_1 - \mathbf{k}_2), \tag{6.39}$$

$$\omega^\sigma_{\mathbf{k}} = -\frac{\beta k_x}{k^2 + F^\sigma}, \tag{6.40}$$

$$D^{\sigma\mu\nu}_{12} = \frac{C^{\sigma\mu\nu}_{12}}{k^2 + F^\sigma}, \tag{6.41}$$

$$C^{\sigma\mu\nu}_{12} = \frac{1}{2}p^\sigma_{\mu\nu}(\mathbf{k}_1 \times \mathbf{k}_2)_z(k_2^2 - k_1^2 + F^\nu - F^\mu). \tag{6.42}$$

We will now take equation (6.38) and introduce canonical variables then symmetrize it. Putting it in symmetric form is an important new step with respect to Kozlov et al. [4] because after symmetrization, as we have seen for the one layer case, derivation of the kinetic equation becomes a standard operation [12, 27].

6.2.2 Introducing the waveaction variable and symmetrization

Now introduce the waveaction variable:

$$a^\pm_{\mathbf{k}} = \frac{(k^2 + F^\pm)}{\sqrt{|\beta k_x s^\pm|}} \hat{\psi}^\pm_{\mathbf{k}}. \tag{6.43}$$

Substituting this into equation (6.38) gives:

$$\dot{a}_{\mathbf{k}}^{\sigma} + i\omega_{\mathbf{k}}^{\sigma} a_{\mathbf{k}}^{\sigma} = -\frac{\lambda}{2} \operatorname{sign}(k_x) \sum_{\mu\nu} \sum_{12} p_{\mu\nu}^{\sigma} |k_{1x} k_{2x} k_x|^{1/2} \bar{a}_1^{\mu} \bar{a}_2^{\nu} |\beta|^{1/2} \left| \frac{s^{\mu} s^{\nu}}{s^{\sigma}} \right|^{1/2} \quad (6.44)$$

$$\times \left(\frac{k_{2y}}{k_1^2 + F^{\mu}} - \frac{k_{2y}}{k_2^2 + F^{\nu}} - \frac{k_{2x} k_y / k_x}{k_1^2 + F^{\mu}} + \frac{k_{2x} k_y / k_x}{k_2^2 + F^{\nu}} \right) \delta_{\mathbf{k}12}.$$

To make the equation more symmetric rewrite the Kronecker delta, $\delta_{12}^{\mathbf{k}} = \delta(\mathbf{k} - \mathbf{k}_1 - \mathbf{k}_2)$ as $\delta_{\mathbf{k}12} = \delta(\mathbf{k} + \mathbf{k}_1 + \mathbf{k}_2)$. In order to do this change $\mathbf{k}_1 \to -\mathbf{k}_1$ and $\mathbf{k}_2 \to -\mathbf{k}_2$. Consequently $a_{-\mathbf{k}_1} = \bar{a}_{\mathbf{k}_1}$ and $a_{-\mathbf{k}_2} = \bar{a}_{\mathbf{k}_2}$, where $\bar{a}$ is now used to denote the complex conjugate instead of a^*. Finally, symmetrize under the assumption that dominant interactions occur on the resonant manifold, i.e. the resonant condition $-\omega_{\mathbf{k}}^{\sigma} = \omega_1^{\mu} + \omega_2^{\nu}$ is correct to get:

$$\dot{a}_{\mathbf{k}}^{\sigma} + i\omega_{\mathbf{k}}^{\sigma} a_{\mathbf{k}}^{\sigma} = \operatorname{sign}(k_x) \sum_{\mu\nu} \sum_{12} V_{\mathbf{k}12}^{\sigma\mu\nu} p_{\mu\nu}^{\sigma} \bar{a}_1^{\mu} \bar{a}_2^{\nu} \left| \frac{s^{\mu} s^{\nu}}{s^{\sigma}} \right|^{1/2} \delta_{\mathbf{k}12}, \quad (6.45)$$

where:

$$V_{12}^{\sigma\mu\nu} = \frac{\lambda}{2} \sqrt{|\beta k_x k_{1x} k_{2x}|} \left(\frac{k_{1y}}{k_1^2 + F^{\mu}} + \frac{k_{2y}}{k_2^2 + F^{\nu}} + \frac{k_y}{k^2 + F^{\sigma}} \right), \quad (6.46)$$

is the nonlinear interaction coefficient for the waveaction variable. For a more detailed derivation of this see appendix B.

6.2.3 Time-scale separation

Rewrite equation (6.45) in terms of an interaction representation variable:

$$b_{\mathbf{k}}^{\pm} = a_{\mathbf{k}}^{\pm} e^{i\omega_{\mathbf{k}}^{\pm} t}, \quad (6.47)$$

to obtain the following:

$$i\dot{b}_{\mathbf{k}}^{\sigma} = \operatorname{sign}(k_x) \sum_{\mu\nu} \sum_{12} V_{\mathbf{k}12}^{\sigma\mu\nu} p_{\mu\nu}^{\sigma} \bar{b}_1^{\mu} \bar{b}_2^{\nu} e^{i\omega_{\mathbf{k}12}^{\sigma\mu\nu} t} \left| \frac{s^{\mu} s^{\nu}}{s^{\sigma}} \right|^{1/2} \delta_{\mathbf{k}12}, \quad (6.48)$$

89

where $\omega_{\mathbf{k}12}^{\sigma\mu\nu} = \omega_{\mathbf{k}}^{\sigma} + \omega_1^{\mu} + \omega_2^{\nu}$. Assume that the wave amplitudes are small and non-linearity is weak, and separate the linear and nonlinear time scales as follows:

$$\tau_L = \frac{2\pi}{\omega_{\mathbf{k}}} \ll \tau_{NL} = \frac{2\pi}{\epsilon^2\omega_{\mathbf{k}}}, \tag{6.49}$$

in order to filter out the fast oscillatory motions and describe the slowly changing wave statistics. Now introduce an intermediate time $T = 2\pi/\epsilon\omega_{\mathbf{k}}$ and find a solution for the wave amplitudes $b_{\mathbf{k}}^{\pm}$ at time $t = T$ using the following expansion in the small nonlinearity parameter $\epsilon \ll 1$ [12]:

$$b_{\mathbf{k}}^{\pm}(T) = b_{\mathbf{k}}^{\pm(0)} + \epsilon b_{\mathbf{k}}^{\pm(1)} + \epsilon^2 b_{\mathbf{k}}^{\pm(2)} + ... \tag{6.50}$$

The first term in the expansion $O(\epsilon^0)$ corresponds to the linear approximation in which the interaction representation amplitude is time independent:

$$b_{\mathbf{k}}^{\pm(0)}(T) = b_{\mathbf{k}}^{\pm(0)}(0). \tag{6.51}$$

Now substitute $b_{\mathbf{k}}^{\pm(0)}$ into the RHS of equation (6.48) to get $O(\epsilon^1)$:

$$i\dot{b}_{\mathbf{k}}^{\sigma(1)} = \text{sign}(k_x) \sum_{\mu\nu} \sum_{12} V_{\mathbf{k}12}^{\sigma\mu\nu} p_{\mu\nu}^{\sigma} \bar{b}_1^{\mu(0)} \bar{b}_2^{\nu(0)} e^{i\omega_{\mathbf{k}12}^{\sigma\mu\nu}t} \left| \frac{s^{\mu}s^{\nu}}{s^{\sigma}} \right|^{1/2} \delta_{\mathbf{k}12}, \tag{6.52}$$

and integrate to get:

$$b_{\mathbf{k}}^{\sigma(1)}(T) = -i\,\text{sign}(k_x) \sum_{\mu\nu} \sum_{12} V_{\mathbf{k}12}^{\sigma\mu\nu} p_{\mu\nu}^{\sigma} \bar{b}_1^{\mu(0)} \bar{b}_2^{\nu(0)} \Delta_T(\omega_{\mathbf{k}12}^{\sigma\mu\nu}) \left| \frac{s^{\mu}s^{\nu}}{s^{\sigma}} \right|^{1/2} \delta_{\mathbf{k}12}, \tag{6.53}$$

where all time dependence is contained in the integral:

$$\Delta_T(\omega_{\mathbf{k}12}^{\sigma\mu\nu}) = \int\limits_0^T e^{i\omega_{\mathbf{k}12}^{\sigma\mu\nu}t}dt. \tag{6.54}$$

The $O(\epsilon^2)$ term is:

$$i\dot{b}_{\mathbf{k}}^{\sigma(2)} = 2\,\text{sign}(k_x) \sum_{\mu\nu} \sum_{12} V_{\mathbf{k}12}^{\sigma\mu\nu} p_{\mu\nu}^{\sigma} \bar{b}_1^{\mu(1)} \bar{b}_2^{\nu(0)} e^{i\omega_{\mathbf{k}12}^{\sigma\mu\nu}t} \left| \frac{s^{\mu}s^{\nu}}{s^{\sigma}} \right|^{1/2} \delta_{\mathbf{k}12}, \tag{6.55}$$

where the two arises due to the symmetry with respect to changing indices $1 \leftrightarrow 2$. Substitute $b_{\mathbf{k}}^{\sigma(1)}$ from equation (6.53) into (6.55) and integrate to get:

$$
\begin{aligned}
b_{\mathbf{k}}^{\sigma(2)}(T) &= -2\,\mathrm{sign}(k_x k_{1x}) \sum_{\mu\nu} \sum_{1234} V_{\mathbf{k}12}^{\sigma\mu\nu} V_{134}^{\nu\sigma\mu} p_{\mu\nu}^{\sigma} p_{\sigma\mu}^{\nu} |s^{\mu}| \qquad (6.56) \\
&\quad \times \bar{b}_2^{\nu(0)} b_3^{\mu(0)} b_4^{\nu(0)} E(\omega_{134}^{\nu\sigma\mu}, \omega_{\mathbf{k}12}^{\sigma\mu\nu}) \delta_{\mathbf{k}12} \delta_{134},
\end{aligned}
$$

where:

$$
E(\omega_{134}^{\nu\sigma\mu}, \omega_{\mathbf{k}12}^{\sigma\mu\nu}) = \int_0^T \Delta_T(\omega_{134}^{\nu\sigma\mu}) e^{i\omega_{\mathbf{k}12}^{\sigma\mu\nu} t} dt. \qquad (6.57)
$$

We do not need to find higher-order terms in the expansion since a non-trivial closure arises in the order ϵ^2.

6.2.4 Statistical averaging

Let us now replace the dynamical description of the wave system by a statistical one in terms of the correlation functions of the field. Begin by carrying out a weak nonlinearity expansion at the intermediate time T as follows:

$$
\begin{aligned}
\langle |b_{\mathbf{k}}^{\pm}(T)|^2 \rangle &= \langle |b_{\mathbf{k}}^{\pm(0)} + \epsilon b_{\mathbf{k}}^{\pm(1)} + \epsilon^2 b_{\mathbf{k}}^{\pm(2)}|^2 \rangle \qquad (6.58) \\
&= \langle |b_{\mathbf{k}}^{\pm(0)}|^2 + \epsilon(|\bar{b}_{\mathbf{k}}^{\pm(0)} b_{\mathbf{k}}^{\pm(1)}| + c.c.) + \epsilon^2 |b_{\mathbf{k}}^{\pm(1)}|^2 + \epsilon^2(|\bar{b}_{\mathbf{k}}^{\pm(0)} b_{\mathbf{k}}^{\pm(2)}| + c.c.) \rangle,
\end{aligned}
$$

where $\langle \rangle$ denotes the average. Now perform statistical averaging over the random phases and amplitudes, starting with the former. The ϵ^1 term using equation (6.53) is:

$$
\begin{aligned}
\langle |\bar{b}_{\mathbf{k}}^{\pm(0)} b_{\mathbf{k}}^{\pm(1)}| \rangle_{\varphi} &= -i\,\mathrm{sign}(k_x) \sum_{\mu\nu} \sum_{\mathbf{k}12} V_{\mathbf{k}12}^{\sigma\mu\nu} p_{\mu\nu}^{\sigma} \left| \frac{s^{\mu} s^{\nu}}{s^{\sigma}} \right|^{1/2} \qquad (6.59) \\
&\quad \times \langle \bar{b}_{\mathbf{k}}^{\pm(0)} \bar{b}_1^{\mu(0)} \bar{b}_2^{\nu(0)} \rangle_{\varphi} \Delta_T(\omega_{\mathbf{k}12}^{\sigma\mu\nu}) \delta_{\mathbf{k}12} + c.c.
\end{aligned}
$$

Wick's contraction rule [12] states that $\langle \psi_{l1}, \psi_{l2}, ..., \bar{\psi}_{m1}, \bar{\psi}_{m2} \rangle$ is zero unless the number of ψ's in it equals the number of $\bar{\psi}$'s. So by Wick's contraction rule, since the correlation function in equation (6.59) has an odd number of terms, it and its complex conjugate are zero.

The first ϵ^2 term is:

$$
\begin{aligned}
\langle |b_\mathbf{k}^{\pm(1)}|^2 \rangle_\varphi &= \sum_{\mu\nu} \sum_{1234} V_{\mathbf{k}12}^{\sigma\mu\nu} \bar{V}_{\mathbf{k}34}^{\sigma\mu\nu} (p_{\mu\nu}^\sigma)^2 \left| \frac{s^\mu s^\nu}{s^\sigma} \right| \langle b_1^{\mu(0)} b_2^{\nu(0)} \bar{b}_3^{\mu(0)} \bar{b}_4^{\nu(0)} \rangle_\varphi \quad (6.60) \\
&\times \Delta_T(\omega_{\mathbf{k}12}^{\sigma\mu\nu}) \bar{\Delta}_T(\omega_{\mathbf{k}34}^{\sigma\mu\nu}) \delta_{\mathbf{k}12} \delta_{\mathbf{k}34}.
\end{aligned}
$$

Look for combinations of wave vectors in the fourth-order correlator $\langle b_1^{\mu(0)} b_2^{\nu(0)} \bar{b}_3^{\mu(0)} \bar{b}_4^{\nu(0)} \rangle_\varphi$ that give a non-zero phase average. Replacing the four-point function by a product of two two-point functions gives:

$$
\begin{aligned}
\langle b_1^{\mu(0)} b_2^{\nu(0)} \bar{b}_3^{\mu(0)} \bar{b}_4^{\nu(0)} \rangle &= \langle b_1^{\mu(0)} \bar{b}_3^{\mu(0)} \rangle \langle b_2^{\nu(0)} \bar{b}_4^{\nu(0)} \rangle \quad (6.61) \\
&+ \langle b_1^{\mu(0)} \bar{b}_4^{\nu(0)} \rangle \langle b_2^{\nu(0)} \bar{b}_3^{\mu(0)} \rangle + \langle b_1^{\mu(0)} \bar{b}_{-2}^{\nu(0)} \rangle \langle \bar{b}_3^{\mu(0)} b_{-4}^{\nu(0)} \rangle,
\end{aligned}
$$

i.e. wavenumbers $\mathbf{k}_1 = \mathbf{k}_3$ and $\mathbf{k}_2 = \mathbf{k}_4$ or $\mathbf{k}_1 = \mathbf{k}_4$ and $\mathbf{k}_2 = \mathbf{k}_3$. Since $\bar{b}_\mathbf{k} = b_{-\mathbf{k}}$, there is also $\mathbf{k}_1 = -\mathbf{k}_2$ and $\mathbf{k}_3 = -\mathbf{k}_4$. The first two are the same from the $1 \leftrightarrow 2$ symmetry. The last combination has zero deltas because $\mathbf{k}_1 = -\mathbf{k}_2 \Rightarrow \mathbf{k} - \mathbf{k}_2 + \mathbf{k}_2 = 0$, which is impossible since $\mathbf{k} \neq 0$, and similarly for $\mathbf{k}_3 = -\mathbf{k}_4$.

Now define the amplitude:

$$
J_\mathbf{k}^\pm = |b_\mathbf{k}^\pm|^2, \quad (6.62)
$$

and substitute it into equation (6.60):

$$
\langle |b_\mathbf{k}^{\pm(1)}|^2 \rangle_\varphi = 2 \sum_{\mu\nu} \sum_{12} |V_{\mathbf{k}12}^{\sigma\mu\nu}|^2 (p_{\mu\nu}^\sigma)^2 \left| \frac{s^\mu s^\nu}{s^\sigma} \right| J_1^\mu J_2^\nu |\Delta_T(\omega_{\mathbf{k}12}^{\sigma\mu\nu})|^2 \delta_{\mathbf{k}12}. \quad (6.63)
$$

The second ϵ^2 term is found using equation (6.56) and is:

$$
\begin{aligned}
\langle |\bar{b}_\mathbf{k}^{\pm(0)} b_\mathbf{k}^{\pm(2)}| \rangle_\varphi &= -2 \, \text{sign}(k_x k_{1x}) \sum_{\mu\nu} \sum_{1234} V_{\mathbf{k}12}^{\sigma\mu\nu} V_{134}^{\nu\sigma\mu} p_{\mu\nu}^\sigma p_{\sigma\mu}^\nu |s^\mu| \quad (6.64) \\
&\times \langle \bar{b}_\mathbf{k}^{\pm(0)} \bar{b}_2^{\nu(0)} b_3^{\mu(0)} b_4^{\nu(0)} \rangle_\varphi E(\omega_{134}^{\nu\sigma\mu}, \omega_{\mathbf{k}12}^{\sigma\mu\nu}) \delta_{\mathbf{k}12} \delta_{134} + c.c.
\end{aligned}
$$

Again, look for combinations of wave vectors in the fourth order correlator $\langle \bar{b}_\mathbf{k}^{\pm(0)} \bar{b}_2^{\nu(0)} b_3^{\mu(0)} b_4^{\nu(0)} \rangle_\varphi$ that give a non-zero phase average. There is $\mathbf{k} = \mathbf{k}_3$ and $\mathbf{k}_2 = \mathbf{k}_4$ or $\mathbf{k} = \mathbf{k}_4$ and $\mathbf{k}_2 = \mathbf{k}_3$ or $\mathbf{k} = -\mathbf{k}_2$ and $\mathbf{k}_3 = -\mathbf{k}_4$. The first two are the same from the $3 \leftrightarrow 4$ symmetry. The last combination is ruled out as the deltas are

zero, so the second ϵ^2 term becomes:

$$\langle|\bar{b}_{\mathbf{k}}^{\pm(0)}b_{\mathbf{k}}^{\pm(2)}|\rangle_\varphi = -4 \,\text{sign}(k_x k_{1x}) \sum_{\mu\nu}\sum_{12}|V_{\mathbf{k}12}^{\sigma\mu\nu}|^2 p_{\mu\nu}^\sigma p_{\sigma\mu}^\nu |s^\mu| \quad (6.65)$$
$$\times J_{\mathbf{k}}^\sigma J_2^\nu E(\omega_{134}^{\nu\sigma\mu}, \omega_{\mathbf{k}12}^{\sigma\mu\nu})\delta_{\mathbf{k}12}.$$

Finally, perform amplitude averaging and introduce the wave spectrum:

$$\langle J_{\mathbf{k}}^\pm\rangle = \left(\frac{2\pi}{L}\right)^2 n_{\mathbf{k}}^\pm, \quad (6.66)$$

into equations (6.63) and (6.65). Combining the resulting equations gives:

$$\langle|b_{\mathbf{k}}^\pm(T)|^2 - |b_{\mathbf{k}}^\pm(0)|^2\rangle = 2\left(\frac{2\pi}{L}\right)^4 \sum_{\mu\nu}\sum_{12}|V_{\mathbf{k}12}^{\sigma\mu\nu}|^2 (p_{\mu\nu}^\sigma)^2\left|\frac{s^\mu s^\nu}{s^\sigma}\right| \quad (6.67)$$
$$\times n_1^\mu n_2^\nu |\Delta_T(\omega_{\mathbf{k}12}^{\sigma\mu\nu})|^2\delta_{\mathbf{k}12} - 4\left(\frac{2\pi}{L}\right)^4 \text{sign}(k_x k_{1x})\sum_{\mu\nu}\sum_{12}$$
$$\times |V_{\mathbf{k}12}^{\sigma\mu\nu}|^2 p_{\mu\nu}^\sigma p_{\sigma\mu}^\nu |s^\mu| n_{\mathbf{k}}^\sigma n_2^\nu E(\omega_{134}^{\nu\sigma\mu}, \omega_{\mathbf{k}12}^{\sigma\mu\nu})\delta_{\mathbf{k}12}.$$

Take the large-box limit ($L \to \infty$) where:

$$\sum_{12} \to \int d\mathbf{k}_1 d\mathbf{k}_2 \left(\frac{L}{2\pi}\right)^4, \quad (6.68)$$

to get:

$$\langle|b_{\mathbf{k}}^\pm(T)|^2 - |b_{\mathbf{k}}^\pm(0)|^2\rangle = 2\sum_{\mu\nu}\int|V_{\mathbf{k}12}^{\sigma\mu\nu}|^2 (p_{\mu\nu}^\sigma)^2\left|\frac{s^\mu s^\nu}{s^\sigma}\right| n_1^\mu n_2^\nu \quad (6.69)$$
$$\times |\Delta_T(\omega_{\mathbf{k}12}^{\sigma\mu\nu})|^2\delta_{\mathbf{k}12}d\mathbf{k}_{12} - 4\,\text{sign}(k_x k_{1x})\sum_{\mu\nu}\int|V_{\mathbf{k}12}^{\sigma\mu\nu}|^2$$
$$\times p_{\mu\nu}^\sigma p_{\sigma\mu}^\nu |s^\mu| n_{\mathbf{k}}^\sigma n_2^\nu E(\omega_{134}^{\nu\sigma\mu}, \omega_{\mathbf{k}12}^{\sigma\mu\nu})\delta_{\mathbf{k}12}d\mathbf{k}_{12}.$$

Then take the weak nonlinearity limit ($\epsilon \to 0$) such that intermediate time $T \to \infty$, giving:

$$|\Delta_T(\omega_{\mathbf{k}12}^{\sigma\mu\nu})|^2 \to 2\pi T\delta(\omega_{\mathbf{k}12}^{\sigma\mu\nu}) \quad \text{and} \quad E(\omega_{134}^{\nu\sigma\mu}, \omega_{\mathbf{k}12}^{\sigma\mu\nu}) \to 2\pi T\delta(\omega_{\mathbf{k}12}^{\sigma\mu\nu}), \quad (6.70)$$

in equation (6.69). Next define:

$$\frac{\partial n_{\mathbf{k}}^{\pm}}{\partial t} \simeq \frac{\langle |b_{\mathbf{k}}^{\pm}(T)|^2 - |b_{\mathbf{k}}^{\pm}(0)|^2 \rangle}{T},$$

(6.71)

and putting it all together gives the two-layer kinetic equation:

$$\frac{\partial n_{\mathbf{k}}^{\sigma}}{\partial t} = 4\pi \sum_{\mu\nu} \int |V_{\mathbf{k}12}^{\sigma\mu\nu}|^2 [(p_{\mu\nu}^{\sigma})^2 \left| \frac{s^{\mu}s^{\nu}}{s^{\sigma}} \right| n_1^{\mu} n_2^{\nu}$$

$$- 2p_{\mu\nu}^{\sigma} p_{\sigma\mu}^{\nu} |s^{\mu}| n_{\mathbf{k}}^{\sigma} n_1^{\mu} \text{sign}(k_x k_{2x})] \delta(\omega_{\mathbf{k}12}^{\sigma\mu\nu}) \delta_{\mathbf{k}12} d\mathbf{k}_{12}.$$

(6.72)

Now take the eight different combinations of $\sigma, \mu, \nu = \pm$, i.e. $\{++-\}, \{-++\}, \{--+\}, \{+--\}, \{+-+\}, \{-+-\}, \{+++\}, \{---\}$ and substitute the coupling coefficients $p_{\mu\nu}^{\sigma}$ from (6.31) into equation (6.72). We finally obtain the two-layer kinetic equation in symmetric form:

$$\frac{\partial n_{\mathbf{k}}^{\sigma}}{\partial t} = \sum_{\mu\nu} \int W_{\mathbf{k}12}^{\sigma\mu\nu} n_1^{\mu} [n_2^{\nu} + 2n_{\mathbf{k}}^{\sigma} \text{sign}(k_x k_{2x})] \delta(\omega_{\mathbf{k}12}^{\sigma\mu\nu}) \delta_{\mathbf{k}12} d\mathbf{k}_{12}.$$

(6.73)

Here:

$$W_{\mathbf{k}12}^{++-} = 4\pi |V_{\mathbf{k}12}^{++-}|^2 (1 + s^-)^2 (s^+)^2 s^-,$$

(6.74)

and the same for permutations of $+, +$ and $-$.

Symmetrically,

$$W_{\mathbf{k}12}^{+--} = 4\pi |V_{\mathbf{k}12}^{+--}|^2 (1 + s^+)^2 (s^-)^2 s^+,$$

(6.75)

and the same for permutations of $-, -$ and $+$.

$$W_{\mathbf{k}12}^{+++} = 4\pi |V_{\mathbf{k}12}^{+++}|^2 (s^+ + (s^-)^2) s^+,$$

(6.76)

and symmetrically,

$$W_{\mathbf{k}12}^{---} = 4\pi |V_{\mathbf{k}12}^{---}|^2 (s^- + (s^+)^2) s^-.$$

(6.77)

We are considering a model of the ocean in which the top layer is significantly thinner than the bottom layer, i.e. $H_1 \ll H_2$. This is more realistic than equal layers,

as typical layer depths have a ratio of $1:7$ [52]. As a result:

$$s^- \simeq -1 \quad \text{and} \quad s^+ \simeq \frac{H_2}{H_1} \gg 1. \tag{6.78}$$

Substituting s^- into $W_{\mathbf{k}12}^{++-}$, it can be seen that it vanishes. Since $s^+ \gg 1$, $W_{\mathbf{k}12}^{+--}$ is the most dominant term, since it contains an $(s^+)^3$ term and $W_{\mathbf{k}12}^{+++}$ and $W_{\mathbf{k}12}^{---}$ only contain $(s^+)^2$ terms. Hence, leaving only permutations of $\{+--\}$, the two-layer kinetic equation (6.73) reduces to the following:

$$\partial_t n_{\mathbf{k}}^+ = \int W_{\mathbf{k}12}^{+--}[n_1^- n_2^- + 2n_1^- n_{\mathbf{k}}^+ sign(k_x k_{2x})]\delta(\omega_{\mathbf{k}}^+ + \omega_1^- + \omega_2^-) \tag{6.79}$$
$$\times \delta(\mathbf{k} + \mathbf{k}_1 + \mathbf{k}_2)d\mathbf{k}_{12},$$

$$\partial_t n_{\mathbf{k}}^- = \int W_{\mathbf{k}12}^{-+-}[n_1^+ n_2^- + n_1^+ n_{\mathbf{k}}^- sign(k_x k_{2x}) + n_2^- n_{\mathbf{k}}^- sign(k_x k_{1x})] \tag{6.80}$$
$$\times \delta(\omega_{\mathbf{k}}^- + \omega_1^+ + \omega_2^-)\delta(\mathbf{k} + \mathbf{k}_1 + \mathbf{k}_2)d\mathbf{k}_{12}.$$

Here, $\{+--\}$ is a triad with two baroclinic components and one barotropic component. In the barotropic part of the kinetic equation (6.79), $\mathbf{k}$ is the barotropic wavenumber and $\mathbf{k}_1, \mathbf{k}_2$ are the baroclinic wavenumbers. In the baroclinic part (6.80), $\mathbf{k}_1$ is the barotropic wavenumber and $\mathbf{k}, \mathbf{k}_2$ are the baroclinic wavenumbers. Equally, it could be $W_{\mathbf{k}12}^{--+}$ in (6.80) so that $\mathbf{k}_2$ is then the barotropic wavenumber and $\mathbf{k}, \mathbf{k}_1$ are the baroclinic wavenumbers.

Equations (6.79) and (6.80) have never been derived or studied before. We will now go on and use these kinetic equations to better understand the transfer of energy between the barotropic and baroclinic modes in the two-layer ocean model from a WT perspective. From their derivation, it can be seen that, in the case of a thin upper layer, the most dominant triad is $\{+--\}$ and therefore this triad will be considered in the most detail, even though $\{+++\}$ and $\{---\}$ triads may of course exist.

6.2.5 Conservation of energy and potential enstrophy

The two-layer kinetic equation (6.73) conserves the total (barotropic plus baroclinic) energy:

$$E = \sum_\sigma \int |\omega_{\mathbf{k}}^\sigma| n_{\mathbf{k}}^\sigma d\mathbf{k}, \tag{6.81}$$

and the total potential enstrophy:

$$\Omega = \sum_\sigma \int |k_x| n_{\mathbf{k}}^\sigma d\mathbf{k}. \tag{6.82}$$

To prove this, substitute equation (6.73):

$$\dot{n}_{\mathbf{k}}^\sigma = \sum_{\mu\nu} \int W_{\mathbf{k}12}^{\sigma\mu\nu}[n_1^\mu n_2^\nu + n_{\mathbf{k}}^\sigma n_1^\mu \mathrm{sign}(\omega_{\mathbf{k}}\omega_2) + n_{\mathbf{k}}^\sigma n_2^\nu \mathrm{sign}(\omega_{\mathbf{k}}\omega_1)]\delta(\omega_{\mathbf{k}12}^{\sigma\mu\nu})\delta_{\mathbf{k}12} d\mathbf{k}_{12}, \tag{6.83}$$

into (6.81) and (6.82):

$$
\begin{aligned}
\dot{E} &= \sum_\sigma \int |\omega_{\mathbf{k}}^\sigma| \dot{n}_{\mathbf{k}}^\sigma d\mathbf{k} \\
&= \sum_{\sigma\mu\nu} \int \omega_{\mathbf{k}}^\sigma \mathrm{sign}(\omega_{\mathbf{k}}) W_{\mathbf{k}12}^{\sigma\mu\nu}[n_1^\mu n_2^\nu + n_{\mathbf{k}}^\sigma n_1^\mu \mathrm{sign}(\omega_{\mathbf{k}}\omega_2) + n_{\mathbf{k}}^\sigma n_2^\nu \mathrm{sign}(\omega_{\mathbf{k}}\omega_1)] \\
&\qquad \times \delta(\omega_{\mathbf{k}12}^{\sigma\mu\nu})\delta_{\mathbf{k}12} d\mathbf{k}_{12}.
\end{aligned} \tag{6.84}
$$

Exchanging $\mathbf{k} \leftrightarrow \mathbf{k}_3$ we have:

$$\sum_{\sigma\mu\nu} \int W_{312}^{\sigma\mu\nu}[n_1^\mu n_2^\nu \omega_3^\sigma \mathrm{sign}(\omega_3) + n_3^\sigma n_1^\mu \omega_3^\sigma \mathrm{sign}(\omega_2) + n_3^\sigma n_2^\nu \omega_3^\sigma \mathrm{sign}(\omega_1)] \tag{6.85}$$
$$\times \delta(\omega_{312}^{\sigma\mu\nu})\delta_{312} d\mathbf{k}_{123},$$

then swapping $3 \leftrightarrow 2$ in the second term and $3 \leftrightarrow 1$ in the third term gives:

$$\frac{1}{3} \int W_{312}^{\sigma\mu\nu} n_1^\mu n_2^\nu \mathrm{sign}(\omega_3)(\omega_3^\sigma + \omega_2^\nu + \omega_1^\mu)\delta(\omega_{312}^{\sigma\mu\nu})\delta_{312} d\mathbf{k}_{123}, \tag{6.86}$$

which is zero by the frequency resonance condition. Similarly for the potential enstrophy:

$$
\begin{aligned}
\dot{\Omega} &= \sum_{\sigma} \int |k_x| \dot{n}_{\mathbf{k}}^{\sigma} d\mathbf{k} \tag{6.87}\\
&= \sum_{\sigma\mu\nu} \int k_x \mathrm{sign}(k_x) W_{\mathbf{k}12}^{\sigma\mu\nu} [n_1^{\mu} n_2^{\nu} + n_{\mathbf{k}}^{\sigma} n_1^{\mu} \mathrm{sign}(k_x k_{2x}) + n_{\mathbf{k}}^{\sigma} n_2^{\nu} \mathrm{sign}(k_x k_{1x})] \\
&\qquad \times \delta(\omega_{\mathbf{k}12}^{\sigma\mu\nu}) \delta_{\mathbf{k}12} d\mathbf{k}_{12} \\
&= \sum_{\sigma\mu\nu} \int W_{312}^{\sigma\mu\nu} [n_1^{\mu} n_2^{\nu} k_{3x} \mathrm{sign}(k_{3x}) + n_3^{\sigma} n_1^{\mu} k_{3x} \mathrm{sign}(k_{2x}) + n_3^{\sigma} n_2^{\nu} k_{3x} \mathrm{sign}(k_{1x})] \\
&\qquad \times \delta(\omega_{312}^{\sigma\mu\nu}) \delta_{312} d\mathbf{k}_{312} \\
&= \sum_{\sigma\mu\nu} \int W_{312}^{\sigma\mu\nu} n_1^{\mu} n_2^{\nu} \mathrm{sign}(k_{3x})(k_{3x} + k_{2x} + k_{1x}) \delta(\omega_{312}^{\sigma\mu\nu}) \delta_{312} d\mathbf{k}_{312},
\end{aligned}
$$

which is zero by the wavenumber resonance condition.

6.3 Non-local interaction between baroclinic and barotropic modes

6.3.1 Energy transfer in two layers

In the introduction, a schematic construction of energy flow in two layers was mentioned, which was first suggested by Salmon in 1978 [52] and has since become the standard picture in geophysical literature. This picture is summarized in Salmon's diagram reproduced in figure 6.2 (except for the diagonal arrow). It is important to realise that in his work Salmon considered equivalent layers, i.e. equal depth and equal density. This means that $s^+ = 1$ and $s^- = -1$ and as a consequence only two types of triads $\{+ - -\}$ and $\{+ + +\}$ can exist (this can be seen from equations (6.74) to (6.77)).

In Salmon's picture, energy is injected at the largest scale, k_F, via wind created by a temperature difference between the poles and the equator. Baroclinic modes then transfer this energy via non-local $\{+ - -\}$ triad interactions to the baroclinic and barotropic modes at the Rossby deformation scale, k_R (one over the Rossby deformation radius). Being non-local implies that waves interact over a range of scales. A small proportion of this energy will continue to flow to the smallest scale,
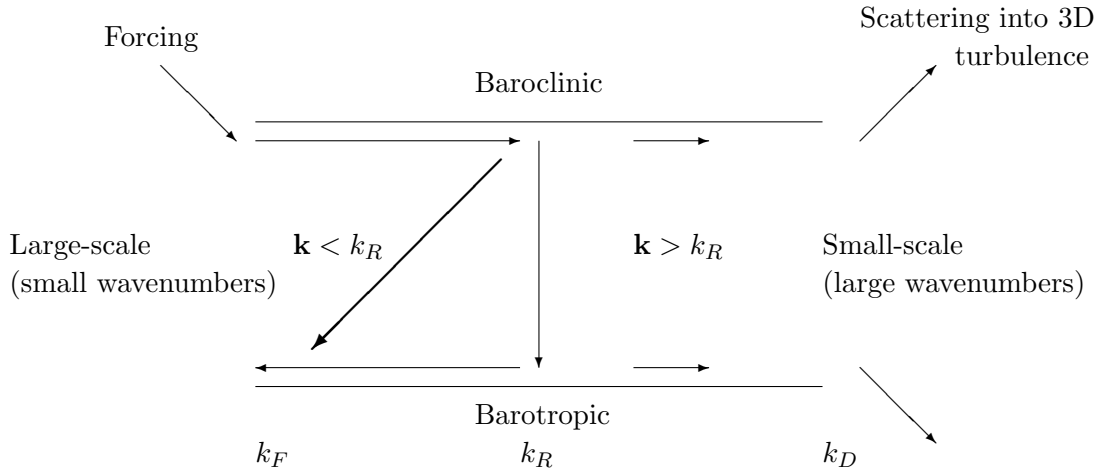
Figure 6.2: Salmon's energy flux diagram for a two-layer system. The potential enstrophy flux present on the original diagram is omitted. The bold diagonal arrow is new. It indicates the direction that energy is thought to transfer when taking the WT approach.

k_D, where it is scattered into 3D turbulence. However, the majority of the energy will undergo barotropization at the deformation scale and will be transferred to the large scales via local $\{+++\}$ triad interactions. By local we mean that interactions take place between waves which are of approximately the same scale.

We will not consider scales less than the Rossby deformation scale, $\mathbf{k} > k_R$, instead we will concentrate on the energy transfer loop whereby the majority of the energy is transferred in $\{+--\}$ triads from the large-scale baroclinic mode to the large-scale barotropic mode in two steps:

1. The energy is transferred from the large-scale baroclinic modes to the baroclinic and barotropic modes at the Rossby deformation scale, $\mathbf{k} \sim k_R$.

2. It is then transferred from the baroclinic and barotropic modes at the Rossby deformation scale to the large-scale barotropic modes (indicated by the diagonal arrow in figure 6.2).

A frequently discussed candidate mechanism for step 1 of this loop is BI, caused by a vertical shear, where one layer slides with respect to the other layer. See figure 6.3. The vertical shear is a result of the meridional temperature gradient created by tropical heating and polar cooling.
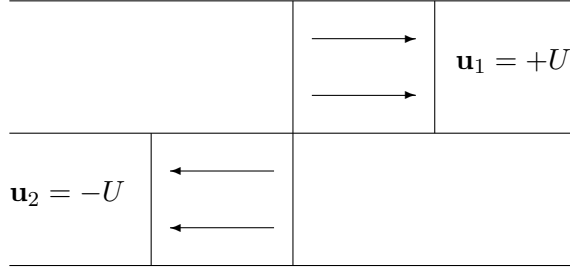
Figure 6.3: Baroclinic flow in a two-layer fluid.

For a derivation of BI in the two-layer equations see [76, 77, 78]. In the latter, it is shown that a necessary condition for instability is:

$$U > \beta k_R^{-2}. \tag{6.88}$$

However, this does not coincide with the necessary condition for weak WT. Weak WT is applicable when the nonlinear terms in an equation are much less than the linear terms. In the case of the two-layer equations this is when:

$$J[\psi, \nabla^2 \psi] \ll \beta \partial_x \psi. \tag{6.89}$$

Letting $k_x \sim k_y \sim \partial_x \sim \partial_y$ we can see that:

$$\partial_x \psi \partial_y \nabla^2 \psi \ll \beta \partial_x \psi \Rightarrow U k^2 \ll \beta. \tag{6.90}$$

Putting together equations (6.88) and (6.90) gives:

$$\beta k_R^{-2} k^2 < U k^2 \ll \beta \Rightarrow k_R^{-2} k^2 \ll 1, \tag{6.91}$$

but BI is maximum at k_R and this is not described by WT. Thus it can be concluded that WT and BI cannot operate simultaneously. For BI to be considered a different WT theory may be needed but this would require a different dispersion relation and

interaction coefficient and this is something to consider in future work. When BI isn't present, other sources of instability could include differential radiative heating which is forced at large scales or in the case of Jupiter, interior convection. For more information on these instabilities see [71].

Let us consider the locality of these two transfers. For step 1 of the loop, consider the possibility of a non-local interaction from a WT perspective. The frequency resonance condition, $\omega_{\mathbf{k}}^+ + \omega_1^- + \omega_2^- = 0$ (which was not considered in Salmon's paper) must be satisfied along with the wavenumber resonance condition, $\mathbf{k} + \mathbf{k}_1 + \mathbf{k}_2 = 0$. If $\mathbf{k}_1$ is small (since it is baroclinic), then $\mathbf{k}_2 \cong -\mathbf{k}$ and the frequency condition gives $\omega_{\mathbf{k}}^+ = \omega_{\mathbf{k}}^-$, which cannot be true. Hence, in this case the transfer of energy from the large-scale baroclinic modes to the Rossby deformation scale cannot be non-local and instead must be local.

At step 2 of the loop, the energy accumulated at the Rossby deformation scale will be transferred into large-scale barotropic modes via an inverse transfer. In the one-layer case [12, 39, 46] the inverse energy transfer becomes anisotropic, with dominant zonal scales, due to the presence of a third invariant, zonostrophy. This is known as zonostrophic turbulence which was defined in [59]. Drawing intuition from the one-layer case, it would be natural to assume that in this two-layer system the inverse energy transfer to the barotropic mode is also non-local. It may start off as a local cascade, but will eventually lead to formation of strong (interaction with) zonal jets, which will become dominant for $\mathbf{k} \sim k_R$ modes. This is what we will now consider, using a similar scale separation technique to that used for the one-layer model [79, 80], but now for dominant $\{+--\}$ triads instead of the one-layer $\{+++\}$ triads.

6.3.2   Scale separation and the diffusion equation

Consider a scale separated system in which the barotropic (+) modes have wavenumbers much less than those of the baroclinic (-) modes and much less than the Rossby deformation scale, $\mathbf{k}_+ \ll \mathbf{k}_-, k_R$ (see figure 6.4).

First, consider the evolution of the small-scale, baroclinic modes (with wave vector $\mathbf{k}$) and their non-local interaction with the large-scale zonal flows. To do this,
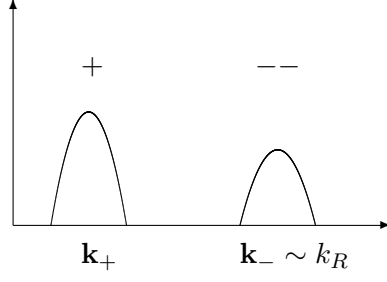
Figure 6.4: Scale separation with $\mathbf{k}_+ \ll \mathbf{k}_-,\, k_R$.

take the baroclinic part of the kinetic equation (6.80) where the wavenumbers $\mathbf{k}, 1, 2$ used for simplicity before will be changed back to $\mathbf{k}, \mathbf{k}_1, \mathbf{k}_2$:

$$\partial_t n_\mathbf{k}^- = \int W_{\mathbf{k},\mathbf{k}_1,\mathbf{k}_2}^{-+-}[n_{\mathbf{k}_1}^+ n_{\mathbf{k}_2}^- + n_{\mathbf{k}_1}^+ n_\mathbf{k}^- sign(\omega_\mathbf{k}\omega_{\mathbf{k}_2}) + n_{\mathbf{k}_2}^- n_\mathbf{k}^- sign(\omega_\mathbf{k}\omega_{\mathbf{k}_1})] \quad (6.92)$$
$$\times \delta(\omega_\mathbf{k}^- + \omega_{\mathbf{k}_1}^+ + \omega_{\mathbf{k}_2}^-)\delta(\mathbf{k} + \mathbf{k}_1 + \mathbf{k}_2)d\mathbf{k}_{12}.$$

The third term, $n_{\mathbf{k}_2}^- n_\mathbf{k}^-$, can be neglected because it is quadratic with respect to the small scales. In the second term, $sign(\omega_\mathbf{k}\omega_{\mathbf{k}_2}) \to -1$, since $\mathbf{k}_1$ is the barotropic wavenumber and small so, from the resonance conditions, $\mathbf{k}_2 \simeq -\mathbf{k}$ and $\omega_{\mathbf{k}_2} \simeq -\omega_\mathbf{k}$. Hence equation (6.92) reduces to:

$$\partial_t n_\mathbf{k}^- = \int W_{\mathbf{k},\mathbf{k}_1,-\mathbf{k}-\mathbf{k}_1}^{-+-} n_{\mathbf{k}_1}^+[n_{-\mathbf{k}-\mathbf{k}_1}^- - n_\mathbf{k}^-]\delta(\omega_\mathbf{k}^- + \omega_{\mathbf{k}_1}^+ + \omega_{-\mathbf{k}-\mathbf{k}_1}^-)d\mathbf{k}_1, \quad (6.93)$$

where $\mathbf{k}_2$ has been integrated out, writing it as $-\mathbf{k} - \mathbf{k}_1$. Now let:

$$\partial_t n_\mathbf{k}^- = \int F(\mathbf{k}, \mathbf{k}_1)d\mathbf{k}_1, \quad (6.94)$$

where:

$$F(\mathbf{k}, \mathbf{k}_1) = W_{\mathbf{k},\mathbf{k}_1,-\mathbf{k}-\mathbf{k}_1}^{-+-} n_{\mathbf{k}_1}^+[n_{-\mathbf{k}-\mathbf{k}_1}^- - n_\mathbf{k}^-]\delta(\omega_\mathbf{k}^- + \omega_{\mathbf{k}_1}^+ + \omega_{-\mathbf{k}-\mathbf{k}_1}^-). \quad (6.95)$$

Using the symmetries:

$$W_{\mathbf{k},\mathbf{k}_1,-\mathbf{k}-\mathbf{k}_1}^{-+-} = W_{-\mathbf{k}-\mathbf{k}_1,\mathbf{k}_1,\mathbf{k}}^{-+-},$$

101

and:

$$W^{-+-}_{\mathbf{k},\mathbf{k}_1,-\mathbf{k}-\mathbf{k}_1} = W^{-+-}_{-\mathbf{k},-\mathbf{k}_1,\mathbf{k}+\mathbf{k}_1},$$

gives:

$$F(\mathbf{k},\mathbf{k}_1) = -F(-\mathbf{k}-\mathbf{k}_1,\mathbf{k}_1) = -F(\mathbf{k}+\mathbf{k}_1,-\mathbf{k}_1), \qquad (6.96)$$

so:

$$
\begin{aligned}
\partial_t n^-_{\mathbf{k}} &= \frac{1}{2}\int (F(\mathbf{k},\mathbf{k}_1) - F(\mathbf{k}+\mathbf{k}_1,-\mathbf{k}_1))d\mathbf{k}_1 \qquad (6.97)\\
&= \frac{1}{2}\int (F(\mathbf{k},\mathbf{k}_1) - F(\mathbf{k}-\mathbf{k}_1,\mathbf{k}_1))d\mathbf{k}_1.
\end{aligned}
$$

Taylor expand $F(\mathbf{k}-\mathbf{k}_1,\mathbf{k}_1)$ with respect to $\mathbf{k}_1$ and neglect terms of $O(\mathbf{k}_1^2)$ to obtain the following:

$$\partial_t n^-_{\mathbf{k}} = \frac{1}{2}\int \mathbf{k}_1 \cdot \nabla_{\mathbf{k}} F(\mathbf{k},\mathbf{k}_1)d\mathbf{k}_1. \qquad (6.98)$$

Using Taylor expansion in equation (6.95), F can be rewritten as:

$$F(\mathbf{k},\mathbf{k}_1) \approx W^{-+-}_{\mathbf{k},\mathbf{k}_1,\mathbf{k}+\mathbf{k}_1}\delta(\omega^-_{\mathbf{k}} + \omega^+_{\mathbf{k}_1} + \omega^-_{\mathbf{k}+\mathbf{k}_1})(\mathbf{k}_1 \cdot \nabla_{\mathbf{k}} n^-_{\mathbf{k}})n^+_{\mathbf{k}_1}. \qquad (6.99)$$

Combining equation (6.98) and (6.99) gives:

$$\partial_t n^-_{\mathbf{k}} = \frac{1}{2}\int \mathbf{k}_1 \cdot \nabla_{\mathbf{k}}\left(W^{-+-}_{\mathbf{k},\mathbf{k}_1,\mathbf{k}+\mathbf{k}_1}\delta(\omega^-_{\mathbf{k}} + \omega^+_{\mathbf{k}_1} + \omega^-_{\mathbf{k}+\mathbf{k}_1})(\mathbf{k}_1 \cdot \nabla_{\mathbf{k}} n^-_{\mathbf{k}})n^+_{\mathbf{k}_1}\right)d\mathbf{k}_1. \quad (6.100)$$

Similar to work done in the one-layer case in [80], the kinetic equation for the small scales, $n^-_{\mathbf{k}}$, can be written as the following anisotropic diffusion equation in $\mathbf{k}$-space:

$$\frac{\partial n^-_{\mathbf{k}}}{\partial t} = \frac{\partial}{\partial k_i} S_{ij} \frac{\partial n^-_{\mathbf{k}}}{\partial k_j}, \qquad (6.101)$$

where the diffusion tensor:

$$S_{ij} = \frac{1}{2}\int W^{-+-}_{\mathbf{k},\mathbf{k}_1,\mathbf{k}+\mathbf{k}_1}\delta(\omega^-_{\mathbf{k}} + \omega^+_{\mathbf{k}_1} + \omega^-_{\mathbf{k}+\mathbf{k}_1})n^+_{\mathbf{k}_1}k_{1i}k_{1j}d\mathbf{k}_1, \qquad (6.102)$$

depends on the structure of the large scales, $n^+_{\mathbf{k}_1}$. Now look at the delta term, the

frequency resonant condition:

$$\omega_{\mathbf{k}}^- + \omega_{\mathbf{k}_1}^+ + \omega_{\mathbf{k}+\mathbf{k}_1}^- = 0, \tag{6.103}$$

can be written using the dispersion relations as follows:

$$\frac{k_x}{F_- + k^2} + \frac{k_{1x}}{F_+ + k_1^2} + \frac{-k_x - k_{1x}}{F_- + (k + k_1)^2} = 0. \tag{6.104}$$

Since $F_- = F_+ \times H^2/h_1 h_2$ [see 4], $F_+ \ll F_-$ so let $F_+ \to 0$ and remove it from the above equation. Assume that the scaling:

$$k_{1y}^3 \sim k_{1x}, \tag{6.105}$$

is true. Using this assumption the following is obtained:

$$\frac{k_x}{F_- + k^2} + \frac{k_{1x}}{k_{1y}^2} - \frac{k_x + k_{1x}}{F_- + k^2 + 2k_x k_{1x} + 2k_y k_{1y} + k_{1y}^2} \tag{6.106}$$
$$= \frac{k_x}{F_- + k^2} + \frac{k_{1x}}{k_{1y}^2} + \frac{k_x}{F_- + k^2}\left(-1 + \frac{2k_y k_{1y}}{F_- + k^2}\right) + O(k_{1y}^2).$$

So:

$$\delta(\omega_{\mathbf{k}}^- + \omega_{\mathbf{k}_1}^+ + \omega_{\mathbf{k}+\mathbf{k}_1}^-) = \delta\left(\frac{k_{1x}}{k_{1y}^2} + \frac{2k_x k_y k_{1y}}{(F_- + k^2)^2}\right) \tag{6.107}$$
$$= k_{1y}^2 \delta\left(k_{1x} + \frac{2k_x k_y k_{1y}^3}{(F_- + k^2)^2}\right).$$

From the bracket:

$$k_{1x} = -k_{1y}^3 \frac{2k_x k_y}{(F_- + k^2)^2}, \tag{6.108}$$

which is much smaller than k_{1y}^2 and hence:

$$k_{1x} \ll k_{1y}^2. \tag{6.109}$$

From equation (6.109), terms containing k_{1x} can be removed from the diffusion

equation (6.101), leaving:

$$\frac{\partial n_{\mathbf{k}}^-}{\partial t} = \frac{\partial}{\partial k_{1y}} S_{yy} \frac{\partial n_{\mathbf{k}}^-}{\partial k_{1y}}, \qquad (6.110)$$

which describes diffusion in the k_y direction with k_x constant. From (6.102):

$$S_{yy} = \frac{1}{2} \int_{-\infty}^{\infty} W_{\mathbf{k},\mathbf{k}_1,\mathbf{k}+\mathbf{k}_1}^{-+-} k_{1y}^2 \delta \left(k_{1x} + \frac{2k_x k_y k_{1y}^3}{(F_- + k^2)^2} \right) n_{\mathbf{k}_1}^+ k_{1y}^2 dk_{1x} dk_{1y} \quad (6.111)$$

$$= \frac{1}{2} \int_{-\infty}^{\infty} W_{\mathbf{k},\mathbf{k}_1,\mathbf{k}+\mathbf{k}_1}^{-+-} \delta(k_{1x} + \theta k_{1y}^3) n_{\mathbf{k}_1}^+ k_{1y}^4 dk_{1x} dk_{1y}, \qquad (6.112)$$

where:

$$\theta = \frac{2k_x k_y}{(F_- + k^2)^2}. \qquad (6.113)$$

Since $k_{1x} = -\theta k_{1y}^3$, from equation(6.108):

$$S_{yy} = \frac{1}{2} \int_{-\infty}^{\infty} \left[W_{\mathbf{k},\mathbf{k}_1,\mathbf{k}+\mathbf{k}_1}^{-+-} n_{\mathbf{k}_1}^+ \right]_{k_{1x}=-\theta k_{1y}^3} k_{1y}^4 dk_{1y}. \qquad (6.114)$$

To close the system, baroclinic equation (6.110) has to be complemented by a barotropic equation, which is obtained from equation (6.79) in which the term $n_{\mathbf{k}_1}^- n_{\mathbf{k}_2}^-$ is neglected. This gives:

$$\partial_t n_{\mathbf{k}}^+ = 2 \int W_{\mathbf{k},\mathbf{k}_1,\mathbf{k}_2}^{+--} n_{\mathbf{k}_1}^- n_{\mathbf{k}}^+ sign(k_x k_{2x}) \delta(\omega_{\mathbf{k}}^+ + \omega_{\mathbf{k}_1}^- + \omega_{\mathbf{k}_2}^-) \delta_{\mathbf{k}12} d\mathbf{k}_{12}. \qquad (6.115)$$

Thus a system of coupled equations (6.110) and (6.115) are obtained for the small-scale baroclinic component and the large-scale barotropic component. One can see that the total waveaction is conserved in the small-scale baroclinic component alone. This is natural because the non-local process that is considered can be interpreted as scattering of small-scale baroclinic wave packets off a slowly varying barotropic flow. The number of wave packets in such a process is conserved. On the other hand, the total energy in the small-scale component is not conserved. Only the sum of the energies of the small-scale baroclinic and the large-scale barotropic components are conserved. Thus the energy may be exchanged between the small-scale baroclinic and large-scale barotropic components. The dominant transfer direction

is from small to large scales. Indeed, consider an initial small-scale spectrum that is concentrated near the meridional axis with $\mathbf{k} \sim (k_{x0}, 0)$. According to the diffusion equation (6.110), this spectrum will spread in k_y, which means that the frequency will spread towards larger k_y's with k_x remaining fixed. As k_y, increases the frequency of the respective modes $\omega_{\mathbf{k}}^- = k_x/(F^- + k_x^2 + k_y^2)$ decreases. Considering that the total waveaction is conserved, this means that the total small-scale baroclinic energy $\int \omega_{\mathbf{k}}^- n_{\mathbf{k}}^- d\mathbf{k}$ will decrease. Since the total barotropic plus baroclinic energy is conserved, the baroclinic energy loss will be compensated by the growth of the barotropic energy at large scales. As the barotropic waves that interact with the small-scale baroclinic modes are mostly zonal (6.105), this transfer of energy will be mostly anisotropic and mostly to the large-scale zonal component (see figure 6.5).

It is possible that a negative feedback loop forms, similar to the one-layer case [81]. Energy lost by the small scales is transferred to the large-scale zonal flows, which grow more intense. This will result in a larger diffusion coefficient and consequently an increased rate of dissipation of small-scale waveaction. Hence, the growth of large scales may turn off the energy source at small scales. One can answer this by direct numerical simulation (DNS) of the two-layer model and this is something to consider in future work.
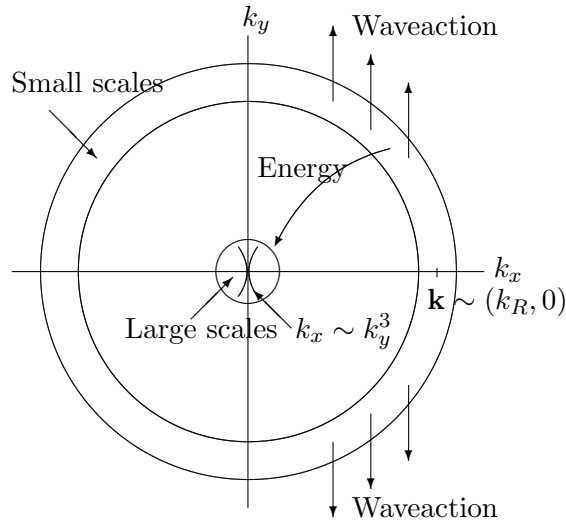

Figure 6.5: Diagram to show the direction of waveaction and energy transfer.

Conclusion

This thesis begins by considering Rossby waves within the one-layer CHM equation from a WT perspective. Three different regimes of WT exist, kinetic, discrete and mesoscopic. Discrete WT exists in the limit of very small amplitudes where only waves that are resonant can interact and exchange energy. As wave vectors are discrete variables any $\mathbf{k}$ may be a member of only a few resonant triads. Conversely, as wave amplitudes increase, kinetic WT develops whereby the wave vectors are continuous variables and consequently may be a member of infinitely many resonant triads.

Kinetic WT for one-layer Rossby waves has been extensively studied. It is well known that three invariants exist, the energy, enstrophy and zonostrophy and they undergo a triple cascade with the zonostrophy directing the energy to zonal scales. In this thesis we considered the problem of finding quadratic invariants in the discrete regime. It turns out that the condition for existence of an invariant is identical for both kinetic and discrete WT, namely the $\mathbf{k}$-space density of the quadratic invariant must satisfy the same resonance conditions as does the wave vector and the frequency. Finding invariants is equivalent to finding the null space of the cluster matrix $\mathbb{A}$ whose vertical dimension M is given by the number of triads and horizontal dimension N is given by the number of modes. The total number of invariants is equal to $J \equiv N - M^* \geq N - M$ where M^* is the number of linearly independent rows in $\mathbb{A}$. Since the resonance conditions are much harder to satisfy in a discrete system, there are fewer triads and therefore many more invariants compared to the kinetic case.

An algorithm is presented which allows one to see how the various quadratic invariants are related to certain parts of a cluster. This is the first time that the

relationship between the structure of the cluster (in terms of connectivity, geometry, etc.) and the most efficient interactions has been addressed. It allows local invariants associated with triads with two loose ends to be identified. In fact it was found that in symbolic cluster space, typically only a few invariants depend on all triads' amplitudes. The majority of the invariants are quite local in symbolic cluster space, involving one or only a few triads. If forcing occurs near a triad with two loose ends, energy may become trapped in it and if forcing does not occur near it, it may contain no energy at all. Hence triads with two loose ends restrict energy movement in the cluster. The more modes involved, the more efficiently the invariant is stirred through the cluster. The next step would be to find out if global invariants with many amplitudes involved, like zonostrophy, directs cascades in an anisotropic way, e.g. making energy transfer to zonal scales, like in kinetic WT. The algorithm also allows us to construct explicitly cases when the number of independent invariants is larger than $N - M$, explaining how these situations are related to the degeneracy of smaller blocks within the matrix. We illustrate our algorithm by applying it to the 104-triad cluster arising in the large-scale CHM system, and show that it has $N - M + 2$ invariants.

The second part of this thesis considers in more detail the large-scale limit of the CHM equation, for which a new quadratic invariant, semi-action, has recently been discovered. As a consequence of its conservation, it was proposed that the following triads are prohibited: $M \to M + M, M \to Z + Z, Z \to M + Z$ and $Z \to M + M$. In this thesis it has been shown, both theoretically and numerically, that this proposition is correct and certain triads are prohibited when nonlinearity is weak. Numerical simulations showed that if the initial spectrum is in the zonal sector it remains in the zonal sector. On the other hand, when the initial spectrum is in the meridional sector, small amounts can move into the zonal sector, but not all can transfer as otherwise semi-action would be lost. However, when nolinearity is strong and the three-wave interactions no longer dominate the proposition doesn't hold. It was also considered when ρ^2 is small but finite and it was discovered that forbidden triads exist. They are concentrated along the zonal/meridional boundary and the deviation of k_y/k_x from $\sqrt{3}$ shrinks as $\rho^2 \to 0$.

In the final part of the thesis we considered Rossby waves in a two-layer QG ocean. Two-layer models are more realistic than one-layer models when describing the oceans, as less dense, warmer surface waters float on top of denser, colder waters. Work on two-layer turbulence in the 1970's by Rhines [51] and Salmon [52] put forward a description of energy transfer which is still the standard picture today. However, they made major assumptions such as equal layers and Salmon only took into account non-resonant triad interactions.

In this thesis two-layer Rossby waves were studied using WT theory. An advantage of using WT theory is that since it deals with weakly nonlinear, dispersive waves, strong interactions can be ruled out which allows us to advance further with the analysis so we can better understand the spectral energy transfer in the ocean. Under the assumptions of weak nonlinearity and random phases, it is possible to derive a kinetic equation. This was done using canonical waveaction variables which make it simple and symmetric and therefore easier to use in the analysis of energy transfer in two layers. Another advantage of WT theory is that the waves are in resonance, meaning that *both* the wavenumber and frequency conditions must be satisfied. By imposing this extra condition, it can be seen which modes interact and how strongly. From the interaction coefficient, it is clear that $\{+ - -\}$ is the dominant triad interaction, with two baroclinic components and one barotropic component.

The kinetic equation was then used to study the turbulent cascade of energy between the barotropic and baroclinic modes. It was shown, using the resonant conditions, that the direct cascade of energy from the large-scale baroclinic modes to baroclinic and barotropic modes at the Rossby deformation scale is *local*. It was then assumed that energy is transferred to the large-scale barotropic modes via an inverse *non-local* transfer and this non-locality was studied via scale separation. A system of coupled equations were obtained for the small-scale baroclinic component and the large-scale barotropic component. It was found that since the baroclinic energy of the small scales is not conserved but the total energy (barotropic plus baroclinic) of the large and small scales together is conserved, the baroclinic energy lost by small scales will be compensated by the growth of the barotropic energy at large scales. And using the frequency resonance condition, it was seen that the

barotropic transfer of energy is in the zonal direction.

This work can be extended to models with more than two layers, which would lead to longer but conceptually similar kinetic equations. In fact, Soomere [82] suggests that both barotropic and two-layer models of geophysical flows often inadequately represent the vertical structure of the ocean as at medium latitudes, the seasonal thermocline occasionally creates a three-layer structure. With this in mind they extended Kozlov et als work [4] to a three-layer ocean obtaining explicit analytical expressions for the coupling coefficients describing energy exchange intensity between different modes.

The simplifying assumptions of WT, i.e. weak nonlinearity and the extra resonance condition, could be too restrictive. However, this approach allows us to understand important processes occurring in nature using simplified models that are tractable analytically. In the one-layer case, important predictions were made and verified numerically regarding the formation of anisotropy and zonal jets. The next step is therefore to test the theoretical results using numerical simulations.

A lot of studies in the literature have condensed spectral transfer calculations onto quasi-isotropic one-dimensional (1D) profiles. However, these do not take into account the anisotropy that results from considering the beta-effect. In this thesis we have considered three or more invariants and shown that consequently the $\mathbf{k}$-space can no longer be divided up in an isotropic way. Therefore it would be a good idea for future studies to take into account triple or multiple anisotropic cascades.

Appendix A

Deriving Kozlov el al.'s kinetic equation (6.30)

From the two-layer equations (6.27) and (6.28):

$$\frac{\partial}{\partial t}\left[\nabla^2\psi_1 + \frac{f_0^2}{g'H_1}(\psi_2 - \psi_1)\right] + \beta\frac{\partial\psi_1}{\partial x} = -J\left[\psi_1, \nabla^2\psi_1 + \frac{f_0^2}{g'H_1}(\psi_2 - \psi_1)\right],$$

$$\frac{\partial}{\partial t}\left[\nabla^2\psi_2 + \frac{f_0^2}{g'H_2}(\psi_1 - \psi_2)\right] + \beta\frac{\partial\psi_2}{\partial x} = -J\left[\psi_2, \nabla^2\psi_2 + \frac{f_0^2}{g'H_2}(\psi_1 - \psi_2)\right],$$

we want to derive a single equation which contains only one unknown function:

$$\psi^\sigma = \psi_1 + s^\sigma\psi_2, \quad \sigma = +, -.$$

We begin by writing out $M_1 + s^\sigma M_2$, where M_1 and M_2 are the linear parts of the two-layer equations for layers 1 and 2 respectively, which gives:

$$\frac{\partial}{\partial t}\left[\nabla^2\psi_1 + \frac{f_0^2}{g'H_1}\psi_2 - \frac{f_0^2}{g'H_1}\psi_1 + s^\sigma\nabla^2\psi_2 + s^\sigma\frac{f_0^2}{g'H_2}\psi_1 - s^\sigma\frac{f_0^2}{g'H_2}\psi_2\right] + \beta\frac{\partial\psi_1}{\partial x} + s^\sigma\beta\frac{\partial\psi_2}{\partial x}.$$

We now want to write this in terms of ψ^σ :

$$\frac{\partial}{\partial t}\left[\nabla^2(\psi_1 + s^\sigma\psi_2) - \left(\frac{f_0^2}{g'H_1} - \frac{f_0^2}{g'H_2}s^\sigma\right)(\psi_1 + s^\sigma\psi_2)\right] + \beta\frac{\partial}{\partial x}(\psi_1 + s^\sigma\psi_2)$$
$$= \frac{\partial}{\partial t}(\nabla^2\psi^\sigma - F^\sigma\psi^\sigma) + \beta\frac{\partial\psi^\sigma}{\partial x},$$

where:

$$F^\sigma = \frac{f_0^2}{g' H_1} - \frac{f_0^2}{g' H_2} s^\sigma.$$

Let us now move on to the working for the nonlinear part. From the RHS of the two-layer equations we get:

$$-J\left[\psi_1, \nabla^2 \psi_1 + \frac{f_0^2}{g' H_1} \psi_2\right] - s^\sigma J\left[\psi_2, \nabla^2 \psi_2 + \frac{f_0^2}{g' H_2} \psi_1\right]$$

$$= -J[\psi_1, \nabla^2 \psi_1] - J\left[\psi_1, \frac{f_0^2}{g' H_1} \psi_2\right] - s^\sigma J[\psi_2, \nabla^2 \psi_2] - s^\sigma J\left[\psi_2, \frac{f_0^2}{g' H_2} \psi_1\right]$$

$$= -J[\psi_1, \nabla^2 \psi_1] - s^\sigma J[\psi_2, \nabla^2 \psi_2] - \left(\frac{f_0^2}{g' H_1} - s^\sigma \frac{f_0^2}{g' H_2}\right) J[\psi_1, \psi_2].$$

Rearranging the normal modes gives:

$$\psi_1 = \frac{s^- \psi^+ - s^+ \psi^-}{s^- - s^+} \quad \text{and} \quad \psi_2 = \frac{\psi^+ - \psi^-}{s^+ - s^-},$$

and substituting these in we get:

$$-J\left[\frac{s^- \psi^+ - s^+ \psi^-}{s^- - s^+}, \nabla^2 \left(\frac{s^- \psi^+ - s^+ \psi^-}{s^- - s^+}\right)\right] - s^\sigma J\left[\frac{\psi^+ - \psi^-}{s^+ - s^-}, \nabla^2 \left(\frac{\psi^+ - \psi^-}{s^+ - s^-}\right)\right]$$

$$- \left(\frac{f_0^2}{g' H_1} - s^\sigma \frac{f_0^2}{g' H_2}\right) J\left[\frac{s^- \psi^+ - s^+ \psi^-}{s^- - s^+}, \frac{\psi^+ - \psi^-}{s^+ - s^-}\right].$$

Take out the fraction as a common denominator:

$$-\frac{1}{(s^+ - s^-)^2}[J[s^-\psi^+ - s^+\psi^-, \nabla^2(s^-\psi^+ - s^+\psi^-)] + s^\sigma J[\psi^+ - \psi^-, \nabla^2(\psi^+ - \psi^-)]$$

$$-\left(\frac{f_0^2}{g'H_1} - s^\sigma \frac{f_0^2}{g'H_2}\right) J[s^-\psi^+ - s^+\psi^-, \psi^+ - \psi^-]]$$

$$= -\frac{1}{(s^+ - s^-)^2}[(s^-)^2 J[\psi^+, \nabla^2\psi^+] - s^- s^+ J[\psi^+, \nabla^2\psi^-]$$

$$-s^+ s^- J[\psi^-, \nabla^2\psi^+] + (s^+)^2 J[\psi^-, \nabla^2\psi^-] + s^\sigma J[\psi^+, \nabla^2\psi^+]$$

$$-s^\sigma J[\psi^+, \nabla^2\psi^-] - s^\sigma J[\psi^-, \nabla^2\psi^+] + s^\sigma J[\psi^-, \nabla^2\psi^-]$$

$$-(\frac{f_0^2}{g'H_1} - s^\sigma \frac{f_0^2}{g'H_2})(s^- \cancel{J[\psi^+,\psi^+]} - s^- J[\psi^+,\psi^-] - s^+ J[\psi^-,\psi^+] + s^+ \cancel{J[\psi^-,\psi^-]}))]$$

$$= -\frac{1}{(s^+ - s^-)^2}[((s^-)^2 + s^\sigma)J[\psi^+, \nabla^2\psi^+] - (s^- s^+ + s^\sigma)J[\psi^+, \nabla^2\psi^-]$$

$$-(s^+ s^- + s^\sigma)J[\psi^-, \nabla^2\psi^+] + ((s^+)^2 + s^\sigma)J[\psi^-, \nabla^2\psi^-]$$

$$-(\frac{f_0^2}{g'H_1} - s^\sigma \frac{f_0^2}{g'H_2})(s^+ - s^-)J[\psi^+, \psi^-]]$$

$$= -\frac{1}{\lambda^2}\sum_{\mu\nu}[p^\sigma_{\mu\nu}J(\psi^\mu, \nabla^2\psi^\nu) + g^\sigma_{\mu\nu}F^\sigma J(\psi^\mu, \psi^\nu)],$$

where $\lambda = (s^+ - s^-)$ and the coupling coefficients are:

$$p^+_{++} = s^+ + (s^-)^2, \quad p^+_{--} = s^+(1 + s^+), \quad p^+_{+-} = -s^+(1 + s^-) = p^+_{-+},$$

$$p^-_{++} = s^-(1 + s^-), \quad p^-_{--} = s^- + (s^+)^2, \quad p^-_{+-} = -s^-(1 + s^+) = p^-_{-+},$$

$$g^+_{+-} = -g^+_{-+} = -\frac{1}{2}(s^+ - s^-) = g^-_{+-} = -g^-_{-+}.$$

Putting the linear and nonlinear parts together we get Kozlov et al.'s kinetic equation (6.30):

$$\frac{\partial}{\partial t}(\nabla^2\psi^\sigma - F^\sigma\psi^\sigma) + \beta\frac{\partial\psi^\sigma}{\partial x} = -\frac{1}{\lambda^2}\sum_{\mu\nu}[p^\sigma_{\mu\nu}J(\psi^\mu, \nabla^2\psi^\nu) + F^\sigma g^\sigma_{\mu\nu}J(\psi^\mu, \psi^\nu)].$$

Appendix B

Deriving the two-layer interaction coefficient (6.46)

Begin by introducing the waveaction variable:

$$a_{\mathbf{k}}^{\pm} = \frac{(k^2 + F^{\pm})}{\sqrt{|\beta k_x s^{\pm}|}} \hat{\psi}_{\mathbf{k}}^{\pm},$$

into equation (6.38):

$$\partial_t \hat{\psi}_{\mathbf{k}}^{\sigma} + i\omega_{\mathbf{k}}^{\sigma} \hat{\psi}_{\mathbf{k}}^{\sigma} = \frac{\lambda}{2(k^2 + F^{\sigma})} \sum_{\mu\nu} \sum_{12} p_{\mu\nu}^{\sigma}(\mathbf{k}_1 \times \mathbf{k}_2)_z (k_2^2 - k_1^2 + F^{\nu} - F^{\mu}) \hat{\psi}_1^{\mu} \hat{\psi}_2^{\nu} \delta_{12}^{\mathbf{k}},$$

to get:

$$\dot{a}_{\mathbf{k}}^{\sigma} \frac{\sqrt{|\beta|}\sqrt{|k_x|}\sqrt{|s^{\sigma}|}}{(k^2 + F^{\sigma})} + i\omega_{\mathbf{k}}^{\sigma} a_{\mathbf{k}}^{\sigma} \frac{\sqrt{|\beta|}\sqrt{|k_x|}\sqrt{|s^{\sigma}|}}{(k^2 + F^{\sigma})} = \frac{\lambda}{2(k^2 + F^{\sigma})} \sum_{\mu\nu} \sum_{12} p_{\mu\nu}^{\sigma}$$

$$\times (k_{1x}k_{2y} - k_{2x}k_{1y})(k_2^2 - k_1^2 + F^{\nu} - F^{\mu}) \bar{a}_1^{\mu} \bar{a}_2^{\nu} \frac{|\beta|\sqrt{|k_{1x}|}\sqrt{|k_{2x}|}\sqrt{|s^{\mu}|}\sqrt{|s^{\nu}|}}{(k_1^2 + F^{\mu})(k_2^2 + F^{\nu})} \delta_{\mathbf{k}12}.$$

Rewriting $\delta_{12}^{\mathbf{k}}$ as $\delta_{\mathbf{k}12}$ and consequently $a_{-\mathbf{k}_1} = \bar{a}_{\mathbf{k}_1}$ and $a_{-\mathbf{k}_2} = \bar{a}_{\mathbf{k}_2}$ and rearranging the above equation gives:

$$
\begin{aligned}
\dot{a}_{\mathbf{k}}^\sigma + i\omega_{\mathbf{k}}^\sigma a_{\mathbf{k}}^\sigma &= -\frac{\lambda}{2} \sum_{\mu\nu} \sum_{12} p_{\mu\nu}^\sigma (k_x k_{2y} - k_{2x} k_y) \\
&\quad \times \frac{(k_2^2 - k_1^2 + F^\nu - F^\mu)}{(k_1^2 + F^\mu)(k_2^2 + F^\nu)} \bar{a}_1^\mu \bar{a}_2^\nu |\beta|^{1/2} \left|\frac{k_{1x}k_{2x}}{k_x}\right|^{1/2} \left|\frac{s^\mu s^\nu}{s^\sigma}\right|^{1/2} \delta_{\mathbf{k}12} \\[2mm]
&= -\frac{\lambda}{2} \operatorname{sign}(k_x) \sum_{\mu\nu} \sum_{12} p_{\mu\nu}^\sigma |k_{1x}k_{2x}k_x|^{1/2} (k_{2y} - k_{2x}k_y/k_x) \\
&\quad \times \left(\frac{1}{k_1^2 + F^\mu} - \frac{1}{k_2^2 + F^\nu}\right) \bar{a}_1^\mu \bar{a}_2^\nu |\beta|^{1/2} \left|\frac{s^\mu s^\nu}{s^\sigma}\right|^{1/2} \delta_{\mathbf{k}12} \\[2mm]
&= -\frac{\lambda}{2} \operatorname{sign}(k_x) \sum_{\mu\nu} \sum_{12} p_{\mu\nu}^\sigma |k_{1x}k_{2x}k_x|^{1/2} \bar{a}_1^\mu \bar{a}_2^\nu |\beta|^{1/2} \left|\frac{s^\mu s^\nu}{s^\sigma}\right|^{1/2} \\
&\quad \times \left(\frac{k_{2y}}{k_1^2 + F^\mu} - \frac{k_{2y}}{k_2^2 + F^\nu} - \frac{k_{2x}k_y/k_x}{k_1^2 + F^\mu} + \frac{k_{2x}k_y/k_x}{k_2^2 + F^\nu}\right) \delta_{\mathbf{k}12}.
\end{aligned}
$$

Substituting the resonant conditions $k_{2y} = -k_y - k_{1y}$ and $k_{2x} = -k_x - k_{1x}$ into the brackets we get:

$$
\begin{aligned}
\dot{a}_{\mathbf{k}}^\sigma + i\omega_{\mathbf{k}}^\sigma a_{\mathbf{k}}^\sigma &= -\frac{\lambda}{2} \operatorname{sign}(k_x) \sum_{\mu\nu} \sum_{12} p_{\mu\nu}^\sigma |k_{1x}k_{2x}k_x|^{1/2} \bar{a}_1^\mu \bar{a}_2^\nu \left|\frac{s^\mu s^\nu}{s^\sigma}\right|^{1/2} |\beta|^{1/2} \\
&\quad \times \left(\frac{-k_y - k_{1y}}{k_1^2 + F^\mu} - \frac{k_{2y}}{k_2^2 + F^\nu} - \frac{(-k_x - k_{1x})k_y/k_x}{k_1^2 + F^\mu} + \frac{k_{2x}k_y/k_x}{k_2^2 + F^\nu}\right) \delta_{\mathbf{k}12} \\[2mm]
&= -\frac{\lambda}{2} \operatorname{sign}(k_x) \sum_{\mu\nu} \sum_{12} p_{\mu\nu}^\sigma |k_{1x}k_{2x}k_x|^{1/2} \bar{a}_1^\mu \bar{a}_2^\nu \left|\frac{s^\mu s^\nu}{s^\sigma}\right|^{1/2} |\beta|^{1/2} \\
&\quad \times \left(\frac{-k_{1y}}{k_1^2 + F^\mu} - \frac{k_{2y}}{k_2^2 + F^\nu} + \frac{k_{1x}k_y/k_x}{k_1^2 + F^\mu} + \frac{k_{2x}k_y/k_x}{k_2^2 + F^\nu}\right) \delta_{\mathbf{k}12}.
\end{aligned}
$$

Finally, symmetrize under the assumption that dominant interactions occur on the resonant manifold, i.e. the resonant condition $-\omega_{\mathbf{k}}^\sigma = \omega_1^\mu + \omega_2^\nu$ is correct to get:

$$
\dot{a}_{\mathbf{k}}^\sigma + i\omega_{\mathbf{k}}^\sigma a_{\mathbf{k}}^\sigma = \operatorname{sign}(k_x) \sum_{\mu\nu} \sum_{12} V_{\mathbf{k}12}^{\sigma\mu\nu} p_{\mu\nu}^\sigma \bar{a}_1^\mu \bar{a}_2^\nu \left|\frac{s^\mu s^\nu}{s^\sigma}\right|^{1/2} \delta_{\mathbf{k}12},
$$

where the nonlinear interaction coefficient (6.46) for the waveaction variable is:

$$V_{12}^{\sigma\mu\nu} = \frac{\lambda}{2}\sqrt{|\beta k_x k_{1x} k_{2x}|}\left(\frac{k_{1y}}{k_1^2 + F^\mu} + \frac{k_{2y}}{k_2^2 + F^\nu} + \frac{k_y}{k^2 + F^\sigma}\right).$$

Bibliography

[1] K. Harper, M. Bustamante, and S. Nazarenko, "Quadratic invariants for discrete clusters of weakly interacting waves," *J. Phys. A: Math. Theor.*, vol. 46, p. 245501, 2013.

[2] K. Harper, S. Nazarenko, S. Medvedev, and C. Connaughton, "Wave turbulence in the two-layer ocean model," *J. Fluid Mech.*, vol. 756, pp. 309–327, 2014.

[3] R. Salmon, *Lectures on Geophysical Fluid Dynamics*. Oxford University Press, 1998.

[4] O. Kozlov, G. Reznik, and T. Soomere, "Kinetic equation for Rossby waves in two-layer ocean," *Izv. Akad. Nauk SSSR Ser. Fiz. Atmosfer. i Okeana*, vol. 23, pp. 1165–1173, 1987.

[5] J. Charney, "Dynamics of long waves in a baroclinic westerly current," *J. Meteor.*, vol. 4, p. 135, 1947.

[6] J. Pedlosky, *Geophysical Fluid Dynamics*. Springer, 1987.

[7] B. Cushman-Roisin, *Introduction to Geophysical Fluid Dynamics*. Prentice Hall, 1994.

[8] G. Vallis, *Atmospheric and Oceanic Fluid Dynamics*. Cambridge University Press, 2006.

[9] A. Hasegawa and K. Mima, "Pseudo-three-dimensional turbulence in magnetized nonuniform plasma," *Phys. Fluids*, vol. 21, pp. 87–92, 1978.

[10] C. Rossby, "Relations between variations in the intensity of the zonal circulation of the atmosphere and the displacements of the semi-permanent pressure systems," *J. Mar. Res.*, vol. 2, pp. 38–55, 1939.

[11] D. Chelton and M. Schlax, "Global observations of oceanic Rossby waves," *Science*, vol. 272, pp. 234–238, 1996.

[12] S. Nazarenko, *Wave Turbulence (Lecture notes in Physics 825)*. Springer, 2011.

[13] R. Peierls *Annalen Physik*, vol. 3, p. 1055, 1929.

[14] A. Vedenov, "Theory of weakly turbulent plasma," *Reviews of Plasma Phys.*, vol. 3, p. 229, 1967.

[15] K. Hasselmann, "On the nonlinear energy transfer in gravity-wave spectrum Part 1. General theory," *J. Fluid Mech.*, vol. 12, pp. 481–500, 1962.

[16] V. Zakharov, F. Dias, and A. Pushkarev, "One-dimensional wave turbulence," *Physics Reports*, vol. 398, pp. 1–65, 2004.

[17] V. Zakharov, "Weak turbulent spectrum in plasma without magnetic field," *Sov. Phys. JETP*, vol. 24, pp. 455–459, 1967.

[18] V. Zakharov and N. Filonenko, "Energy spectrum for stochastic oscillations of the surface of a liquid," *Sov. Phys. Dokl.*, vol. 11, pp. 881–884, 1967.

[19] V. Zakharov and N. Filonenko, "Weak turbulence of capillary waves," *J. Appl. Mech. Tech. Phys.*, vol. 4, pp. 506–515, 1967.

[20] G. Kolmakov, P. McClintock, and S. Nazarenko, "Wave turbulence in quantum fluids," *Proc. Natl. Acad. Sci. USA*, vol. 111, pp. 4727–4734, 2014.

[21] R. Bedard, S. Lukaschuk, and S. Nazarenko, "Non-stationary regimes of surface gravity wave turbulence," *JETP Lett.*, vol. 97, pp. 529–535, 2013.

[22] A. Pushkarev and V. Zakharov, "Turbulence of capillary waves - theory and numerical simulation," *Physica D*, vol. 135, pp. 98–116, 2000.

[23] S. Galtier, S. Nazarenko, and A. Newell, "On wave turbulence in MHD," *Nonlin. Processes Geophys.*, vol. 8, pp. 141–150, 2001.

[24] N. Tronko, S. Nazarenko, and S. Galtier, "Weak turbulence in two-dimensional magnetohydrodynamics," *Phys. Rev. E*, vol. 87, p. 033103, 2013.

[25] N. Schaeffer and P. Cardin, "Rossby wave turbulence in a rapidly rotating sphere," *Nonlin. Processes in Geophys.*, vol. 12, pp. 947–953, 2005.

[26] Y. Lvov, K. Polzin, and N. Yokoyama, "Wave-wave interactions in stratified fluids: A comparison of approaches," *arXiv:0706.3712v2*, 2014.

[27] V. Zakharov, V. L'vov, and G. Falkovich, *Kolmogorov Spectra of Turbulence I: Wave Turbulence.* Springer, 1992.

[28] E. Kartashova, *Nonlinear Resonance Analysis: Theory, computation, applications.* Cambridge University Press, 2010.

[29] V. L'vov and S. Nazarenko, "Discrete and mesoscopic regimes of finite-size wave turbulence," *Phys. Rev. E*, vol. 82, p. 056322, 2010.

[30] E. Kartashova and M. Bustamante, "Resonance clustering in wave turbulence regimes: Integral dynamics," *Commun. Comput. Phys.*, vol. 10, pp. 1211–1240, 2011.

[31] V. L'vov, A. Pomyalov, I. Procaccia, and O. Rudenko, "Finite-dimensional turbulence of planetary waves," *Phys. Rev. E*, vol. 80, p. 066319, 2009.

[32] M. Bustamante and E. Kartashova, "Dynamics of nonlinear resonances in hamiltonian systems," *EPL*, vol. 85, p. 14004, 2009.

[33] M. Bustamante and E. Kartashova, "Effect of the dynamical phases on the nonlinear amplitudes' evolution," *EPL*, vol. 85, p. 34002, 2009.

[34] M. Bustamante and U. Hayat, "Complete classification of discrete resonant Rossby/drift wave triads on periodic domains," *Commun. Nonlin. Sci. Numer. Simulat.*, vol. 18, pp. 2402–2419, 2013.

[35] S. Nazarenko, "Sandpile behaviour in discrete water-wave turbulence," *J. Stat. Mech.*, p. L02002, 2006.

[36] N. Fitzmaurice, D. Gurarie, F. Mccaughan, and W. Woyczynski, *Nonlinear Waves and Weak Turbulence with Applications in Oceanography and Condensed Matter Physics*. Birkhauser Verlag, 1994.

[37] V. Zakharov and E. Schulman, "Degenerative dispersion laws, motion invariants and kinetic equations," *Physica D*, vol. 1, pp. 192–202, 1980.

[38] V. Zakharov and E. Schulman, "On additional motion invariants of classical Hamiltonian wave systems," *Physica D*, vol. 29, pp. 283–320, 1988.

[39] A. Balk, S. Nazarenko, and V. Zakharov, "A new invariant for drift turbulence," *Phys. Lett. A*, vol. 152, pp. 276–280, 1991.

[40] A. Balk, "A new invariant for Rossby wave systems," *Phys. Lett. A*, vol. 155, pp. 20–24, 1991.

[41] L. Richardson, *Weather Prediction by Numerical Process*. 1922.

[42] A. Kolmogorov *Dokl. Akad. Nauk SSSR*, vol. 30, pp. 301–305, 1941.

[43] A. Kolmogorov *Dokl. Akad. Nauk SSSR*, vol. 31, pp. 538–540, 1941.

[44] R. Kraichnan, "Inertial ranges in two-dimensional turbulence," *Phys. Fluids*, vol. 10, pp. 1417–1423, 1967.

[45] R. Fjørtoft, "On the changes in the spectral distribution of kinetic energy for two-dimensional non-divergent flow," *Tellus*, vol. 5, pp. 225–230, 1953.

[46] S. Nazarenko and B. Quinn, "Triple cascade behaviour in QG and drift turbulence and the generation of zonal jets," *Phys. Rev. Lett.*, vol. 203, p. 118501, 2009.

[47] A. Carpinteri, *Structural mechanics: A unified approach*. 1997.

[48] I. Saito and K. Ishioka, "Angular distribution of energy spectrum in two-dimensional β-plane turbulence in the long-wave limit," *Phys. Fluids*, vol. 25, p. 076602, 2013.

[49] C. Connaughton, S. Nazarenko, and B. Quinn, "Rossby and drift wave turbulence and zonal flows: the Charney-Hasegawa-Mima model and its extensions," *arXiv:1407.1896*, 2014.

[50] N. Phillips, "A simple three-dimensional model for the study of large-scale extra-tropical flow patterns," *J. Meteor.*, vol. 8, pp. 381–394, 1951.

[51] P. Rhines, *The Dynamics of Unsteady Currents*. 1977.

[52] R. Salmon, "Two-layer quasi-geostrophic turbulence in a simple special case," *Geophys. Astrophys. Fluid Dyn.*, vol. 10, pp. 25–52, 1978.

[53] R. Salmon, "Baroclinic instability and geostrophic turbulence," *Geophys. Astrophys. Fluid Dynamics*, vol. 15, pp. 167–211, 1980.

[54] J. Charney, "Geostrophic turbulence," *J. Atmos. Sci.*, vol. 28, pp. 1087–1094, 1971.

[55] P. Rhines, "Geostrophic turbulence," *Ann. Rev. Fluid Mech.*, vol. 11, pp. 401–441, 1979.

[56] A. Venaille, G. Vallis, and S. Griffies, "The catalytic role of beta effect in barotropization processes," *J. Fluid Mech.*, vol. 709, pp. 490–515, 2012.

[57] P. Rhines, "Waves and turbulence on a beta-plane," *J. Fluid Mech.*, vol. 69, pp. 417–443, 1975.

[58] G. Vallis and M. Maltrud, "Generation of mean flows and jets on a beta-plane and over topography," *J. Phys. Oceanog.*, vol. 23, pp. 1346–1362, 1993.

[59] B. Galperin, S. Sukoriansky, N. Dikovskaya, P. Read, Y. Yamazaki, and R. Wordsworth, "Anisotropic turbulence and zonal jets in rotating flows with a beta-effect," *Nonlin. Processes Geophys.*, vol. 13, pp. 83–98, 2006.

[60] L. Fu and G. Flierl, "Nonlinear energy and enstrophy transfers in a realistically stratified ocean," *Dyn. Atmos. Oceans*, vol. 4, pp. 219–246, 1980.

[61] K. Smith and G. Vallis, "Scales and equilibration of mid-ocean eddies: Freely decaying flow," *J. Phys. Oceanogr.*, vol. 31, pp. 554–571, 2001.

[62] B. Arbic, "Generation of mid-ocean eddies: The local baroclinic instability hypothesis," *Ph.D. dissertation*, 2000.

[63] R. Scott and F. Wang, "Direct evidence of an oceanic inverse kinetic energy cascade from satellite altimetry," *J. Phys. Oceanog.*, vol. 35, pp. 1650–1666, 2005.

[64] T. Schneider and C. Walker, "Self-organization of atmospheric macroturbulence into critical states of weak nonlinear eddyeddy interactions," *J. Atmos. Sci.*, vol. 63, pp. 1569–1586, 2006.

[65] R. Wordsworth, P. Read, and Y. Yamazaki, "Turbulence, waves, and jets in a differentially heated rotating annulus experiment," *Phys. Fluids*, vol. 20, p. 126602, 2008.

[66] P. Berloff and I. Kamenkovich, *Dynamics of Baroclinic Multiple Zonal Jets.* 2013.

[67] Y. Kaspi and G. Flierl, "Formation of jets by baroclinic instability on gas planet atmospheres," *J. Atmos. Sci.*, vol. 64, pp. 3177–3194, 2007.

[68] B. Galperin, R. Young, S. Sukoriansky, N. Dikovskaya, P. Read, A. Lancaster, and D. Armstrong, "Cassini observations reveal a regime of zonostrophic macroturbulence on Jupiter," *Icarus*, vol. 229, pp. 295–320, 2014.

[69] J. Marston, "Planetary atmospheres as nonequilibrium condensed matter," *Ann. Rev. Condens. Matt. Phys.*, vol. 3, pp. 285–310, 2012.

[70] K. Srinivasan and W. Young, "Zonostrophic instability," *J. Atmos. Sci.*, vol. 69, pp. 1633–1656, 2012.

[71] T. Schneider and J. Liu, "Formation of jets and equatorial superrotation on Jupiter," *J. Atmos. Sci.*, vol. 66, pp. 597–601, 2009.

[72] A. Ingersoll, P. Gierasch, D. Banfield, A. Vasavada, and the Galileo Imaging Team, "Moist convection as an energy source for the large-scale motions in Jupiter's atmosphere," *Nayure*, vol. 403, pp. 630–632, 2000.

[73] B. Arbic, R. Scott, G. Flierl, A. Morten, J. Richman, and J. Shriver, "Nonlinear cascades of surface oceanic geostrophic kinetic energy in the frequency domain," *J. Phys. Oceanog.*, vol. 42, pp. 1577–1600, 2012.

[74] B. Arbic, M. Muller, J. Richman, J. Shriver, A. Morten, R. Scott, G. Serazin, and T. Penduff, "Geostrophic turbulence in the frequencywavenumber domain: Eddy-driven low-frequency variability," *J. Phys. Oceanog.*, vol. 44, pp. 2050–2069, 2014.

[75] "http://www.columbia.edu/ irs2113/6˙2layerSW.pdf,"

[76] N. Phillips, "Energy transformations and meridional circulation associated with baroclinic waves in a two-level, quasi-geostrophic model," *Tellus*, vol. 6, pp. 273–286, 1954.

[77] J. Pedlosky, "Baroclinic instability in two layer systems," *Tellus*, vol. 15, pp. 20–25, 1963.

[78] J. McWilliams, *Fundamentals of Geophysical Fluid Dynamics*. Cambridge University Press, 2006.

[79] A. Balk, S. Nazarenko, and V. Zakharov, "On the nonlocal turbulence of drift type waves," *Phys. Lett. A*, vol. 146, pp. 217–221, 1990.

[80] C. Connaughton, S. Nazarenko, and B. Quinn, "Nonlocal wave turbulence in the Charney-Hasegawa-Mima equation: a short review," *arXiv:1012.2714*, 2010.

[81] C. Connaughton, S. Nazarenko, and B. Quinn, "Feedback of zonal flows on wave turbulence driven by small-scale instability in the Charney-Hasegawa-Mima model," *EPL*, vol. 96, p. 25001, 2011.

[82] T. Soomere, "Coupling coefficients and kinetic equation for rossy waves in multi-layer ocean," *Nonlinear Processes in Geophysics*, vol. 10, pp. 385–396, 2003.